3-22-2012

Accurate Modeling of Stability and Control Properties for Fighter Aircraft from CFD

Jedediah H. Butler

DETERMINATION OF EFFECTIVE CROSSOVER LOCATION AND DIMENSIONS FOR BRANCHED DETONATION IN A PULSED DETONATION ENGINE

THESIS

Louis A. Camardo II, Major, USMC

AFIT/GAE/ENY/12-M05

DEPARTMENT OF THE AIR FORCE
AIR UNIVERSITY

AIR FORCE INSTITUTE OF TECHNOLOGY

Wright-Patterson Air Force Base, Ohio

AFIT/GAE/ENY/12-M05

DETERMINATION OF EFFECTIVE CROSSOVER LOCATION AND DIMENSIONS FOR BRANCHED DETONATION IN A PULSED DETONATION ENGINE

THESIS

Presented to the Faculty

Department of Aeronautics and Astronautics

Graduate School of Engineering and Management

Air Force Institute of Technology

Air University

Air Education and Training Command

In Partial Fulfillment of the Requirements for the

Degree of Master of Science in Aeronautical Engineering

Louis A. Camardo II

Major, USMC

March 2012

AFIT/GAE/ENY/12-M05

DETERMINATION OF EFFECTIVE CROSSOVER LOCATION AND DIMENSIONS FOR BRANCHED DETONATION IN A PULSED DETONATION ENGINE

Louis A. Camardo II

Major, USMC

Approved:

_____	_____
Paul I. King (Chairman)	Date
_____	_____
Frederick R. Schauer (Member)	Date
_____	_____
James L. Rutledge, Capt, USAF (Member)	Date

Abstract

A study is presented of the optimal crossover duct location and width to obtain consistent branched detonation transition from one detonation tube to another. On a Pulsed Detonation Engine (PDE) with detonation branching, the duct location at which the detonation crosses from one (primary) tube to a branched (secondary) tube impacts the number of successful detonations. In this paper, a comparison is made of the effects of the location and width of the crossover duct for hydrogen, ethylene and an n-alkane. The crossover location is varied from the aft end of the detonation tube to the middle of the detonation tube while the crossover width is varied from 2.5 in to 0.5 in. Detonation wave speeds are measured and compared to Chapman-Jouguet velocities in order to determine successful detonations. Regardless of crossover location, all three fuels are demonstrated 100% of the time to transition between 2 in detonation tubes with a crossover width of 2 in. With a mid-location crossover duct, all three fuels are demonstrated 100% of the time to transition detonations between 2 in detonation tubes with a crossover width between 1.75 in and 2.5 in.

Acknowledgments

Ad majorem Dei gloriam.

I am thankful for the opportunity I have been given to attend the Air Force Institute of Technology and for the chance to learn from the finest individuals that the Air Force Research Laboratory has to offer. I am proud to have been associated with the Detonation Engine Research Facility, even if only for a short time. The individuals who work in D-Bay and 5-Stand are true professionals. I extend my thanks to them for allowing me to take part in the amazing work that they do on a regular basis.

I would like to thank Dr. Paul King, Dr. Fred Schauer, Dr. John Hoke, and Capt Jay Rutledge for taking the time to share their knowledge and experience and for helping further my education.

I would especially like to thank Chris Stevens for the countless hours that he generously contributed to answering my questions, setting up equipment and lending a hand at every opportunity. I owe my thanks to Dr. Brian Sell for always making time to be available to assist with anything that needed to be done. For sharing his expertise running the PDE, and for sharing the snacks from his well-stocked cabinet, I give many thanks to Curt Rice. The tests simply would not have been possible were it not for Justin Goffena's diligent efforts fabricating modifications to the test section. I sincerely thank him for taking extra time to show me how to do the work correctly. I also thank Dave Burris for going out of his way to make sure I had the IT support that I needed and for helping me make use of the software that is smarter than me.

Finally, for their unconditional love, I thank my wonderful wife, Jenny, and our children: Maria, Josephine, Mario, and Antonina.

Deo gratias.

Louis A. Camardo II

Table of Contents

Page

List of Figures

Page

List of Tables

Page

Nomenclature

A	Area [m^2]
a	Slope of Rayleigh line in P-*v* space [$kg/(m^2 \cdot s)$]
B	Bias uncertainty
b	Y-intercept of Rayleigh line in P-*v* space
d	Diameter [mm]
e	Internal energy per unit mass [J/kg]
F	Uninstalled thrust [N]
h	Enthalpy per unit mass [J/kg]
ht	Height [m]
M	Mach number
m	Mass flow rate [kg/s]
m′	Mass flux [$kg/(m^2 \cdot s)$]
P	Pressure [N/m^2]
p	Precision uncertainty
q	Heat addition per unit mass [J/kg]
R	Specific gas constant [$J/(kg \cdot K)$]
r	Ratio
T	Temperature [K]
t	time [s]
U	Overall uncertainty
V	Velocity [m/s]
w	Width [m]

x	Distance between ion probes [m]
Δ	Difference between two parameters
φ	Equivalence ratio
ρ	Density [kg/m^3]
σ	Standard deviation
λ	Detonation cell width [mm]
v	Specific volume [m^3/kg]

Subscripts

c	Critical
cr	Crossover
CJ	Chapman-Jouguet
d	Detonation tube
e	Exit condition
ws	Wave speed
0	Upstream or ambient condition
1	Initial condition of reactants
2	Final condition of products
1-2	Denotes two subsequent measurements of one parameter, e.g. a parameter measured at two ion probes or in two frames of high speed photography
Δt	Uncertainty in time
Δx	Uncertainty in location

DETERMINATION OF EFFECTIVE CROSSOVER LOCATION AND DIMENSIONS FOR BRANCHED DETONATION IN A PULSED DETONATION ENGINE

I. Introduction

A Pulsed Detonation Engine (PDE) makes use of unsteady supersonic combustion to produce thrust. While most air breathing propulsion systems use a combustion process entailing steady deflagration in order to generate thrust, the PDE uses unsteady detonations to provide the desirable characteristics of constant volume combustion and high thermodynamic efficiencies.[1]

Similar technology in aeronautical applications was operational as early as 1944 on the German V-1 "Buzz Bomb" powered by pulse jet engines.[2] This "flying bomb" was the precursor to today's cruise missile and utilized an engine developed by Paul Schmidt, a German inventor, in 1928. Schmidt's work was based on Georges Marconnet's 1908 French patent and V.V. Karavodin's 1906 Russian patent.[3]

Regardless of the design used in an aeronautical engine, the desired result is thrust. Considering a perfect engine, that is, an engine in which drag is not accounted for, thrust may be defined as in Eq. (1)[4].

$$F = m_e V_e - m_0 V_0 + \ P_e - P_0 \ A_e \tag{1}$$

A detonation is an attractive source of thrust in an engine owing to the exit velocity at which the detonation travels and the pressure difference between the exit and ambient conditions. A PDE is also desirable for its scalability and versatile applicability at airspeeds ranging from low subsonic to high supersonic.[5] PDEs offer the potential for high-performance from simple and efficient designs.[6]

The relevance of a PDE is based on its ability to harness and use the thrust produced by a detonation. A detonation is a violent supersonic combustion event. Composed of a shock wave

coupled to a combustion front, a detonation wave produces an overpressure in a constant volume process. In contrast, a deflagration, the more common type of combustion, is subsonic and is often modeled as a constant pressure process.[2]

A detonation can be created in one of several ways, including the following three methods: using a low energy spark with subsequent Deflagration to Detonation Transition (DDT), using a pre-detonator, or applying a large amount of energy to cause direct initiation. A variation of direct initiation, called a branched detonation or tube-to-tube initiation, utilizes one of the three methods mentioned to initiate a detonation in a primary detonation tube. Tube-to-tube initiation then transfers the detonation to a secondary tube via a crossover duct. The advantages and disadvantages of each of these methods have been previously documented.[7]

This research utilizes a PDE with detonation tubes open at one end and closed at the other end where the tube is connected to a source of fuel, oxidizer, and ignition.[7] The engine cycle is divided into three equal phases: fill, fire, and purge. During the fill phase, the engine intake valves allow a pre-determined ratio of pre-mixed fuel and air to enter the detonation tube. The fire phase begins with closure of the fill valves, isolating the combustion event from feed lines upstream of the valves. A spiral in the primary detonation tube accelerates DDT. The purge phase cools and clears the tubes and begins upon opening of the purge valves.

Throughout this research, the closed end of the detonation tube is the head of the tube while the open end of the detonation tube is the tail end of the tube. Tube-to-tube initiation has been successfully shown using the detonation from the tail end of one tube into the head of another tube (tail-head)[8], using the detonation from the tail end of one tube into the tail end of another tube (tail-tail), and using the detonation from the head of one tube into the head of another tube (head-head).[9]

For a self-sustaining, continuous branching PDE, it is necessary to extract energy from on-going detonation cycles to initiate subsequent detonation events. The tube-to-tube initiation offers greater efficiency than the other methods of detonation initiation; however, maintaining the detonation through the crossover duct has proven to be challenging.[10] As the detonation enters the crossover, the shock wave and combustion front begin to decouple.[11]

Assuming the detonation from the last tube in succession crosses over to ignite a detonation in the first tube, then with the exception of the DDT, all detonations are initiated with tube-to-tube initiation in a continuous branching PDE.[9] Although a continuous branching PDE is not utilized in this research, the results regarding crossover location and width documented here should be applicable to the operation of a continuous branching PDE in the future.

In the tail-tail configuration shown in Fig. 1, tube-to-tube detonation initiation requires the detonation in the primary tube to reverse direction via the crossover duct.

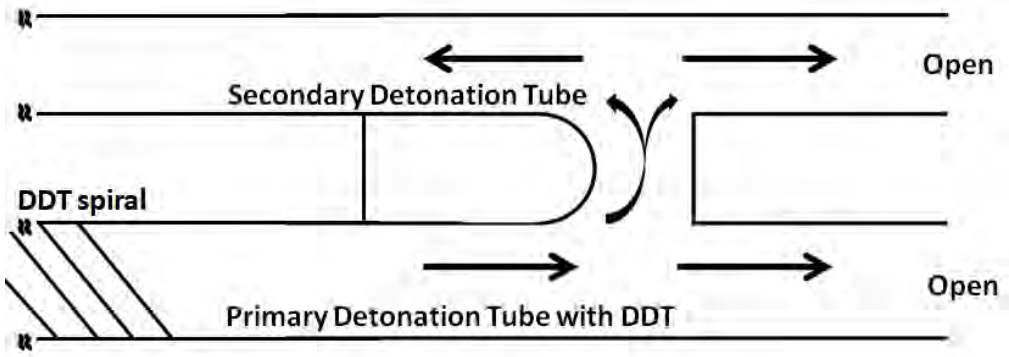

Figure 1. Detonation directions through multiple tubes connected by a crossover duct

Past experiments, however, showed that detonations could propagate through various crossover geometries and in directions different from that of the primary detonation wave.[7, 12]

This research examines at which location and width the crossover duct most consistently results in a viable detonation in the secondary tube.

II. Background and Theory

1. Detonation Properties

Combustion occurs as a deflagration or a detonation. A deflagration propagates subsonically away from the source of ignition through reactants; however, a detonation propagates supersonically.[13]

Figure 2 depicts a detonation wave within a control volume. In a laboratory reference frame the detonation wave propagates from right to left with velocity, V, pressure, P, temperature, T, density, ρ, and Mach number, M. Subscripts 1 and 2 denote reactants and products, respectively. In a reference frame fixed to the detonation wave, as shown in Fig. 2, the reactants enter the detonation wave from left to right at velocity, V_1, as the products leave the detonation wave at velocity, V_2.

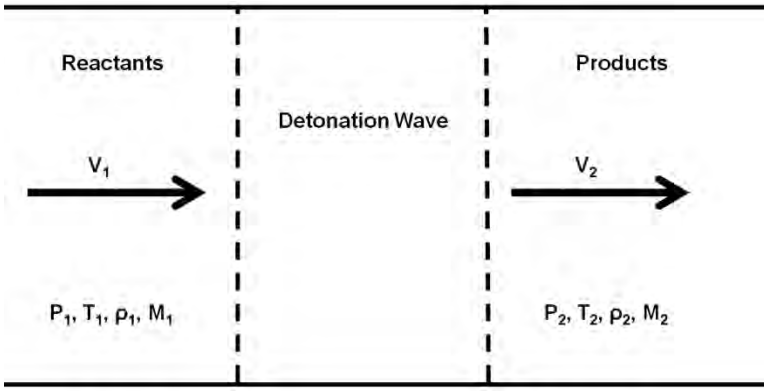

Figure 2. One-dimensional detonation wave in a constant area duct[14]

Table 1 lists the Mach numbers of the reactants and products as well as the ratios of properties across a typical detonation.[14]

Table 1. Standard detonation properties

Property	Detonation
M_1	5-10
M_2	1.0
V_2/V_1	0.4-0.7
P_2/P_1	13-55
T_2/T_1	8-21
ρ_2/ρ_1	1.7-2.6

As seen in Table 1, reactants travel supersonically at M_1 with respect to the detonation wave. Products travel away from the detonation wave at M_2, the local speed of sound. Comparing the properties of products to reactants, a detonation wave produces a decrease in velocity and an increase in pressure, temperature and density of the products.

A detonation is composed of a shock wave coupled to a deflagration front. The compression of reactants and subsequent high temperatures caused by the leading shock wave of a detonation initiate the detonation combustion process. This combustion process is sustained as a result of the energy from the combustion.[14] A shock wave, detonation, and deflagration are very different, however. This is illustrated in Table 2 by the upstream and downstream Mach numbers and by the property ratios of the products and reactants across these three phenomena. The normal shock properties in Table 2 are for air with a ratio of specific heats equal to 1.4. The detonation properties are the standard properties from Table 1. The deflagration properties are for a methane-air mixture.[14]

Table 2. Normal shock, detonation, and deflagration properties[14]

Property	Normal shock	Detonation	Deflagration
M_1	5.0	5-10	0.001
M_2	0.42	1.0	0.003
V_2/V_1	0.20	0.4-0.7	7.5
P_2/P_1	29	13-55	~1
T_2/T_1	5.8	8-21	7.5
ρ_2/ρ_1	5.0	1.7-2.6	0.13

2. Detonation physics

In the following analysis[14], flow properties and the equations of mass continuity and conservation of momentum and energy are utilized to describe the physics of a detonation. Equation (2) uses the internal energy per unit mass, e, to define enthalpy, h.

$$h = e + \frac{P}{\rho} \tag{2}$$

Equation (3) is the ideal gas equation.

$$P = \rho RT \tag{3}$$

Equations (4) – (6) are the equations for continuity of mass and conservation of momentum and energy respectively in a constant area duct.

$$\rho_1 V_1 = \rho_2 V_2 = m' \tag{4}$$

$$P_1 + \rho_1 V_1^2 = P_2 + \rho_2 V_2^2 \tag{5}$$

$$h_1 + \frac{1}{2} V_1^2 + q = h_2 + \frac{1}{2} V_2^2 \tag{6}$$

Combining Eqs. (4) and (5) produces Eq. (7).

$$\rho_1 V_1^{\ 2} = \rho_2 V_2^{\ 2} = m'^2 = -\frac{P_2 - P_1}{\frac{1}{\rho_2} - \frac{1}{\rho_1}} \tag{7}$$

The plot of Eq. (7) in pressure – specific volume space is called a Rayleigh line.[15] The slope, *a*, and the y-intercept, b, of each line can be calculated with Eqs. (8) and (9) respectively.

$$-m'^2 = a \tag{8}$$

$$P_1 + \frac{m'^2}{\rho_1} = b \tag{9}$$

Point A in Fig. 3 represents a given P_1 and ρ_1. The negative slope of the Rayleigh line plotted through point A in Fig. 3 steepens as the mass flux increases. An infinite mass flux would pass vertically through point A, while zero mass flux would pass horizontally through point A. Between an infinite mass flux and zero mass flux all possible mass fluxes are included. Neither a mass flux greater than infinity nor less than zero are possible, therefore, solutions for Rayleigh lines passing through the quadrants labeled I and II in Fig. 3 are not obtainable.

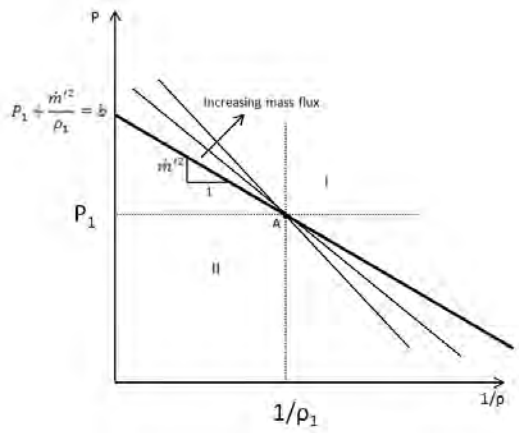

Figure 3. Rayleigh lines of increasing mass flux[14]

Two Rayleigh lines are plotted in Fig. 4 through point A and noted as the Upper and Lower Rayleigh lines. As seen in Fig. 4 proceeding from point A, the Upper Rayleigh line illustrates a high mass flux and the pressure and density increases that are characteristic of a detonation. The Lower Rayleigh line, however, illustrates a lower mass flux and the pressure and density decreases from point A that are characteristic of a deflagration. In Fig. 4 the pressure decrease from point A to point L is small. Deflagrations are often modeled as constant pressure processes due to a small change in pressure.

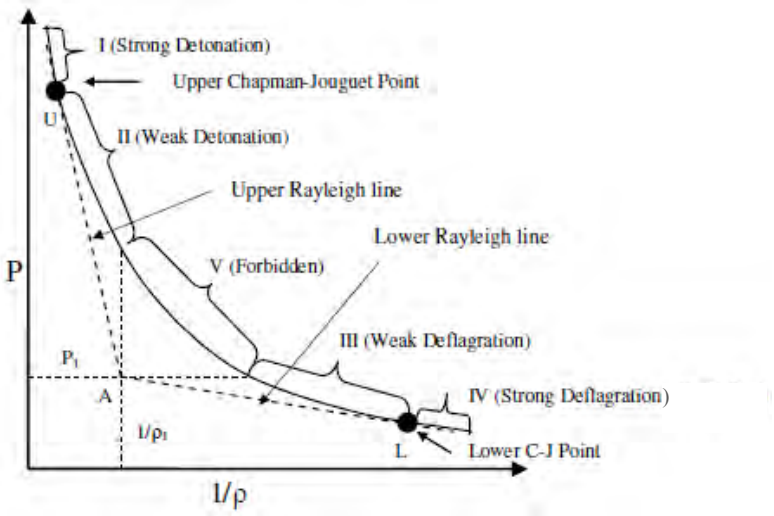

Figure 4. Hugoniot curve and Rayleigh lines[14,16]

Using the definitions in Eqs. (2) and (3) and combining Eqs. (4) – (6) produces Eqs. (10) and (11).[2]

$$h_1 - h_2 + q = \frac{1}{2}\ P_1 - P_2 \quad \frac{1}{\rho_2} - \frac{1}{\rho_1} \tag{10}$$

$$e_1 - e_2 + q = -\frac{1}{2}\ P_1 + P_2 \quad \frac{1}{\rho_1} - \frac{1}{\rho_2} \tag{11}$$

Equations (10) and (11) are the Hugoniot equations. The Hugoniot curve is plotted as the solid line in Fig. 4. A physically possible end state must satisfy the equation of the Rayleigh line (Eq. (7)) and the Hugoniot equations (Eqs. (10) and (11)). Proceeding from P_1 and ρ_1 at point A, the intersection of the Hugoniot curve and the Rayleigh line indicates possible end states in

regions I through IV in Fig 4. Region V indicates an area with an unrealizable mass flux and therefore a physically impossible end state.

Point U in Fig. 4 is the Upper Chapman-Jouguet Point, named after the men who independently discovered, in the late 19th and early 20th centuries respectively, that a detonation sustaining itself is found where the Rayleigh line falls tangent to the Hugoniot curve. Chapman also noted that the velocity of the detonation is at a minimum at this upper tangent point.[13] At the Upper Chapman-Jouguet point, the detonation velocity is referred to as the Chapman-Jouguet velocity (V_{CJ}).[17] When the velocity is greater than the minimum, there are strong and weak detonation solutions as shown in regions I and II of Fig. 4.[13]

Although in theoretical analysis one often assumes one-dimensional detonation waves for simplification, detonations are complex three-dimensional structures composed of triple shock waves. The intersection of the Mach-stem, incident and reflected shocks is known as the triple point and is seen near a wall in Fig. 5.[18] The Mach stem is stronger than the incident shock. The reflected shock wave extends into the reactants in the direction that the detonation is traveling.[13]

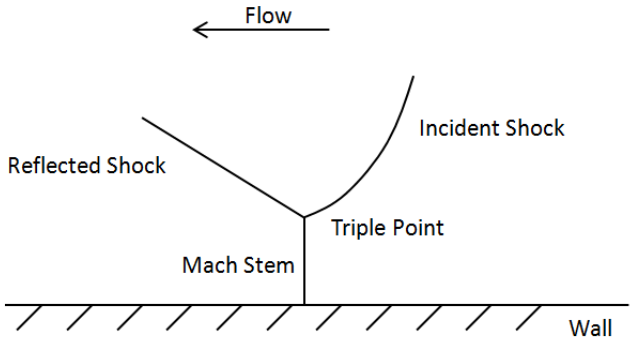

Figure 5. Intersection of detonation incident shock, reflected shock and Mach stem at triple point[18]

The velocity of the detonation varies along these shock waves as the detonation propagates and the shock waves interact. At the triple point, the detonation velocity reaches its maximum. The velocity then decreases along the three shock waves until they intersect again and the local detonation velocity increases. A successful detonation is sustainable within 30% of the theoretical V_{CJ} as the detonation velocity constantly decreases and increases along the shock waves.[7]

3. Cell size

The triple points move and interact in a distinctive pattern throughout a detonation. The triple point pattern is observable after a detonation passes through a tube coated with soot.[13,18] The triple point removes soot from the detonation and leaves behind a diamond shape with a characteristic cell width dimension, λ, unique to the reactants, as seen in Fig. 6.

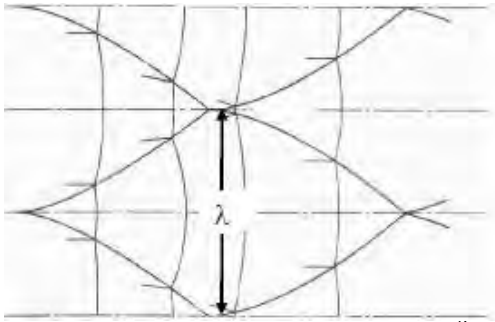

Figure 6. Detonation cell width[9]

The cell width is a characteristic length scale of a detonation. The larger the cell width, the more distance is required for DDT.[12] Also, Fievisohn showed that strong reflections caused detonation reinitiation.[19] Figure 7 shows the transverse wave intersections and cell structure reestablish on the right after strong reflections off the obstacle in the center of the figure and off the wall reinitiate the detonation.

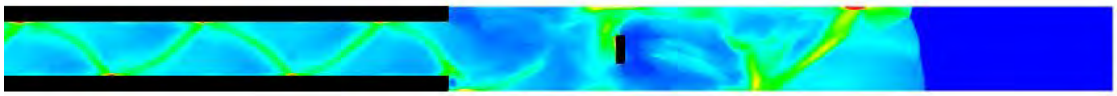

Figure 7. Detonation cell structure reestablishes after interaction with obstacle

A substantial amount of experimental data is available showing the detonation cell widths for most of the common fuel-oxidizer mixtures.[13] Cell width has been shown to vary as a function of equivalence ratio as in Fig. 8.

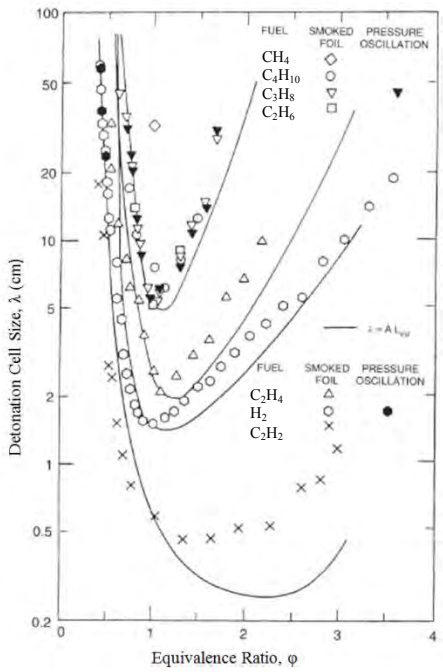

Figure 8. Cell size variation with equivalence ratio.[18]

Another useful characteristic length scale of a detonation is the critical tube diameter.[13] The critical tube diameter, d_c, is the minimum diameter from which a planar detonation confined in a tube can successfully transition into an unconfined area.[13] Zeldovich has shown that while a confined detonation propagates in a plane, the planar detonation transitions, or diffracts, into an unconfined area and propagates spherically.[13] Transitioning from a confined area into an unconfined area occurs during this research, for example, upon exiting a detonation tube or

entering the crossover duct in a branched detonation. Zeldovich showed that a diffracting detonation wave propagating across a change in area will not propagate from a tube having a diameter less than d_c.[20] Instead, the shock wave and combustion front of the detonation decouple and do not recombine without intervention or a change in conditions.

A diffracting detonation from a tube with a diameter greater than d_c is known as supercritical. A supercritical detonation will successfully propagate naturally into the unconfined area. From a tube with a diameter less than d_c, a diffracting detonation is known as subcritical. The shock wave and combustion front of the subcritical detonation will decouple and not reinitiate naturally. From a tube with a diameter equal to d_c, a detonation is critical. The shock wave and combustion front of the critical detonation will initially decouple, but will reinitiate naturally. These different phenomena are depicted in Fig. 9.[21]

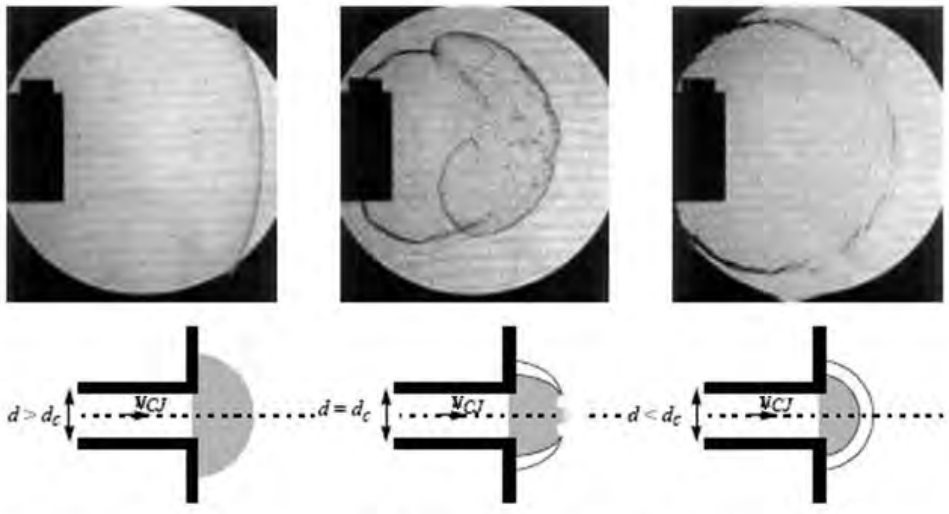

a) Supercritical b) Critical c) Subcritical

Figure 9. Supercritical, critical, and subcritical detonation diffractions

Furthermore, cell width is related to the critical tube diameter as determined by Mitrofanov and Soloukhinin and noted by multiple authors as in Eq. (12) for a circular tube and in Eq. (13) for a planar channel.[18,20]

$$d_c = 13\lambda \tag{12}$$

$$d_c = 10\lambda \tag{13}$$

The crossover section in this research uses planar channels to facilitate Schlieren photography of the detonation as explained in Section III.

Critical tube diameter has also been shown to vary with equivalence ratio as shown in Fig. 10.

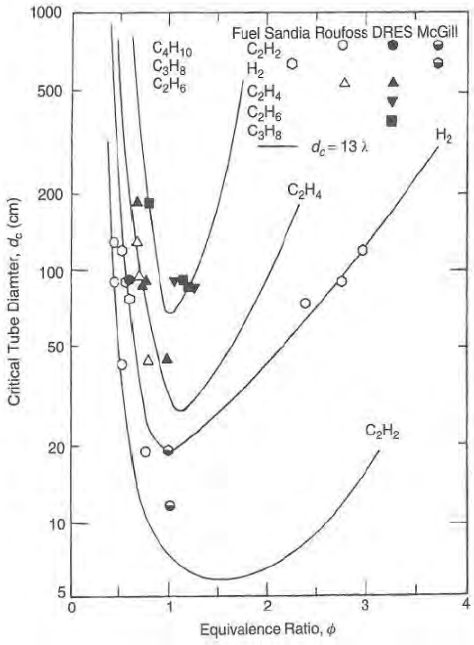

Figure 10. Critical tube diameter variation with equivalence ratio[18]

Table 3 shows the cell sizes used in this research. As a point of reference, this research utilizes detonation tubes of 2 in (50.8 mm). The detonations are expected to be subcritical as they diffract from the tube based on Eq. (13).

Table 3. Pertinent fuels and cell sizes

Fuel	Equivalence Ratio	Cell Size, λ (mm)	Critical tube diameter, d_c (mm)	Actual tube diameter (mm)
Hydrogen	1	8	80	50.8
Ethylene	1.3	26.5	265	50.8
n-Alkane	1.1	50-70	500-700	50.8

4. Previous Research

In recent experiments by Nielsen, the crossover geometry was varied in a tail-tail setup in order to find the configuration that provided the most consistent branched detonation.[7] Based on Nielsen's results with hydrogen, the "D" geometry, with a convex surface in the direction of the primary tube flow and a flat surface facing the flow in the primary tube, consistently reinitiated a detonation in the secondary tube7 (Fig. 11).

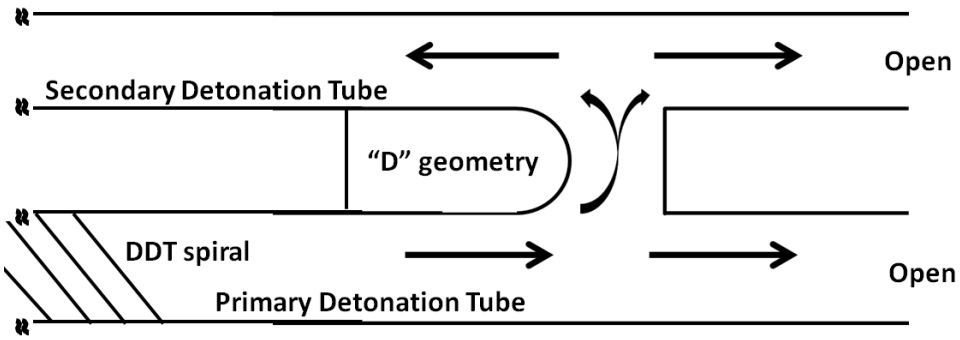

Figure 11. Crossover duct showing "D" geometry and flow direction

Additionally, Nielsen's experiments illustrated one of the challenges with the tail-tail configuration: When the engine valves close after filling the primary detonation tube with fuel and air, the mixture continues moving aft. As the volume of the fuel-air mixture expands, the pressure drops causing the flow in the tube to reverse direction. In the tail-tail configuration when the flow reverses, the local equivalence ratio in the crossover duct decreases due to entrainment of the ambient air.[7] This can be seen in Figs. 12 and 13.

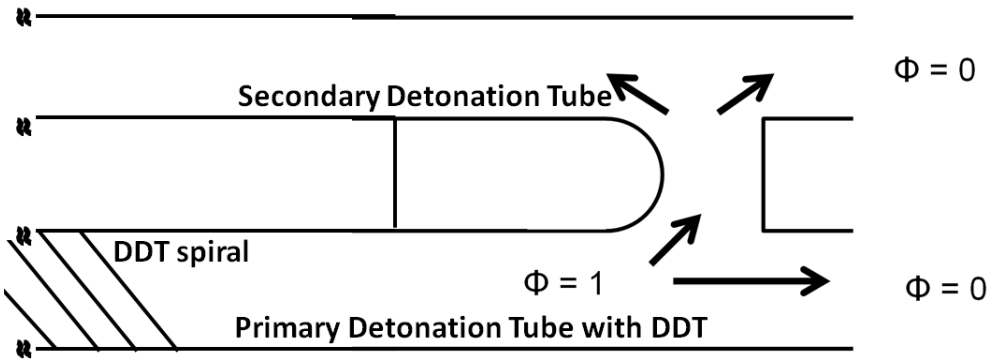

Figure 12. Tail-tail crossover with fuel-air mixture moving aft as intake valves close

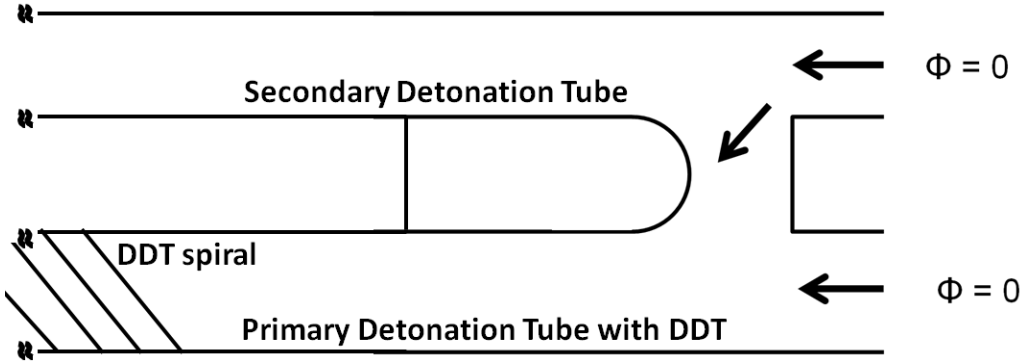

Figure 13. Tail-tail crossover illustrating entrainment of ambient air as lower pressure causes flow reversal

The leaned-out equivalence ratio leads to inconsistent reinitiation after decoupling in the crossover duct.[7] He successfully reduced those inconsistencies by placing a nozzle over the open

end of the primary tube to force fuel and air through the crossover duct and into the secondary detonation tube.[7] Nielsen settled on a "D" geometry, but with a) only a single filling tube, b) only a hydrogen-air mixture and c) with a nozzle on the tail end of the primary tube. The current experiment removes the constraints in a, b and c, and includes testing with hydrocarbon fuels.

5. Research Objectives

This research reports on three main objectives. The first objective of this research is to apply Nielsen's findings regarding crossover geometry to a configuration with two tubes. As a continuous branching PDE would actually fill multiple tubes, this research looks at the more practical case of filling the crossover duct by means of two tubes with a hydrogen-air mixture, an ethylene-air mixture, and an n-alkane-air mixture with none of the two-tube tests having the nozzle on the tail end of the primary detonation tubes. The second objective is to exploit the potential of the "D" geometry by testing it with varied crossover widths in search of an optimal width. The final objective is to address the entrainment of ambient air into the crossover duct in the tail-tail location by varying the location of the crossover from a tail-tail location to a new location in the center of the detonation tube. This location will be referred to as a mid-mid tube-to-tube detonation initiation. Sketches of the two configurations can be seen in Figs. 14 and 15.

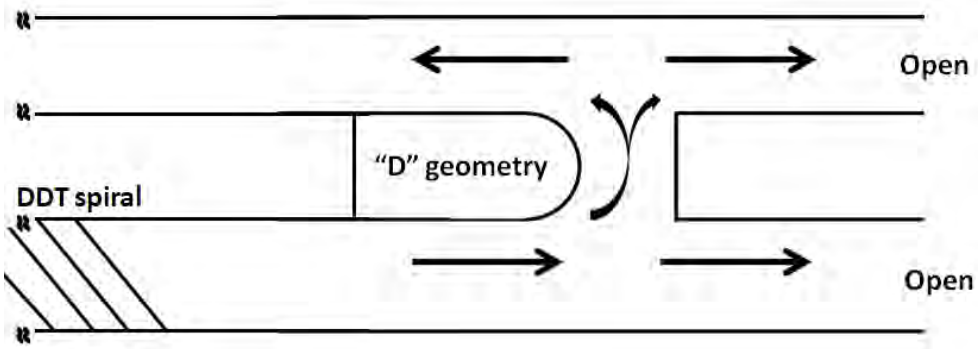

Figure 14. Two-tube tail-tail crossover configuration.

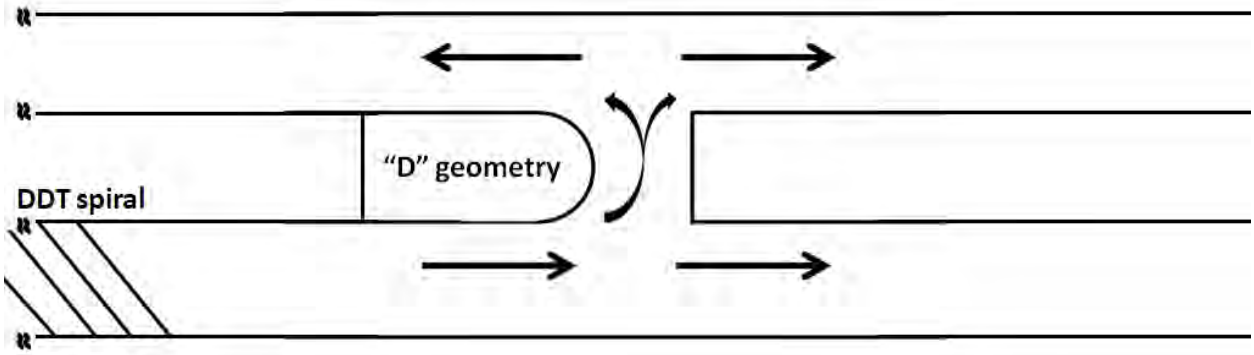

Figure 15. Two-tube mid-mid crossover configuration.

III. Methodology

1. Facility

Experiments were performed in the Detonation Engine Research Facility (DERF) of the Advanced Concepts Group within the Air Force Research Laboratory at Wright-Patterson Air Force Base, Ohio. This facility includes a test cell of over 750,000 cubic feet and a control room, surrounded by reinforced concrete, where systems are controlled remotely, testing is monitored and data acquisition systems are run.[22] The PDE in this study employs a General Motors Quad 4, Dual Overhead Cam cylinder head for filling the tubes with a fuel-air mixture. The engine head can be seen at the top of Fig. 16. The openings where the cylinder head would mount to four cylinders in an internal combustion engine are numbered sequentially from the left in Fig. 16. Also in Fig. 16, tubes 2 and 4 are shown mounted to the cylinder head in the two-tube configuration.

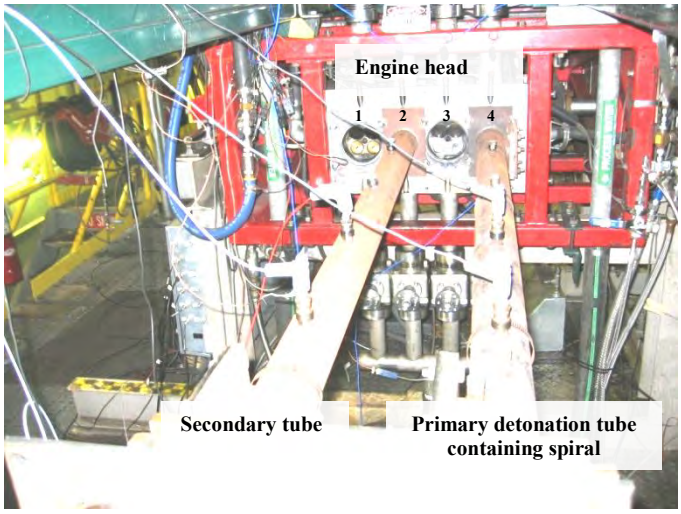

Figure 16. Two-tube setup looking forward from the tail end of the crossover section

Each detonation tube has two valves to fill the tube with a fuel-air mixture and two valves to purge the tube with air. The primary detonation tube uses a spark plug in the cylinder head to ignite the fuel-air mixture. The resulting deflagration accelerates across the DDT spiral and transitions to a detonation. The length of the DDT spiral varies according to the fuel being tested. The lengths of the DDT spirals used in this research for hydrogen, ethylene, and an n-alkane are 18, 24, and 48 in respectively. In Eq. (14) the definition of fill fraction helps to determine the volume of fuel-air mixture to be used. The ratio of the volume of fuel-air mixture to the volume of the detonation tube, less the DDT spiral volume, equals the desired fill fraction.

$$Fill\ fraction = \frac{Volume\ of\ fuel/air\ mixture}{Volume\ of\ detonation\ tube - Volume\ of\ DDT\ spiral} \tag{14}$$

Similarly, the volume of purge air to be used is determined by the desired purge fraction as defined in Eq. (15).

$$Purge\ fraction = \frac{Volume\ of\ purge\ air}{Volume\ of\ detonation\ tube - Volume\ of\ DDT\ spiral} \tag{15}$$

Equivalence ratio is defined in Eq. (16).

$$Equivalence\ Ratio = \frac{\frac{fuel}{air} ratio}{(\frac{fuel}{air} ratio)_{stoichiometric}} \tag{16}$$

Fill fraction, purge fraction, and equivalence ratio are all controlled remotely in the test facility control room. For each run, a fill fraction equal to unity and a purge fraction equal to 0.5 was used. The equivalence ratio was varied to find an equivalence ratio close to unity and which would consistently produce detonations for the given fuel and crossover location. For hydrogen and ethylene, equivalence ratios of unity and 1.3 respectively were used with both the tail-tail and mid-mid configurations. For the n-alkane, however, the mid-mid configuration more consistently produced detonations at a lower equivalence ratio than the tail-tail configuration as shown in Table 4.

Table 4. Equivalence ratio variation between fuels and test configurations

Fuel	Configuration	Equivalence Ratio
Hydrogen	Tail-Tail & Mid-Mid	1
Ethylene	Tail-Tail & Mid-Mid	1.3
n-Alkane	Tail-Tail	1.2
n-Alkane	Mid-Mid	1.1

2. Test configurations

The detonation tubes used in this research are 2 inches in diameter and 4 feet in length. While the PDE can handle up to four detonation tubes, this research used only two tubes. The primary detonation tube contained a DDT spiral. In Fig. 17, the primary detonation tube is connected to a crossover section that contains both a primary and secondary tube connected via a crossover duct. The width of the crossover duct was varied from 0.5 in to 2.5 in. The various test conditions used in this research are tabulated in Tables 8-10 in Section IV.

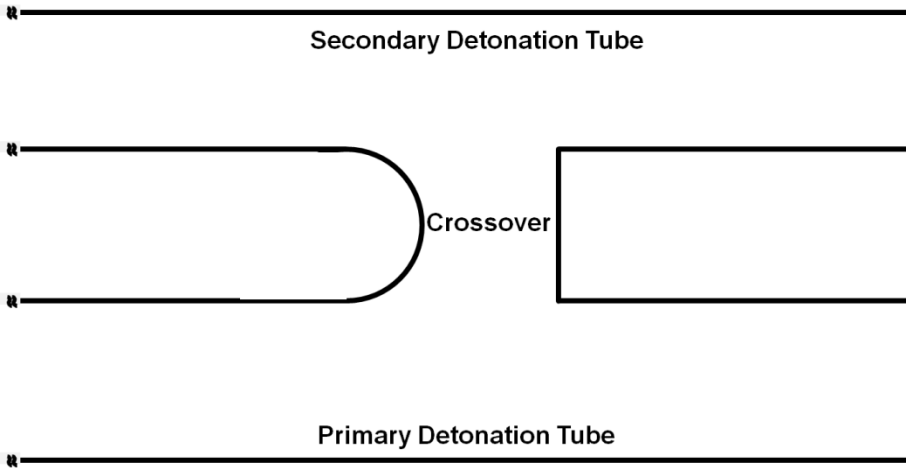

Figure 17. Diagram of crossover section

The two-tube configuration, as the name implies, has two detonation tubes extending from the engine head to the crossover section. The two-tube configuration in this research used tubes 2 and 4 as numbered in Fig. 16. Both tubes are fueled and purged from the head end.

Figure 18 shows the numbered ion probes (1-10) used for measuring detonation wave speeds.

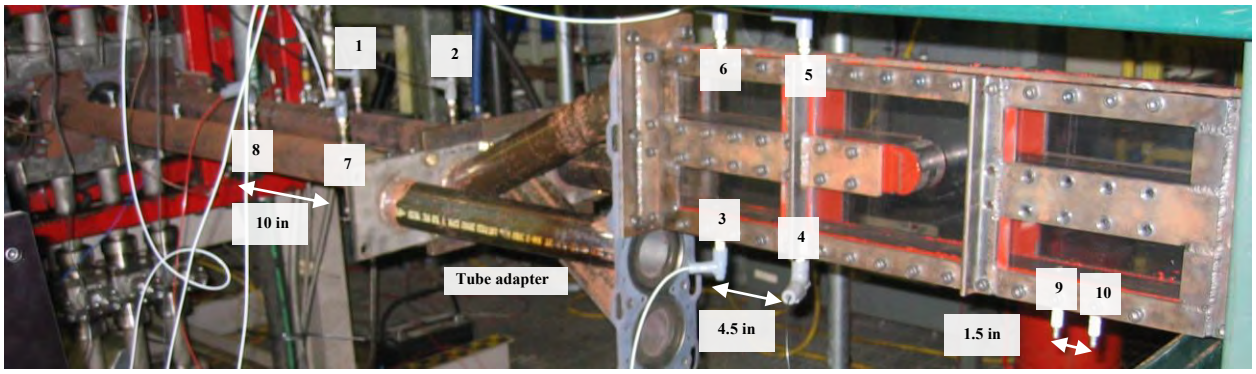

Figure 18. Two-tube configuration with engine head on the left side and crossover section on the right. Ion probes are numbered throughout.

The ion probes are spark plugs and are placed in pairs along the detonation tubes and around the crossover section. The ion probes detect the passing of a combustion wave and allow for calculation of the detonation wave speed. When the ion probes are charged with a voltage they

are utilized as capacitors, storing energy until a combustion wave passes. The ionized combustion wave closes the electrical circuit across the gap in the ion probe, thereby decreasing the circuit voltage. The drop in voltage indicates the passing of the combustion wave. The voltage drop and the time at which the voltage drops are recorded by the data acquisition system. The detonation wave speeds are calculated from the distance between paired ion probes divided by the difference in passing time:[9]

$$Detonation\ wave\ speed = \frac{\Delta x_{1-2}}{\Delta t_{1-2}} \tag{17}$$

The resulting speed is compared with V_{CJ} to determine if the combustion wave is traveling fast enough to be considered an actual detonation for the fuel of interest.[14] It can thus be determined if a detonation has propagated to a region of interest within the test section. This research used V_{CJ} equal to the values in Table 5.

Table 5. V_{CJ} for fuels of interest[23]

Fuel	V_{CJ} (m/s)
Hydrogen	1971
Ethylene	1850
n-Alkane	~1750

The maximum number of available ion probe channels on the data acquisition system is 12. One channel records the spark used to ignite the fuel-air mixture. Ion probe drops follow the spark signal in time (Fig. 19). The observer uses the recorded spark signal as a benchmark in time to help identify at what time to begin looking for ion probe voltage drops. If no ion probe drops are seen between spark signals, no combustion wave passing was recorded. Four sparks were fired at 10 Hz for each run in order to observe multiple detonations without allowing too

many detonations to melt the polycarbonate windows in the crossover section used for Schlieren photography.

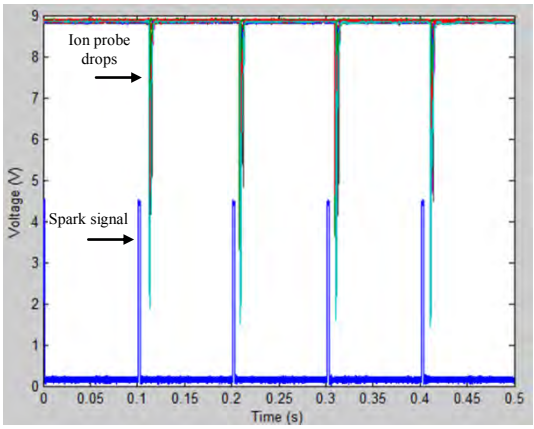

Figure 19. PDE spark signals and ion probe voltage drops

The remaining 11 channels were divided into five pairs, as seen in Fig. 18. Also seen in Fig. 18 are the distances between pairs of ion probes. Ten inches separate ion probe pairs on the detonation tubes. There are 4.5 in between ion probe pairs on the half of the crossover section closest to the engine head. There are 1.5 in between ion probe pairs on the half of the crossover section closest to the tail end.

The two-tube tests included the crossover in the tail-tail location and in the mid-mid location. Figure 20 shows the mid-mid location; the engine head is outside the picture to the left, and the tail end of both tubes is on the far right side of the picture.

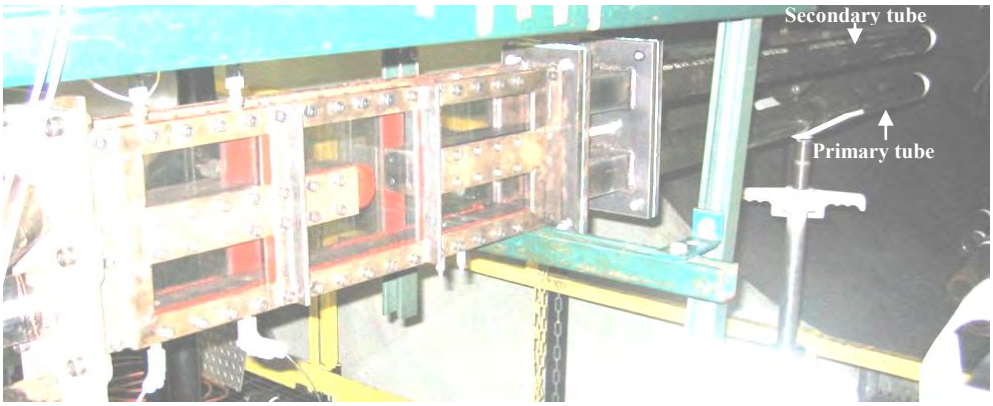

Figure 20. Two-tube setup with crossover at mid-mid location

The two-tube configuration uses a tube adapter shown in Fig. 18 to reorient the flow from the horizontal detonation tubes into the vertical crossover duct. This reorientation of the flow enables the observer to use Schlieren photography through the walls of the crossover section to see the detonation wave.

The crossover section is enclosed by 0.5 inch-thick polycarbonate on either side to allow Schlieren photography through the crossover duct. Schlieren photography is used for two reasons. First, Schlieren photography provides exceptional flow visualization.[24] Schlieren helps in identifying a combined, or coupled, shock and combustion front, as seen in Fig. 21 with hydrogen and air. Second, Schlieren photography helps in secondarily verifying detonation wave speed.[7] From two consecutive digital images, the number of photo pixels that the wave moves is noted. The pixel spacing is computed from a known distance (e.g., the distance between detonation tubes). The calculated wave movement in meters is divided by the frame time in seconds to find the wave speed as in Eq. (17).

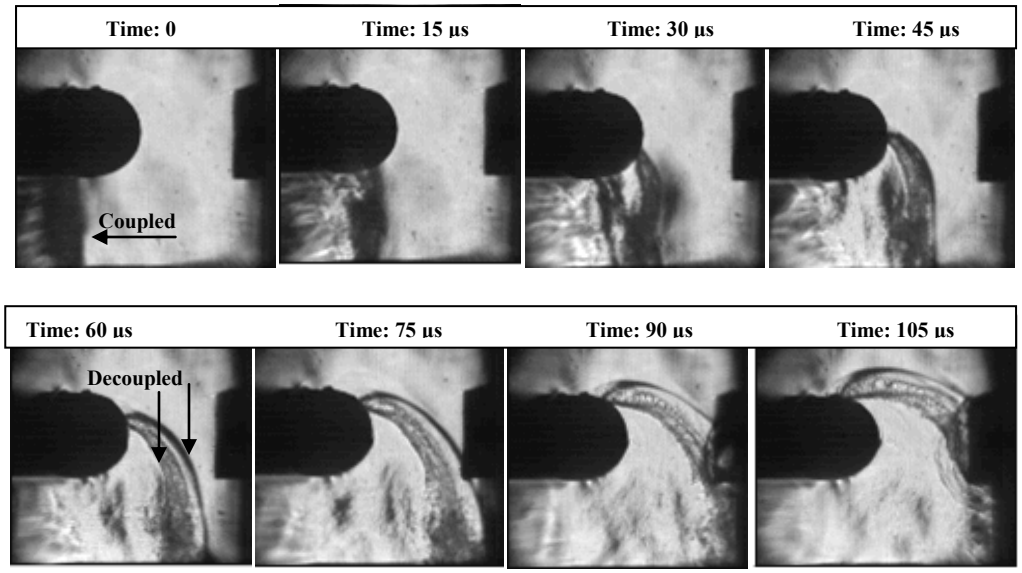

Figure 21. Schlieren photography illustrating the detonation of hydrogen and air at 15 microsecond intervals, sequentially from left to right, top to bottom. The shock and combustion fronts decouple through the crossover duct.

As seen in Fig. 21, the left-to-right running detonation in the primary tube diffracts at the crossover duct causing the shock wave and combustion front to begin decoupling. With 2 in diameter detonation tubes and with the fuels and cell widths listed in Table 3, this is anticipated based on Eq. (13). After the subcritical detonation diffracts into the crossover duct, the detonation is not expected to reinitiate naturally, as discussed in regards to Fig. 9. Nielsen found the "D" geometry consistently reinitiated in the crossover duct with a hydrogen-air mixture as the shock wave and combustion front reflected off the flat portion of the geometry facing the flow and again reflected off the top of the secondary detonation tube.[7] These reflections were sufficient to recouple the shock wave and combustion front and reinitiate the detonation. Ideally, this reinitiation occurs in a short span of tube in order to effectively produce thrust in the secondary tube.

To determine whether detonations exist upstream and downstream of the crossover duct in the primary detonation tube, and to help determine if detonations reinitiate in the secondary tube,

there are three regions of interest within the PDE system. In Fig. 22, Region I is prior to the crossover where DDT occurs. Region II is in the primary tube downstream of the crossover at the tail end of the tube. Region III is in the secondary detonation tube where a detonation reinitiation should occur after decoupling in the crossover. The Schlieren field-of-view captures Regions I and III only.

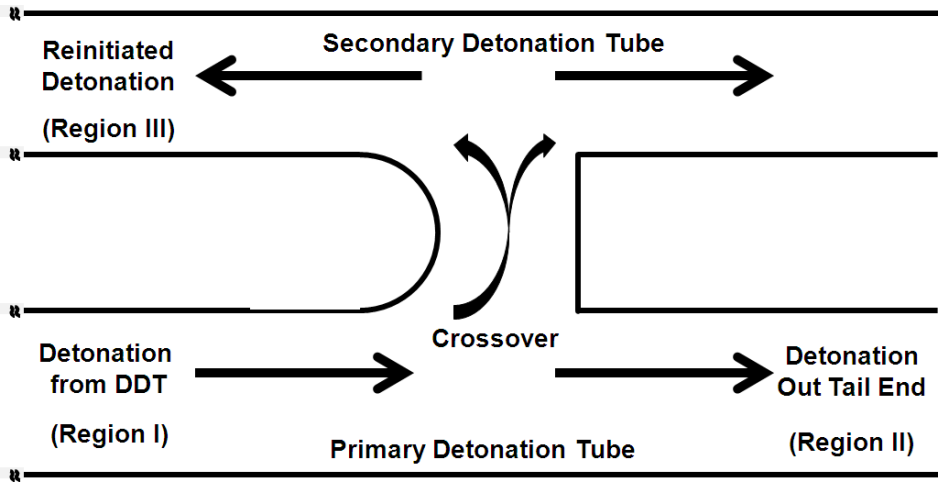

Figure 22. The detonation regions of interest within the crossover section.

3. Uncertainty

The uncertainty of a measured value quantifies the dispersion of the values measured for a particular parameter. For a given probability, the actual value of the measured parameter lies within the uncertainty with a certain confidence.[24] The two types of uncertainty are bias and precision. Bias uncertainty, B, is constant and is calculated as the root sum square of the estimated sources of bias:[24]

$$B = \sqrt{\sum_{k=1}^{K} B_k^2} \tag{18}$$

Precision uncertainty, p, varies randomly with repeated measurements of the same parameter. When repeated measurements were available, the precision uncertainty was calculated within 95% probability using the standard deviation, σ:[24]

$$p_k = 2\sigma_k \tag{19}$$

The overall uncertainty is equal to the root sum square of the bias and precision uncertainties:

$$U = \sqrt{B^2 + p^2} \tag{20}$$

For this research, an uncertainty analysis was conducted for the detonation wave speeds measured with the ion probes and the Schlieren photographs. For the ion probe measurements, the two sources of bias uncertainty are the location of the ion probe and the arrival time of the detonation wave.[9] The bias uncertainty in location, $B_{\Delta x}$, is 2.5 x 10^{-4} in based on the fact that the holes for the ion probes were drilled on a mill with accuracy to 5.0 x 10^{-4} in.[7] The bias uncertainty in arrival time, $B_{\Delta t}$, has two sources of bias uncertainty: ion probe response time and data sampling rate. As shown by Hopper, the ion probe response time is 0.1 μs.[9] The bias uncertainty in ion probe response time is therefore half the response time, or ±0.05 μs.[9] The data

sampling rate is 1 MHz. The bias uncertainty in the data sampling rate is therefore ±0.5 μs. Using Eq. (18), $B_{\Delta t}$ is estimated to be 0.502 μs.[9]

The only source of precision uncertainty that was considered for the ion probe measurements was the arrival time of the detonation wave. The precision uncertainty in the arrival time of the detonation wave, $p_{\Delta t}$, is dominated by the three dimensional effects of the detonation wave and was calculated by Hopper to be ±2.5 μs.[9] For the ion probe measurement uncertainty calculation, the precision uncertainty in location, $p_{\Delta x}$, is zero.

The overall bias and precision uncertainty in the wave speed are calculated as shown by Hopper using Eqs. (21) and (22).[9]

$$B_{ws} = \sqrt{\left(\frac{B_{\Delta x}}{\Delta t}\right)^2 + \left(\frac{\Delta x}{\Delta t^2} B_{\Delta t}\right)^2} \qquad 21$$

$$p_{ws} = \sqrt{\left(\frac{p_{\Delta x}}{\Delta t}\right)^2 + \left(\frac{\Delta x}{\Delta t^2} p_{\Delta t}\right)^2} \qquad 22$$

The values for Δx vary based on the distance between the ion probe pair of interest. The values of Δt vary based on the V_{CJ} of the fuel of interest. The calculated values for B_{ws}, p_{ws}, and U_{ws} are tabulated in Table 6. As seen in Table 6, wave speed uncertainty increases as the distance between ion probe pairs decreases.

Table 6. Bias, precision, and overall uncertainty for detonation wave speeds of multiple fuels and multiple ion probe pairs

Distance between ion probes, Δx (in)	Bias uncertainty, B_{ws} (m/s)			Precision uncertainty, P_{ws} (m/s)			Overall uncertainty, U_{ws} (m/s)		
	Hydrogen	Ethylene	n-Alkane	Hydrogen	Ethylene	n-Alkane	Hydrogen	Ethylene	n-Alkane
1.5	54.64	45.03	41.17	263.85	215.99	196.80	269.45	220.63	201.06
4.5	17.61	15.48	13.72	84.94	74.34	65.60	86.75	75.93	67.02
10.0	7.79	6.75	5.91	37.57	32.40	28.22	39.37	33.09	28.84

The following uncertainty analysis for the detonation wave speeds measured with the Schlieren photography is based on the analysis presented by Nielsen.[7] $B_{\Delta x}$ is 1 pixel due to the difficulty determining exactly where the front of the detonation wave is in a given photograph. $B_{\Delta t}$ is ±1 μs due to the uncertainty of the time between frames. $p_{\Delta x}$ is 0.5 pixels due to the human error associated with selecting the correct pixel. The photography software showed no precision errors after reviewing the elapsed time between 100 frames. Therefore, $p_{\Delta t}$ is assumed to be zero. Using Eqs. (20) - (22) the bias, precision and overall uncertainties are calculated and tabulated in Table 7.

Table 7. Bias, precision, and overall uncertainty for detonation wave speeds of multiple fuels using Schlieren photography

Bias uncertainty, B_{ws} (m/s)			Precision uncertainty, P_{ws} (m/s)			Overall uncertainty, U_{ws} (m/s)		
Hydrogen	Ethylene	n-Alkane	Hydrogen	Ethylene	n-Alkane	Hydrogen	Ethylene	n-Alkane
145.11	137.28	133.41	35.27	35.27	35.27	149.33	141.73	137.99

As seen in Table 7, the uncertainty of the Schlieren photography in measuring detonation wave speeds is high. This is not unexpected. Schlieren photography is excellent for flow visualization, and is primarily used in this research to confirm that shock waves and combustion fronts are coupled. Schlieren photography was not primarily used for measuring speed. Due to the high uncertainty in wave speeds from the Schlieren photography, the ion probe data is used first, provided that voltage drops across the ion probes are noted for a given run. If one or both

ion probes in a pair does not show a voltage drop for a given run, the Schlieren photography is used secondarily to confirm that a detonation is present by examining the photographs for shock waves coupled to combustion fronts and then to measure wave speed. If only one ion probe shows a voltage drop typical of a detonation wave but the ion probe pair is not within the Schlieren field of view, the detonation wave is assumed, although no detonation wave speed is recorded for that region. Figure 23 is a flowchart showing the conditions for using either ion probe data or Schlieren photography to calculate wave speeds.

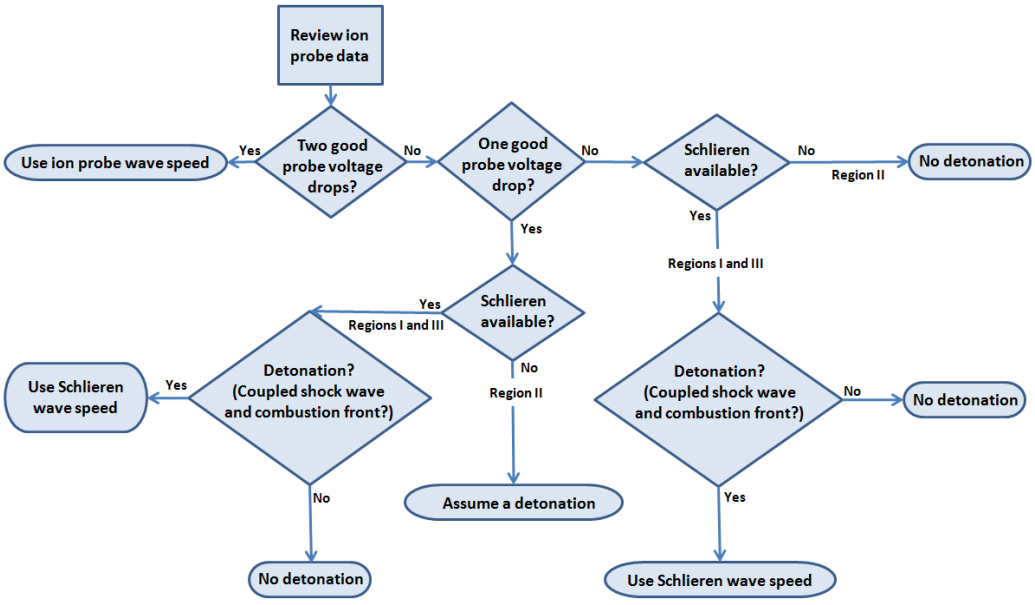

Figure 23. Wave speed data flowchart

IV. Analysis and Results

1. Test configuration

The two-tube tests include the crossover duct filled and purged by both the primary and secondary detonation tubes, a configuration that can be directly applied to a realistic operational application of detonation branching. Both the tail-tail and mid-mid configurations were examined for each fuel-air mixture.

Each test shown in the following tables consisted of four sparks fired at 10 Hz at the indicated crossover width. Firing four sparks at 10 Hz allowed multiple detonations to be observed during each run without concern for the detonations melting the polycarbonate windows used for Schlieren photography. A successful detonation was considered approximately 70% of V_{CJ} or greater to allow for some detonation wavespeed variation from the theoretical V_{CJ} without considering the choked flame in the combustion products as a detonation. The average successful detonation wave speed over the four sparks in each of the three regions of interest is shown in Tables 8-10. Appendix A includes wavespeeds for each of the three regions after each spark was fired.

2. Hydrogen tests

Table 8 shows the tabulated results for the hydrogen-air mixture in both the tail-tail and mid-mid configurations at varying crossover widths. Detonation wave speeds are also shown nondimensionalized by V_{CJ}. Ion probe number 10 (reference Fig. 18) in Region II did not register voltage drops during the hydrogen tests. The voltage drops across ion probe number 9 in Region II were indicative of a detonation. In accordance with the wave speed data flowchart (Fig. 23) these detonations were assumed to have occurred, although no Region II wave speed is recorded.

Hydrogen was successful in producing detonations in all three regions in both the tail-tail and mid-mid configurations, as expected. Hydrogen detonation velocities have been recorded within 30% of stoichiometric V_{CJ} at equivalence ratios as low as 0.4.[23] The 2.5 in crossover width mid-mid configuration test was repeated because the first test produced only two detonations across the four sparks. The second test produced three detonations.

Table 8. Hydrogen test results

Fuel	# Tubes	Spiral Length (in)	Equivalence Ratio	Crossover width (in)	Config	Detonation Wave Speed (m/s)		Nondimensional Detonation Wave Speed	
						Region I	Region III	Region I	Region III
Hydrogen	2	18	1.0	2.50	Tail-Tail	1902	2305	.965	1.17
Hydrogen	2	18	1.0	2.25	Tail-Tail	1909	2337	.969	1.19
Hydrogen	2	18	1.0	2.00	Tail-Tail	1902	2247	.965	1.14
Hydrogen	2	18	1.0	1.75	Tail-Tail	1902	2263	.965	1.15
Hydrogen	2	18	1.0	1.50	Tail-Tail	1884	2284	.956	1.16
Hydrogen	2	18	1.0	0.50	Tail-Tail	1902	2511	.965	1.27
Hydrogen	2	18	1.0	2.50	Mid-Mid	1916	2156	.972	1.09
Hydrogen	2	18	1.0	2.50	Mid-Mid	1909	2244	.969	1.14
Hydrogen	2	18	1.0	2.25	Mid-Mid	1891	2213	.959	1.12
Hydrogen	2	18	1.0	2.00	Mid-Mid	1909	2252	.969	1.14
Hydrogen	2	18	1.0	1.75	Mid-Mid	1891	2333	.959	1.18
Hydrogen	2	18	1.0	1.50	Mid-Mid	1905	2268	.967	1.15
Hydrogen	2	18	1.0	0.50	Mid-Mid	1898	2587	.963	1.31

In Fig. 24, a hydrogen detonation is shown in a tail-tail configuration with a 2.5 in crossover width. Frame 1 shows the coupled shock wave and combustion front in Region I. The planar detonation in Region I is subcritical because the height of the planar channel in Region I (50.8 mm) is less than the critical tube diameter for hydrogen (80 mm); therefore, the detonation

diffracts as it enters the crossover duct, decoupling the shock wave and combustion front. The decoupled shock wave and combustion front are visible in frame 7 of Fig. 24. As the shock wave and combustion front strike the opposing flat face of the crossover geometry in frame 8, they are recoupled. The flash of visible light in frame 8 and subsequent detonation wave propagation in frame 9 indicate the strong reflection and detonation reinitiation respectively. The reinitiated detonation propagates spherically as if unconfined and quickly decouples as seen in frame 11. In frame 12, the decoupled shock wave and combustion front are recoupled again as they strike the top of the secondary detonation tube with a strong reflection. The reinitiated detonation wave in the secondary detonation tube interacts with the transverse shock wave present, enabling the detonation to propagate and exit the Schlieren field of view, as seen in frames 13-17. More hydrogen detonation photographs are located in Appendix B.

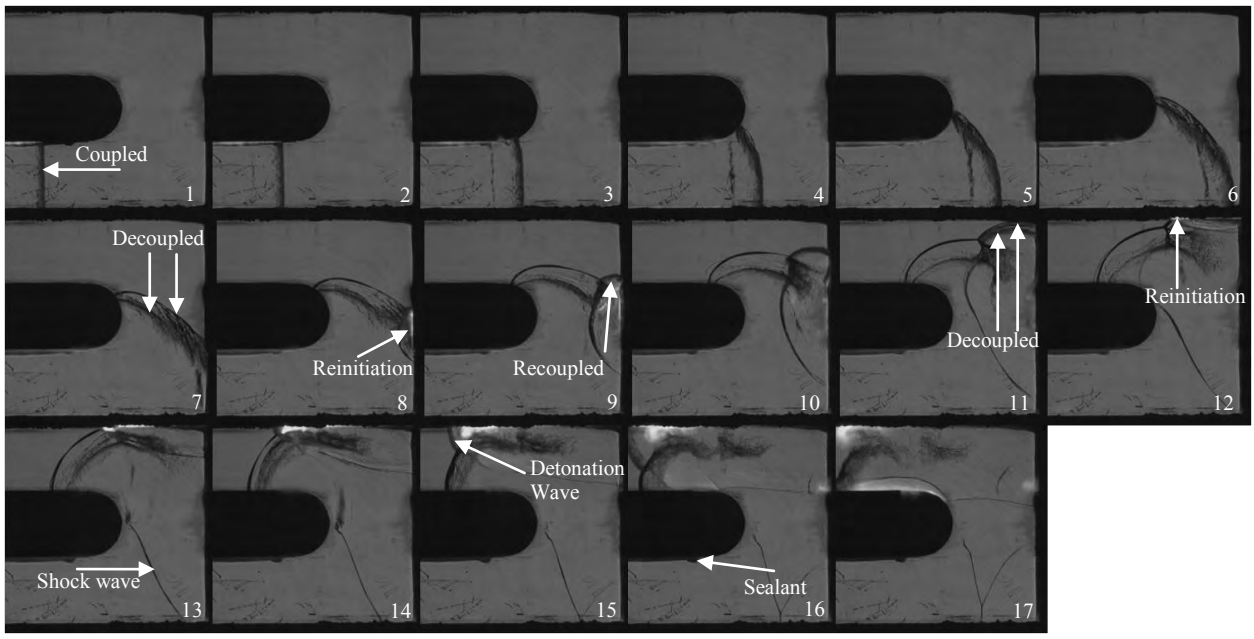

Figure 24. Detonation of hydrogen and air in a tail-tail configuration with 2.5 in crossover width, sequentially from left to right, top to bottom. The detonation resulted in a successful Region III reinitiation.

Figure 24 also shows several things that recur in many of the detonation photographs. After the detonation reinitiates in the crossover duct in frame 8, the shock wave and combustion front recouple and propagate into the secondary detonation tube as labeled in frame 9. The lower portion of the spherically propagating shock wave travels back into the primary detonation tube, starting in frame 9, where it reflects off the bottom of the tube in frame 15. The shock wave is visible in frames 9-17 and labeled in frame 13. Also visible in the photographs, is some high temperature sealant that has spread into the Schlieren field of view. The sealant is labeled in frame 16. Figure 25 shows an example of some sealant that would be visible within the Schlieren field of view. The sealant was not observed to noticeably affect the flow as the effect was confined to the edges and did not significantly alter the bulk flow.

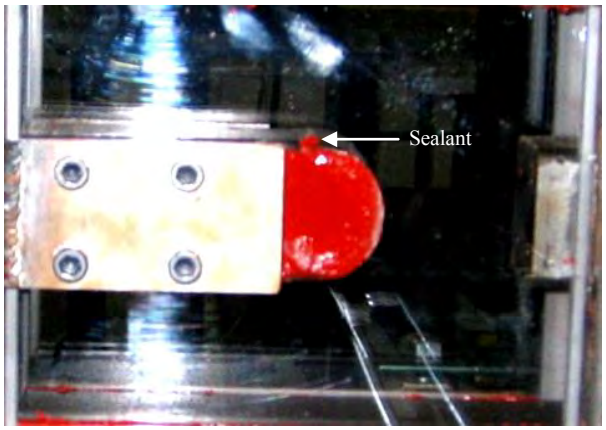

Figure 25. High temperature sealant within the Schlieren field of view. The sealant adheres the polycarbonate to the crossover geometry and keeps the high pressure flow from leaking around the crossover geometry.

3. Ethylene tests

The ethylene test results are tabulated in Table 9 including detonation wave speeds nondimensionalized by V_{CJ}. As seen in Table 9, the first two tests were run at crossover widths of 2.5 in and equivalence ratio of 1.2. During these tests there were no successful detonations in

Region II as indicated by the lack of detonation wave speed in Table 9. Holding the crossover width at 2.5 in, the equivalence ratio was increased to 1.3. The 2.5 in crossver width tests were repeated three times with the increased equivalence ratio. Successful Region II detonations were observed during two of the three tests at 2.5 in and for all subsequent crossover widths. The diffracting subcritical detonation may have had more difficulty reinitiating across a wider crossover duct from Region I to Region II particularly at the lower equivalence ratio. As seen in Table 9, when the crossover width is decreased below 2.5 in and when the equivalence ratio is increased to 1.3, the detonation successfully transitions from Region I to Region II.

The 1.5 in mid-mid configuration test was repeated because the first test produced only one detonation across four sparks. The second test produced two detonations. The ethylene tests run in the tail-tail and mid-mid configurations with the crossover width at 0.5 in did not produce any successful Region III detonations. Ethylene detonations with a crossover width of 0.5 in were not able to reinitiate in the secondary detonation tube because the reinitiation was limited to the crossover duct by the small crossover width as shown later.

Table 9. Ethylene test results

Fuel	# Tubes	Spiral Length (in)	Equivalence Ratio	Crossover width (in)	Config	Detonation Wave Speed (m/s)			Nondimensional Detonation Wave Speed		
						Region I	Region II	Region III	Region I	Region II	Region III
Ethylene	2	24	1.2	2.50	Tail-Tail	2081	-	2099	1.12	-	1.13
Ethylene	2	24	1.2	2.50	Tail-Tail	1940	-	1903	1.05	-	1.03
Ethylene	2	24	1.3	2.50	Tail-Tail	1913	2437	2125	1.03	1.32	1.15
Ethylene	2	24	1.3	2.50	Tail-Tail	2032	-	2116	1.10	-	1.14
Ethylene	2	24	1.3	2.50	Tail-Tail	2078	2447	2303	1.12	1.32	1.24
Ethylene	2	24	1.3	2.25	Tail-Tail	2006	2342	2152	1.08	1.27	1.16
Ethylene	2	24	1.3	2.00	Tail-Tail	1982	2064	2170	1.07	1.12	1.17
Ethylene	2	24	1.3	1.50	Tail-Tail	1880	2120	2018	1.02	1.15	1.09
Ethylene	2	24	1.3	0.50	Tail-Tail	2063	1833	-	1.12	.991	-
Ethylene	2	24	1.3	2.50	Mid-Mid	1969	2439	2174	1.06	1.32	1.18
Ethylene	2	24	1.3	2.25	Mid-Mid	1925	2231	2171	1.04	1.21	1.17
Ethylene	2	24	1.3	2.00	Mid-Mid	1681	2123	2208	.909	1.15	1.19
Ethylene	2	24	1.3	1.75	Mid-Mid	1917	2123	2144	1.04	1.15	1.16
Ethylene	2	24	1.3	1.50	Mid-Mid	1502	2005	1895	.812	1.08	1.02
Ethylene	2	24	1.3	1.50	Mid-Mid	1947	2349	2152	1.05	1.27	1.16
Ethylene	2	24	1.3	0.50	Mid-Mid	1954	1826	-	1.06	.987	-

Figure 26 shows an ethylene detonation in a tail-tail configuration with a 2.5 in crossover width. More visible light is observed in the combustion of ethylene as compared to hydrogen. The ethylene detonation is initially coupled, then diffracts into the crossover duct and is labeled as decoupled in frame 7. Strong reflections and subsequent detonation reinitiations within the crossover tube and at the top of the secondary detonation tube are labeled in frames 9 and 13 respectively. Frame 17 shows the detonation wave as it exits the Schlieren field of view. The detonation that reinitiated at the top of the secondary detonation tube in frame 13 reflects

strongly in frame 17 off the bottom of the secondary detonation tube. The reflection is labeled in frame 18. Figure 26 also shows a common image in many of the detonation photographs. Burn marks are left on the polycarbonate where the crossover geometry and polycarbonate meet. The burn marks are visible in the Schlieren field of view when the crossover width is readjusted to a wider setting. The visible burn marks at each crossover width setting of previous tests are labled in frame 1.

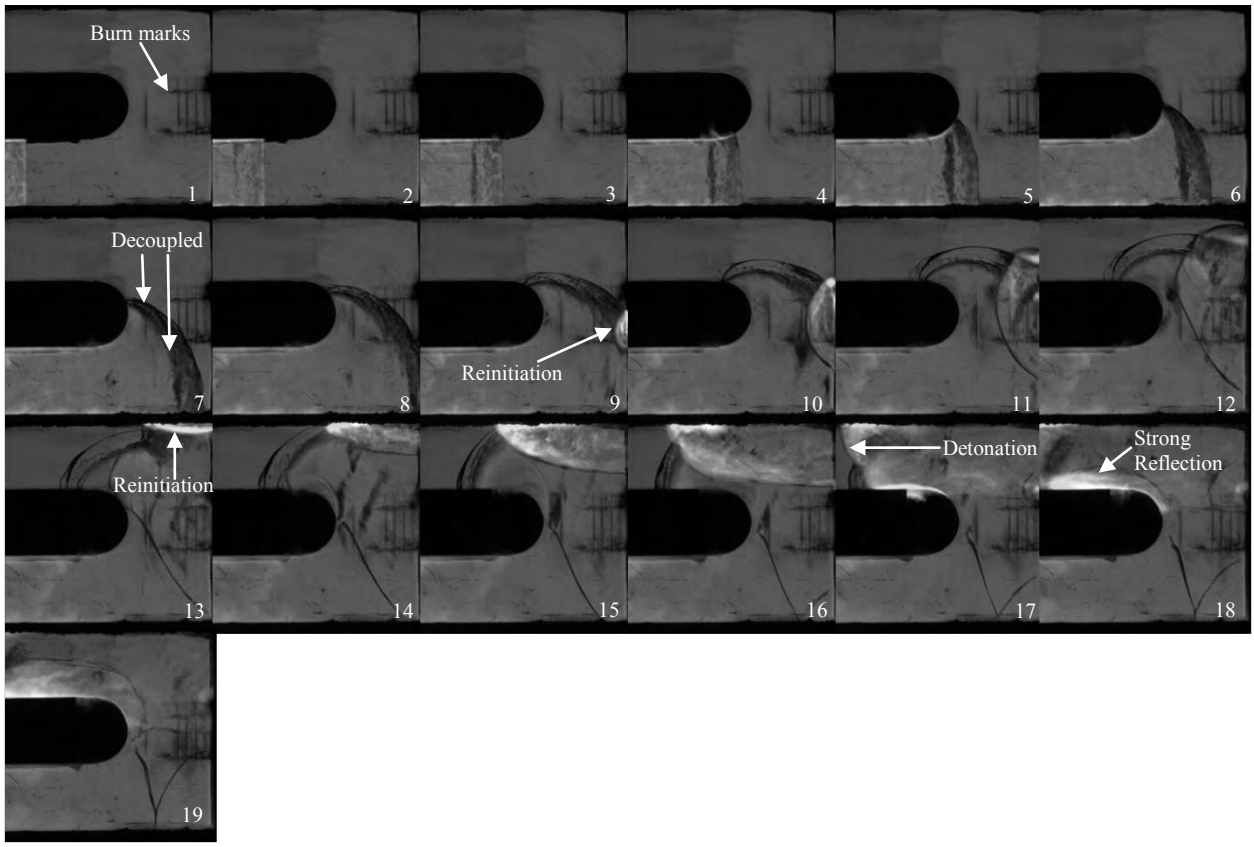

Figure 26. Detonation of ethylene and air in a tail-tail configuration with 2.5 in crossover width, sequentially from left to right, top to bottom. The detonation resulted in a successful Region III reinitiation.

Figure 27 shows an ethylene detonation in a tail-tail configuration with a 0.5 in crossover width. All ethylene detonations with the 0.5 in crossover width failed to reinitiate in Region III

as noted inTable 9. Frame 5 shows the detonation reinitiation in the crossover width. Unlike reinitiations at larger crossover widths, the reinitiation at the 0.5 in crossover width occurs much lower on the crossover geometry. The reinitiation reflects back off the "D" geometry in frame 6. It appears that the detonation emerging from the crossover width into the secondary detonation tube in frame 7 is unable to reinitiate at the top of the secondary detonation tube in frames 11 and 12. The strong reflection and reinitiation were limited to the crossover duct by the smaller crossover width. A deflagration propagates through Region III and exits the Schlieren field of view. The deflagration wave speed is noted in Table A-2 in Appendix A. More ethylene detonation photographs are located in Appendix C.

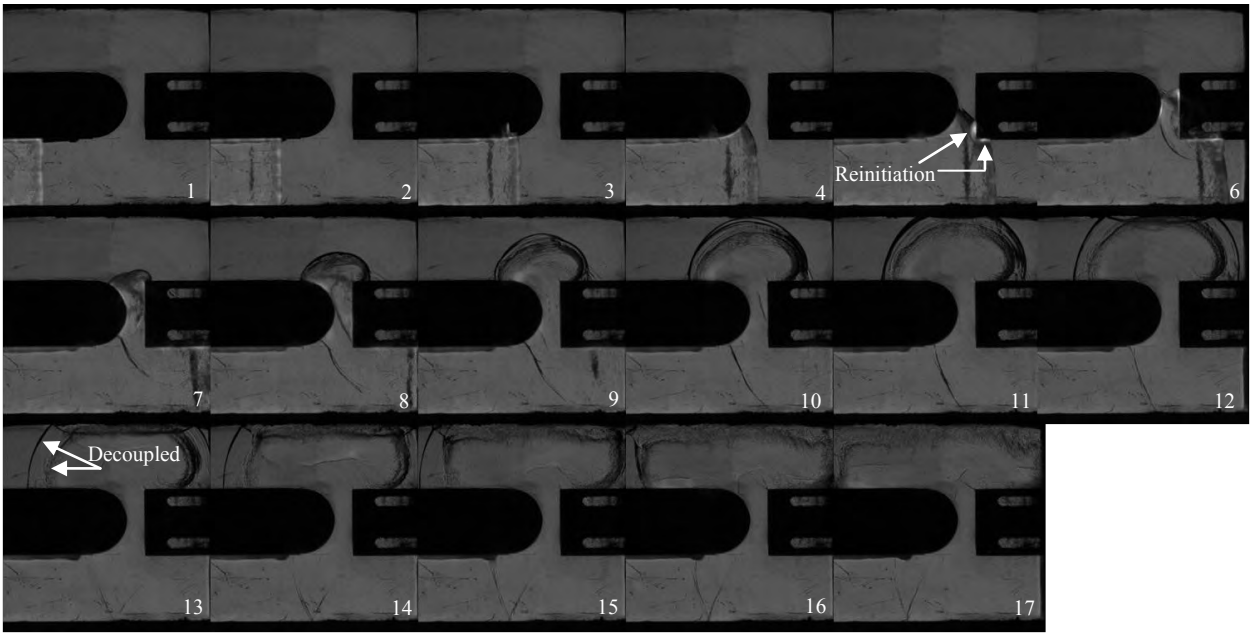

Figure 27. Detonation of ethylene and air in a tail-tail configuration with 0.5 in crossover width, sequentially from left to right, top to bottom. The small crossover width limits the reinitiation to the crossover duct. The detonation resulted in a failed Region III reinitiation.

4. n-Alkane tests

The n-alkane test results are tabulated in Table 10 including detonation wave speeds nondimensionalized by V_{CJ}. The voltage drops across ion probe number 9 (reference Fig. 18) in Region II were indicative of a detonation, although ion probe number 10 did not register voltage drops during the n-alkane tests. In accordance with the wave speed data flowchart (Fig. 23) these detonations were assumed to have occurred although no Region II wave speed was recorded.

The n-alkane Region I detonation wavespeeds in Table 10 are lower than V_{CJ} for all crossover widths in both the tail-tail and mid-mid configurations with the exception of the tail-tail configuration with 2.5 in and 1.5 in crossover widths. The lower wavespeeds may be an indication in Region I that the n-alkane is taking more distance to transition to a detonation and has not fully accelerated to V_{CJ} by Region I due to its large cell size.[12]

No successful Region III detonations were observed with the 0.5 in crossover in either the tail-tail or the mid-mid configuration. Similar to ethylene, the n-alkane detonations do not transition through the crossover when the crossover width is decreased to 0.5 in. The reinitiation is reflected off the crossover geometry within the smaller crossover duct and does not emerge into Region III as shown later.

The tail-tail configuration produced detonations at an equivalence ratio of 1.2 while the mid-mid configuration produced detonations more consistently at an equivalence ratio of 1.1. This may be an indication that the mid-mid configuration is able to run at a leaner equivalence ratio because it is not as affected by entrainment of the ambient air as the tail-tail configuration, however, this research did not extensively examine equivalence ratio variation.

Table 10. n-Alkane test results

Fuel	# Tubes	Spiral Length (in)	Equivalence Ratio	Crossover width (in)	Config	Detonation Wave Speed (m/s)		Nondimensional Detonation Wave Speed	
						Region I	Region III	Region I	Region III
n-Alkane	2	48	1.2	2.50	Tail-Tail	1797	2311	1.03	1.32
n-Alkane	2	48	1.2	2.25	Tail-Tail	1364	1668	.779	.953
n-Alkane	2	48	1.2	2.00	Tail-Tail	1502	2077	.858	1.19
n-Alkane	2	48	1.2	1.50	Tail-Tail	2059	1840	1.18	1.05
n-Alkane	2	48	1.2	0.50	Tail-Tail	1566	-	.895	-
n-Alkane	2	48	1.1	2.25	Mid-Mid	1599	1545	.914	.883
n-Alkane	2	48	1.1	2.00	Mid-Mid	1269	1797	.725	1.03
n-Alkane	2	48	1.1	1.75	Mid-Mid	1685	2253	.963	1.29
n-Alkane	2	48	1.1	1.50	Mid-Mid	1664	1544	.951	.882
n-Alkane	2	48	1.1	2.50	Mid-Mid	1406	1642	.803	.938
n-Alkane	2	48	1.1	0.50	Mid-Mid	1264	-	.722	-

Like the hydrogen and ethylene tests, the n-alkane tests were initially run with the DDT spiral and spark in tube 4 (reference Fig. 16). There was a problem, however, with one of the valves closing in tube 4, and detonations would not initiate in tube 4. The DDT spiral and spark were switched into tube 2 in order to remedy the initiation failures. As a result, the n-alkane detonation photographs depict the primary detonation tube on the top and the secondary detonation tube on the bottom. The detonations proceed from top to bottom as opposed to proceeding from bottom to top as with hydrogen and ethylene. Additionally, oil was sprayed through the leaking valve in tube 4 and covered the polycarbonate window. The Schlieren light source must shine through the oil coated polycarbonate and as a result, the field of view in the Schlieren photographs is darker for the n-alkane detonations. The overall quality of the n-alkane

photographs is lower. More visible light is observed in the combustion of n-alkane as compared to hydrogen and ethylene.

Figure 28 shows an n-alkane detonation in the tail-tail configuration with 2.5 in crossover width. The shock wave and combustion front decouple in frame 6. Strong reflections and detonation reinitiations occur in frame 9 in the crossover width and in frame 13 at the bottom of the secondary detonation tube. The detonation exits the Schlieren field of view in frames 17 and 18.

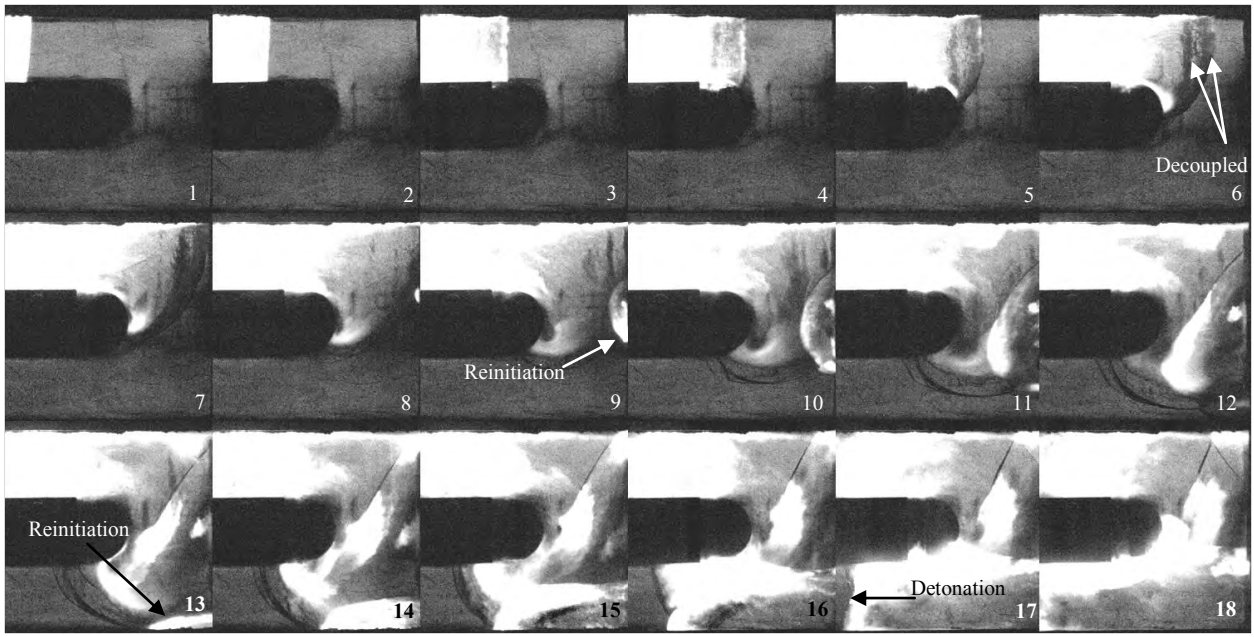

Figure 28. Detonation of an n-alkane and air in a tail-tail configuration with 2.5 in crossover width, sequentially from left to right, top to bottom. The detonation resulted in a successful Region III reinitiation.

Figure 29 shows a decoupled n-alkane shock wave and combustion front in Region I (labeled in frame 1) that successfully reinitiates in Region III. It appears in frames 1-6 that the shock wave and combustion front are coupling as the distance between the two decreases. The coupling is incomplete in frame 6 as the wave diffracts into the crossover duct. The strong reflections in frame 10 in the crossover duct and in frame 15 at the bottom of the secondary

detonation tube successfully initiate a detonation in Region III without a successful detonation in Region I. The reinitiation in frame 11 likely helped recouple the detonation in Region II, although there is no video of Region II to show how the detonation recoupled. The failed Region I detonation may be the result of the n-alkane deflagration taking more distance to transition to a detonation. While the n-alkane deflagration was not completely transitioned to a detonation in Region I, it likely would have completely transitioned given more distance before the crossover duct. The reinitiations in frames 10, 11 and 15 completed the transition resulting in detonations in Regions II and III.

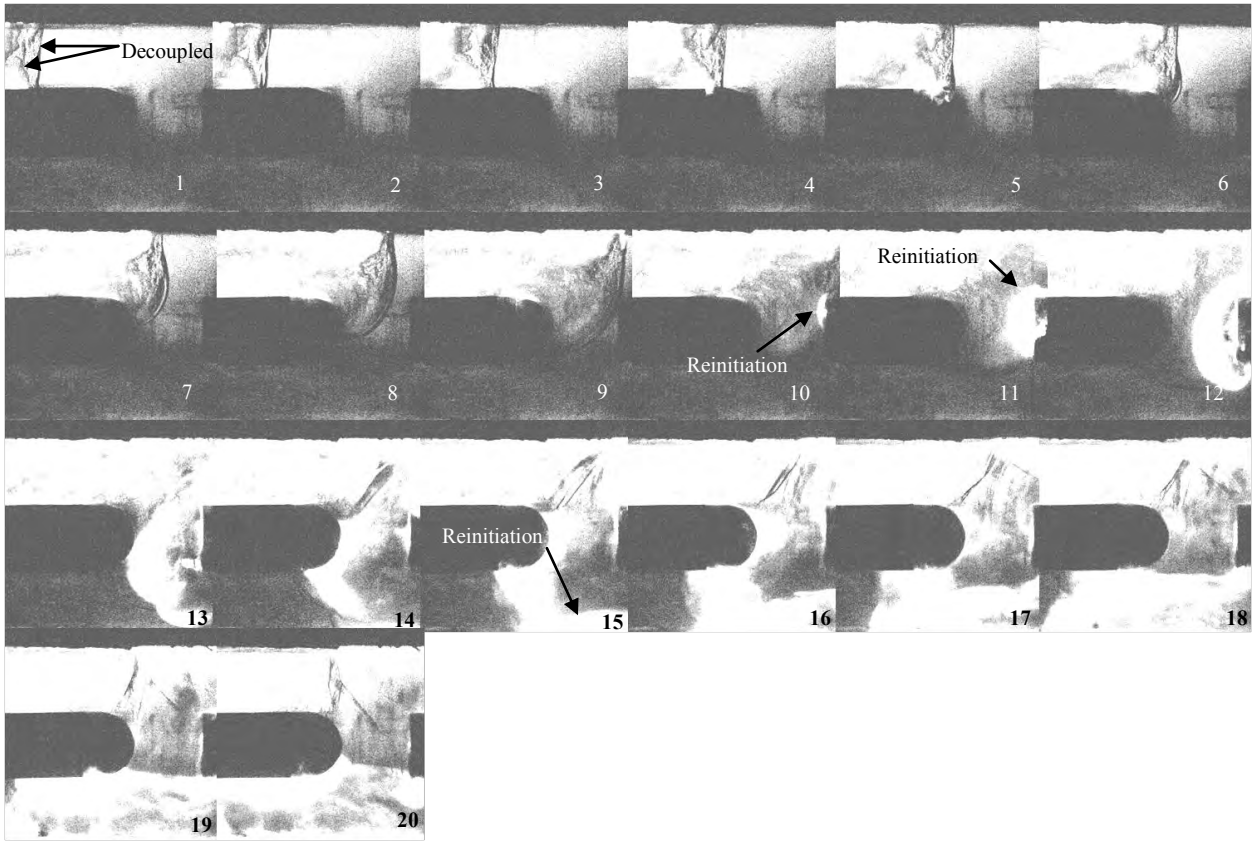

Figure 29. Detonation of an n-alkane and air in a mid-mid configuration with 2.0 in crossover width, sequentially from left to right, top to bottom. A failed Region I detonation enters in frame 1 and successfully reinitiates in Region III.

The n-alkane detonations fail to reinitiate in Region III with the 0.5 in crossover width as shown in Table 10. Figure 30 shows an n-alkane detonation with the 0.5 in crossover width. The reinitiation in frame 6 reflects off the "D" geometry in frame 7. While frame 14 shows somewhat of a reflection at the bottom of the secondary detonation tube, it is too weak to reinitiate the detonation in Region III. The strong reflections were limited to the crossover duct. More n-alkane detonation photographs are located in Appendix D.

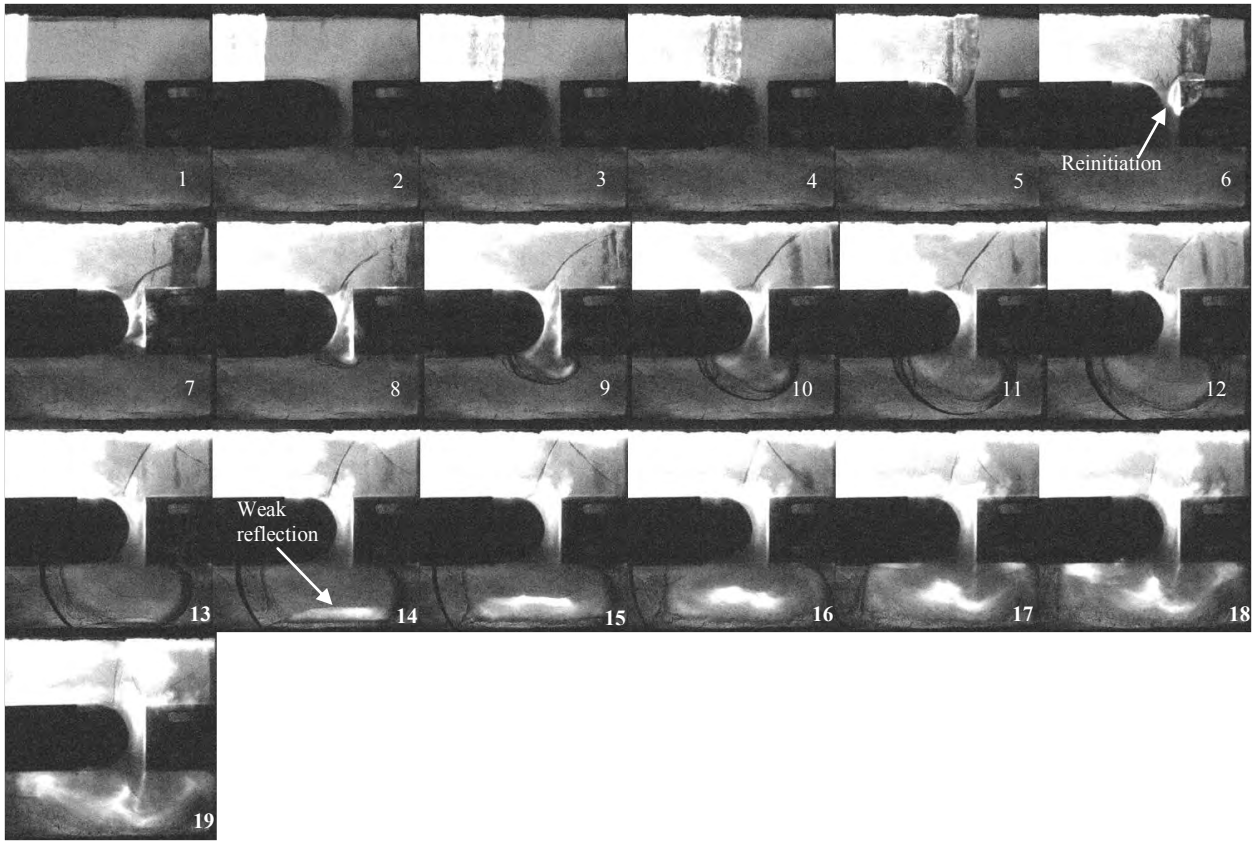

Figure 30. Detonation of an n-alkane and air in a tail-tail configuration with 0.5 in crossover width, sequentially from left to right, top to bottom. The small crossover width limits the strong reflections within the crossover resulting in a failed Region III reinitiation.

5. Region III detonations only

This research was primarily focused on the optimum crossover location and width to achieve branched detonation. The analysis of Regions II and III considers only those runs which originated from a successful Region I detonation. This is done in order to isolate the results as a function of crossover width and location and not as a function of the number of primary tube DDT attempts. Region I detonations will be examined briefly later. Each run at a particular crossover width noted in Tables 8 – 10 consisted of four sparks at 10 Hz in order to observe multiple detonations at each crossover width. Figures 31-33 show the percentage of hydrogen, ethylene, and n-alkane Region III detonations respectively which reinitiate after decoupling in the crossover duct. Data points are connected to show trends only and not to imply linear relationships where no data was recorded.

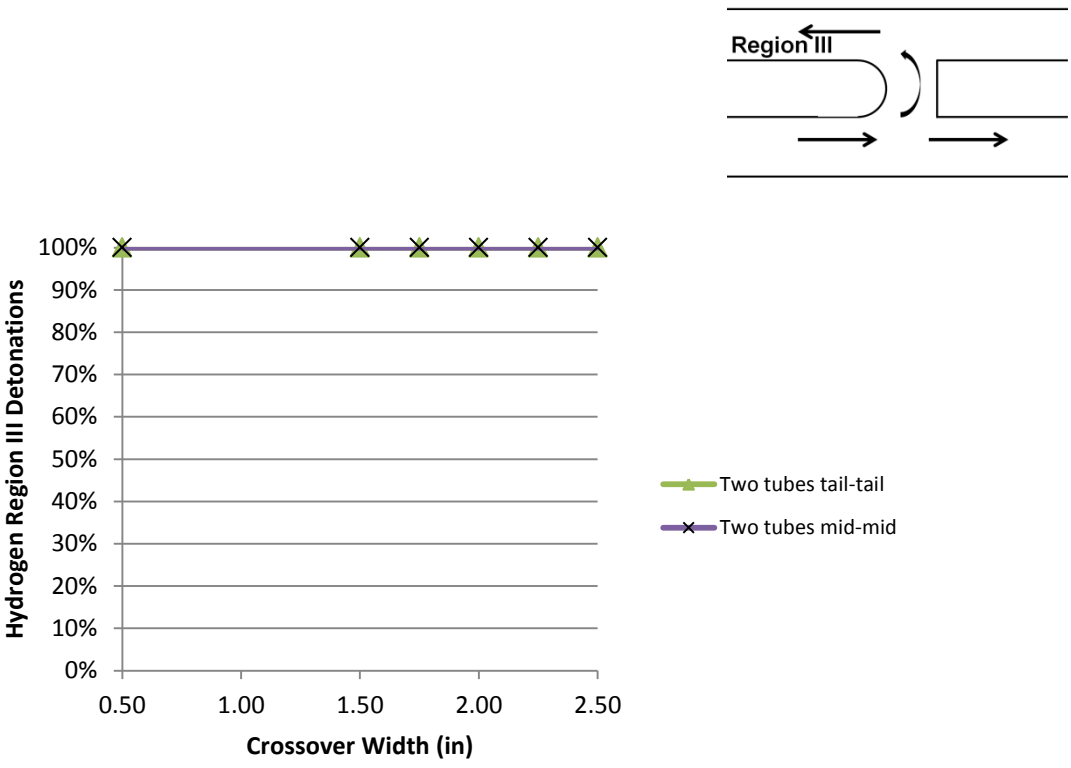

Figure 31. Region III hydrogen detonations for tail-tail and mid-mid configurations

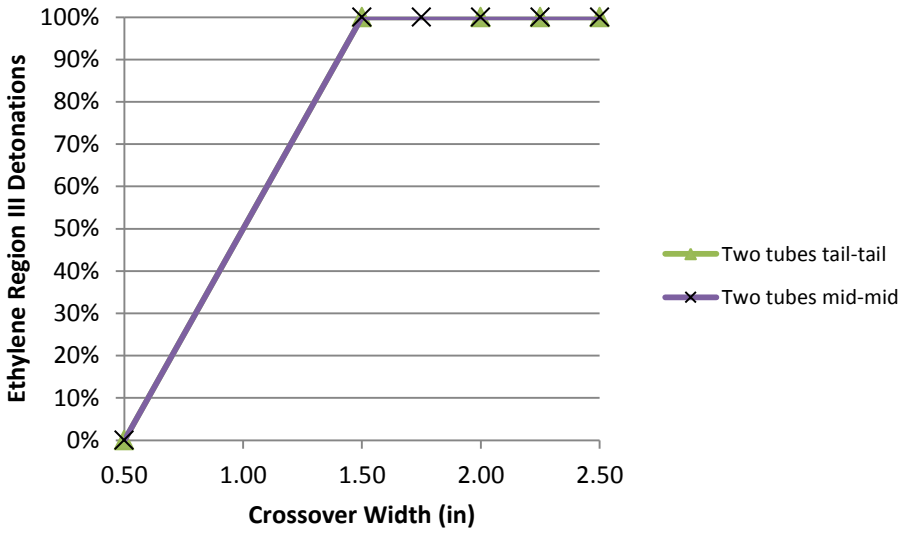

Figure 32. Region III ethylene detonations for tail-tail and mid-mid configurations

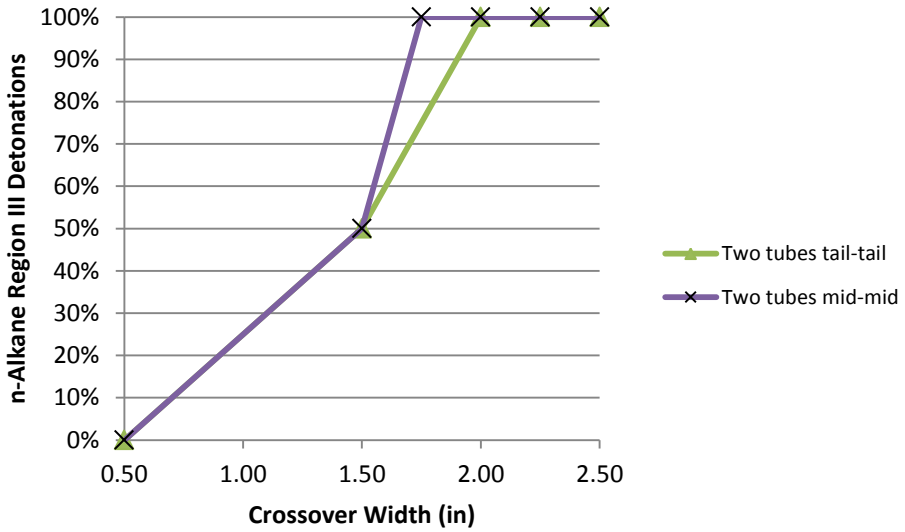

Figure 33. Region III n-alkane detonations for tail-tail and mid-mid configurations

As seen in Fig. 31, regardless of crossover location or crossover width, hydrogen produced Region III detonations 100% of the time. Hydrogen was expected to successfully produce Region III detonations in both the tail-tail and mid-mid configurations across various crossover widths. As mentioned earlier, hydrogen detonates consistently even at low equivalence ratios.[23]

In Fig. 32, there are no ethylene Region III detonations at the 0.5 in crossover for either the tail-tail or mid-mid configuration, however, Region III detonations occur 100% of the time for crossover widths of 1.5 in and greater. Ethylene detonations do not successfully transition through the crossover when the crossover width is 0.5 in because the strong reflection does not propagate successfully into Region III as shown earlier.

In Fig. 33, the n-alkane Region III detonations do not occur at all at the 0.5 in crossover width, then steadily increase to 100% at the 1.75 in and 2.0 in crossover widths for the mid-mid and tail-tail configurations respectively. The trend of increasing successful detonations with increasing crossover widths in Fig. 33 appears to suggest again that the smaller crossover widths are less conducive to detonation propagation. At 0.5 inches the crossover width does not allow the reinitiated detonation to propagate into Region III.

6. Region II detonations only

Figures 34-36 show the percentage of successful Region II detonations originating from a successful Region I detonation. In Fig. 34, hydrogen detonates successfully in Region II 100% of the time for all crossover widths in both the tail-tail and mid-mid configurations. Hydrogen again consistently detonates as expected regardless of varying conditions.

In Fig. 35, the ethylene Region II mid-mid configuration successfully detonates 100% of the time at each of the crossover widths. The ethylene Region II tail-tail configuration, however, detonates 100% of the time at crossover widths of 0.5 in – 2.0 in, but successful detonations steadily decrease as the crossover width is increased up to 2.5 in. It is possible that entrainment of ambient air decreases the number of successful detonations as the crossover width increases in the tail-tail configuration.

Figure 36 shows that the n-alkane consistently detonated 100% of the time in Region II at each of the crossover widths. The n-alkane tail-tail configuration does not appear to be affected by entrainment of the ambient air in Region II. Strong n-alkane reflections off the corner of the crossover duct may have allowed the n-alkane detonation to successfully transition into Region II.[19]

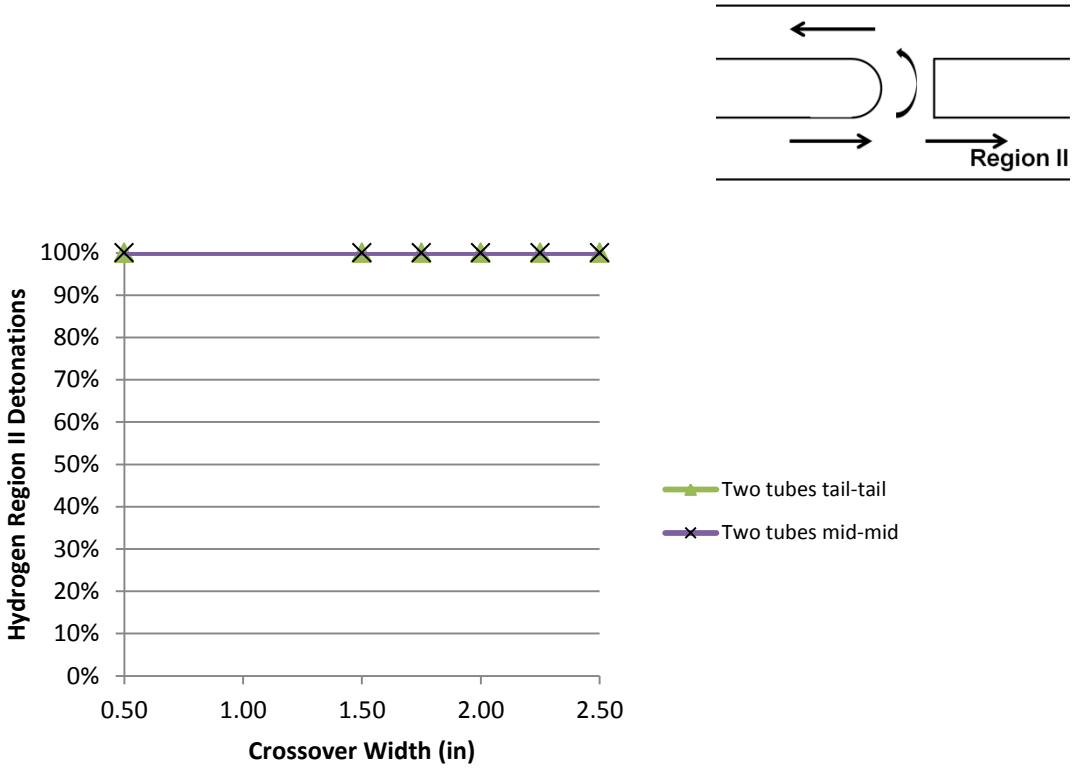

Figure 34. Region II hydrogen detonations for tail-tail and mid-mid configurations

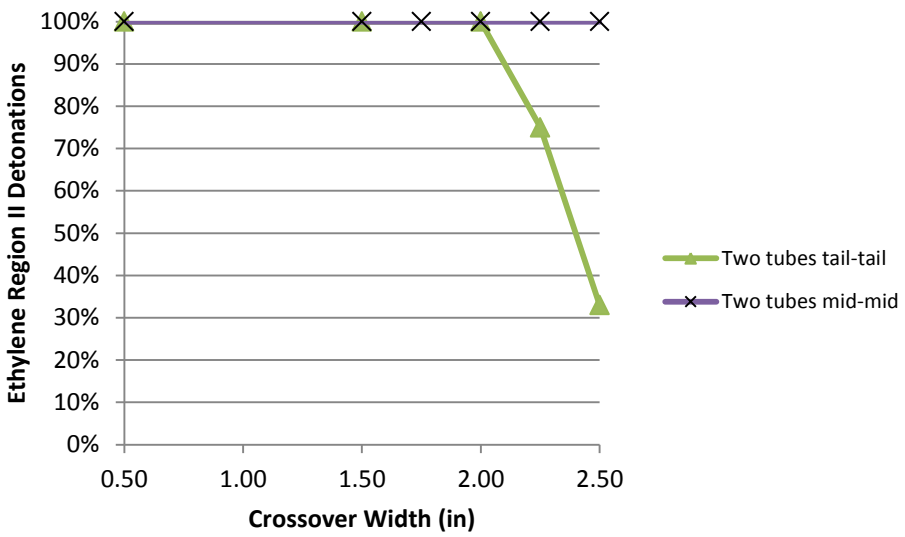

Figure 35. Region II ethylene detonations for tail-tail and mid-mid configurations

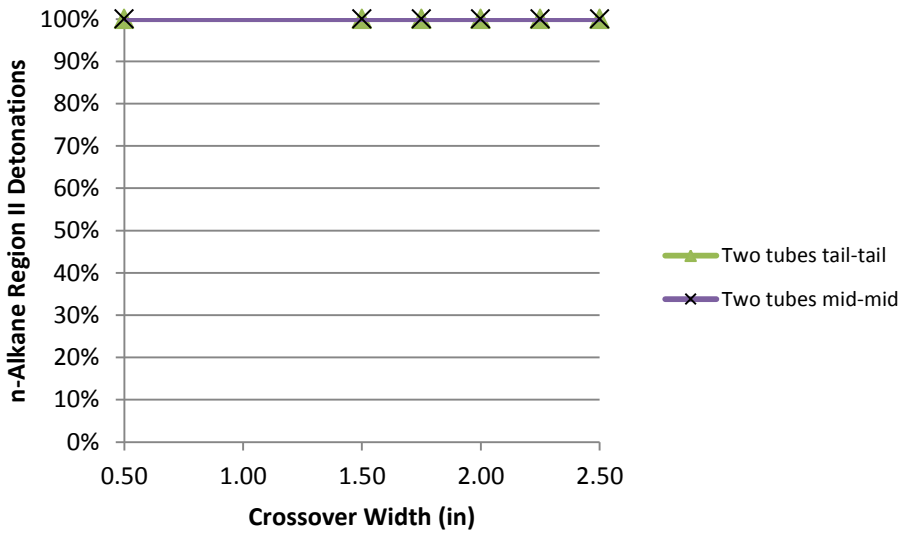

Figure 36. Region II n-alkane detonations for tail-tail and mid-mid configurations

7. Regions II and III simultaneous detonations

A detonation originating in Region I ideally propagates to both Regions II and III. While detonations often propagated to either Region II or Region III, the propagation did not always

occur in both regions. Figures 37 – 39 show successful detonations in both Regions II and III originating from the same Region I detonation.

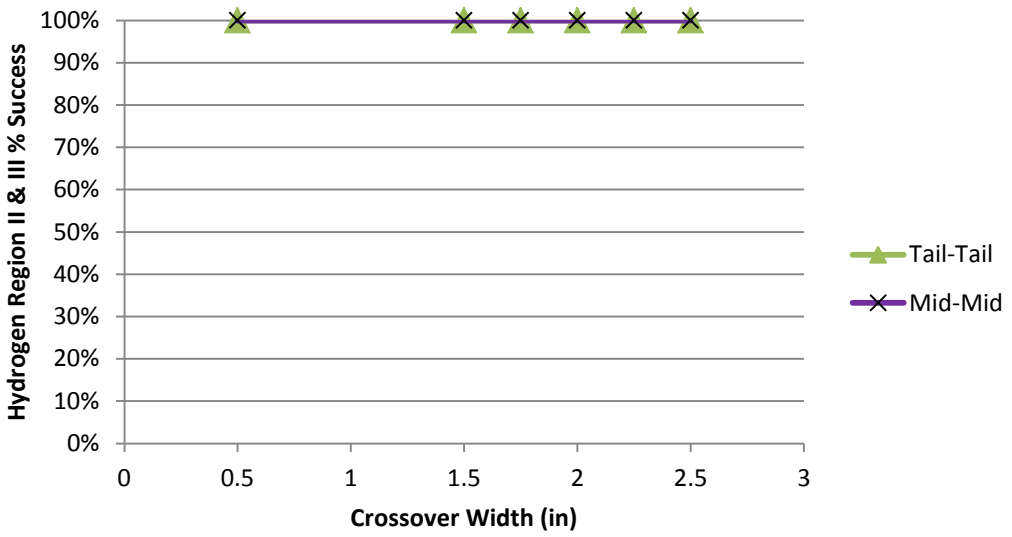

Figure 37. Regions II and III hydrogen detonations for tail-tail and mid-mid configurations

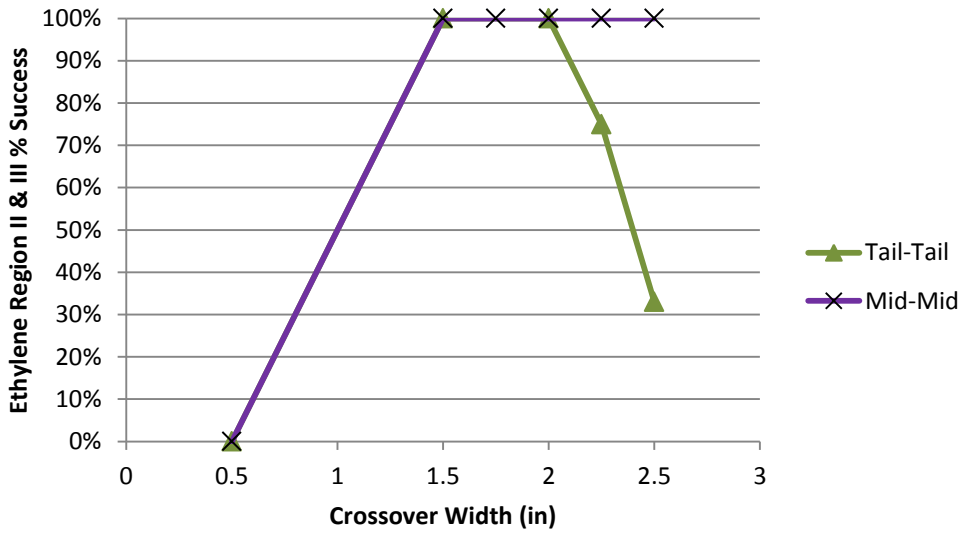

Figure 38. Regions II and III ethylene detonations for tail-tail and mid-mid configurations

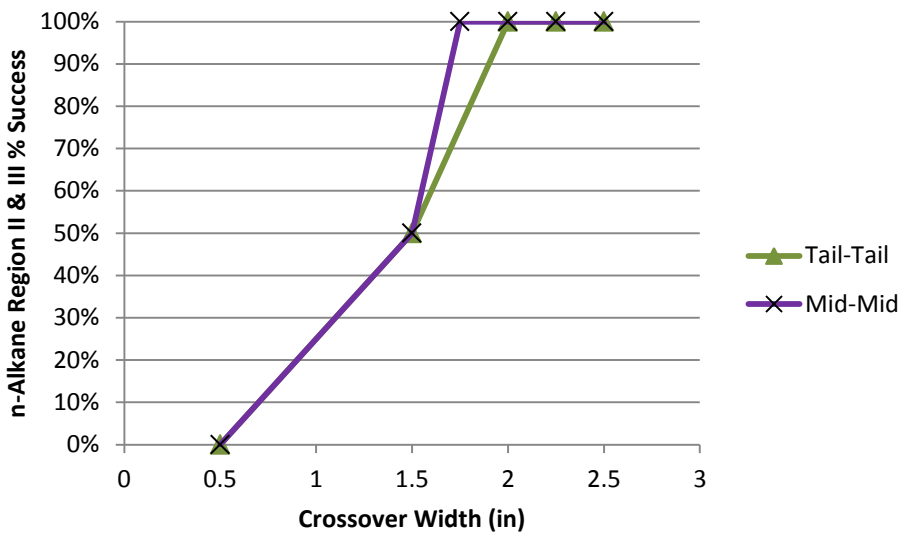

Figure 39. Regions II and III n-alkane detonations for tail-tail and mid-mid configurations

Figure 37 shows that hydrogen again was not affected by a change in crossover width or a change in crossover location. Regardless of the different conditions, hydrogen maintains high detonability.

Figure 38 shows the successful Region II and III ethylene detonations in the tail-tail configuration increase from a crossover width of 0.5 in to 1.5 in then decrease steadily as the crossover width increases above 2.0 in. In the mid-mid configuration, the successful ethylene detonations similarly increase from a crossover width of 0.5 in to 1.5 in, however, the mid-mid configuration then consistently produces 100% detonations for crossover widths greater than 1.5 in.

In the tail-tail configuration at the 0.5 in crossover width, the failure of the detonation reinitiation to propagate into Region III limits detonation success. At crossover widths greater than 2.0 in, however, entrainment of the ambient air may limit detonation success as the mid-mid configuration continued to produce 100% successful detonations in both Regions II and III.

In Fig. 39, the n-alkane detonations increase as the crossover width increases, suggesting that at crossover widths of 0.5 in and 1.5 in, the smaller crossover width limits successful detonation reinitiations. Figures D-5, D-6, D-10, and D-12 show crossover widths of 0.5 in and 1.5 in limiting n-alkane detonation reinitiations in Region III.

The n-alkane appears less affected than ethylene by entrainment of the ambient air at larger crossover widths. As mentioned earlier, strong n-alkane reflections may have contributed to the high detonation success rate in Region II. Both the tail-tail and mid-mid configurations produce detonations in Regions II and III equivalently at all crossover widths with the exception of 1.75 in where there was no tail-tail configuration data.

8. The PDE system

It is beneficial to define the PDE system in terms of inputs and desired outputs in order to establish a baseline for performance. Figure 40 depicts the PDE system as viewed for purposes of this research.

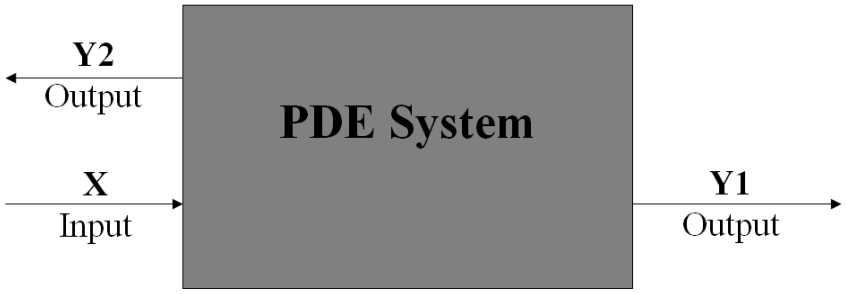

X = Spark
Y1 = Detonation out tail end of primary detonation tube
Y2 = Detonation reinitiation in secondary detonation tube via crossover

Figure 40. The PDE crossover system

As seen in Fig. 40, for every spark in the primary detonation tube there are two desired detonations: one out the tail end of the primary detonation tube and one through the crossover

duct into the secondary detonation tube. For every X, an optimal system would produce 100% Y1 and 100% Y2. A figure of merit, defined as the sum of Y1% plus Y2%, is used as a baseline in order to compare the performance of the different configurations. The desired figure of merit is 200.

Figure 41 compares the hydrogen figures of merit for both tail-tail and mid-mid configurations every time a spark was fired, regardless of a successful detonation in Region I. This research was primarily focused on the optimum crossover location and width to achieve branched detonation. The analyses of Regions II and III considered only those runs which originated from a successful Region I detonation. Analyzing Regions II and III in this manner isolates the results as a function of crossover width and location and not as a function of the number of primary tube DDT attempts. Detonations did not occur in Region I 100% of the time, however. Each run at a particular crossover width noted in Tables 8 – 10 consisted of four sparks at 10 Hz in order to observe multiple detonations at each crossover width. Figure 42 shows the percentage of Region I hydrogen detonations. Comparing Figs. 41 and 42, it is clear that the hydrogen figure of merit is limited by successful Region I detonations at the 2.5 in crossover width in the mid-mid configuration.

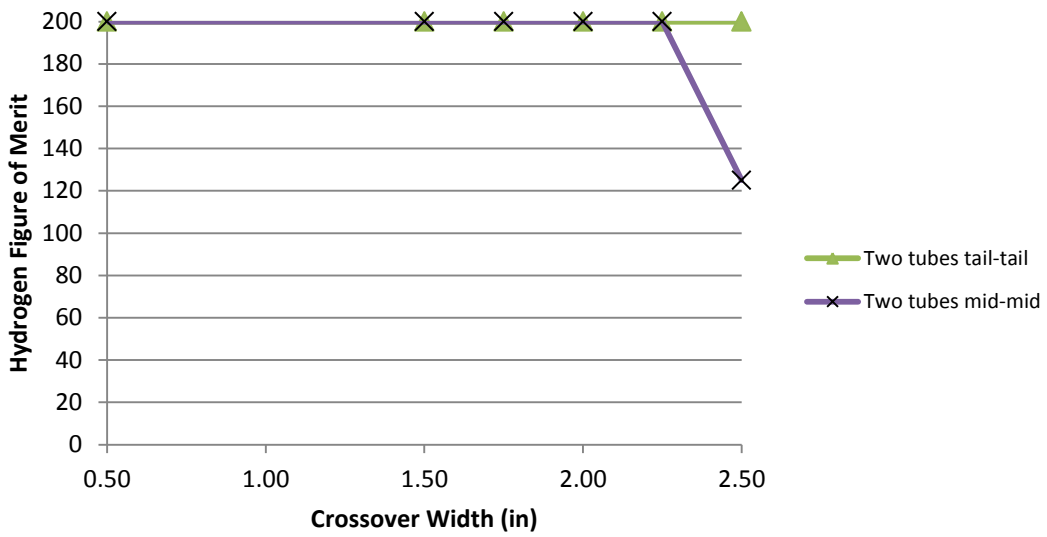

Figure 41. Hydrogen figure of merit for tail-tail and mid-mid configurations

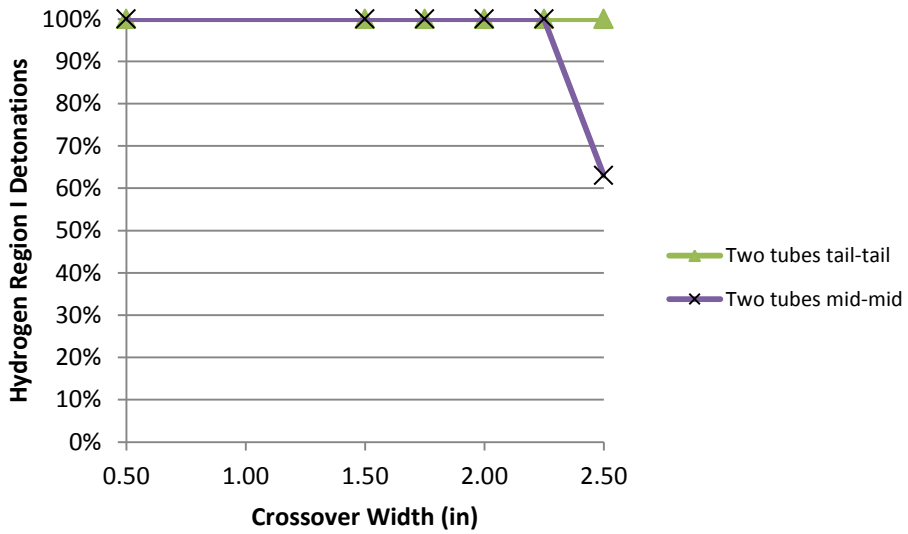

Figure 42. Hydrogen Region I detonations for tail-tail and mid-mid configurations

In Fig. 43, the ethylene tail-tail figure of merit is better than the mid-mid figure of merit. Compared to the Region I data in Fig. 44, the ethylene mid-mid figure of merit appears limited by Region I detonations. In Fig. 38, with a successful Region I detonation, the ethylene mid-mid

configuration produced 100% detonations in Regions II and III more often than the tail-tail configuration. While this research did not examine the variables affecting successful Region I detonations, the higher success rate of Region I detonations in the tail-tail configuration contributed to the higher tail-tail figure of merit.

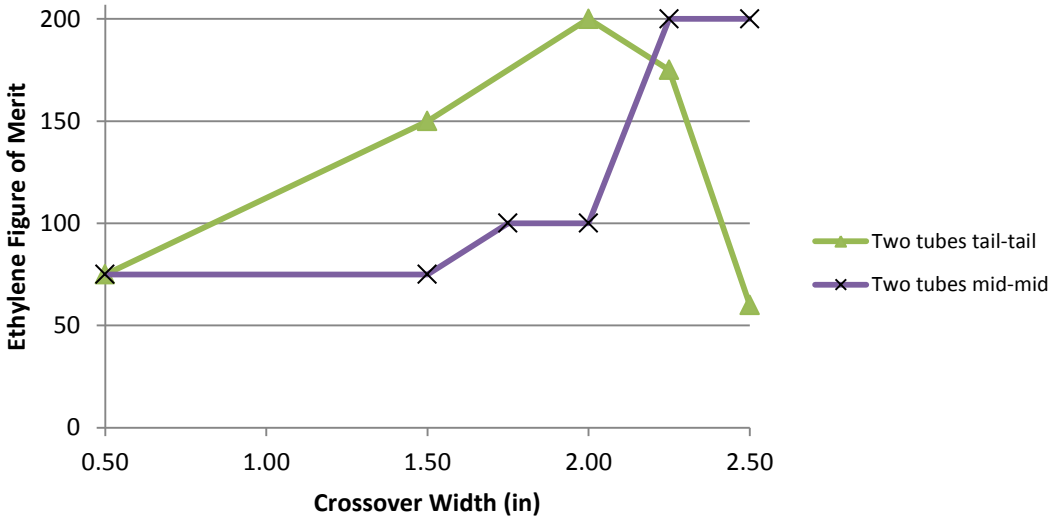

Figure 43. Ethylene figure of merit for tail-tail and mid-mid configurations

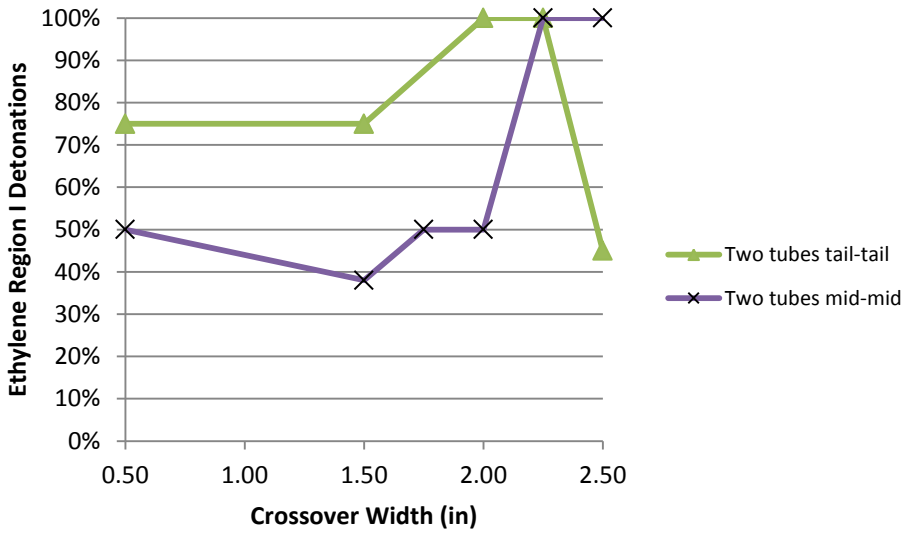

Figure 44. Ethylene Region I detonations for tail-tail and mid-mid configurations

Figure 39 shows that smaller crossover widths (0.5 in and 1.5 in) appear to limit successful n-alkane detonation propagation in both the tail-tail and mid-mid configurations. The smaller crossover width likewise limits the figure of merit in Fig. 45. There appears to be no correlation between Region I detonations and figure of merit for the n-alkane, as seen in Figs. 45 and 46. As shown earlier, the n-alkane detonation can successfully reinitiate and propagate into another region without a Region I detonation.

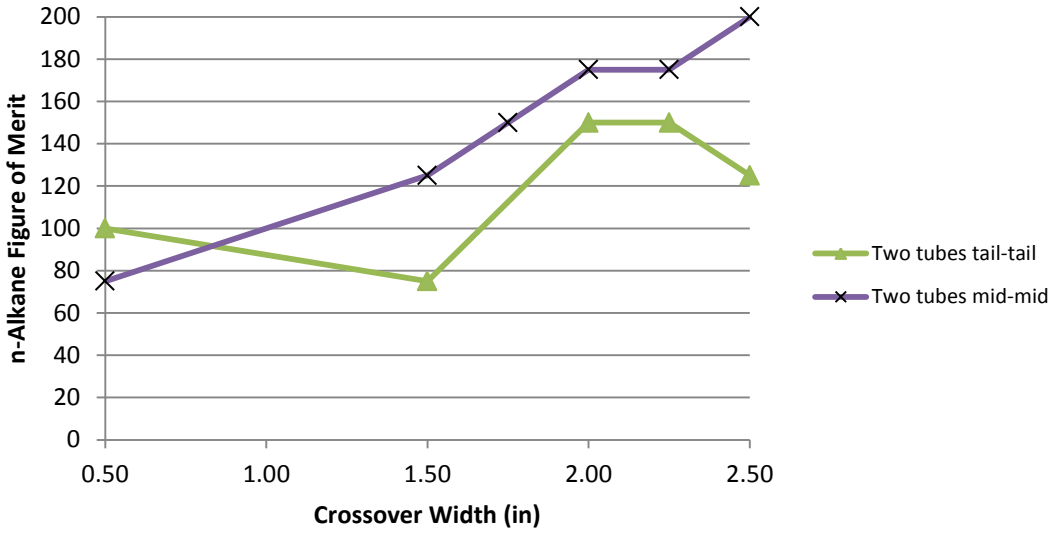

Figure 45. n-Alkane figure of merit for tail-tail and mid-mid configurations

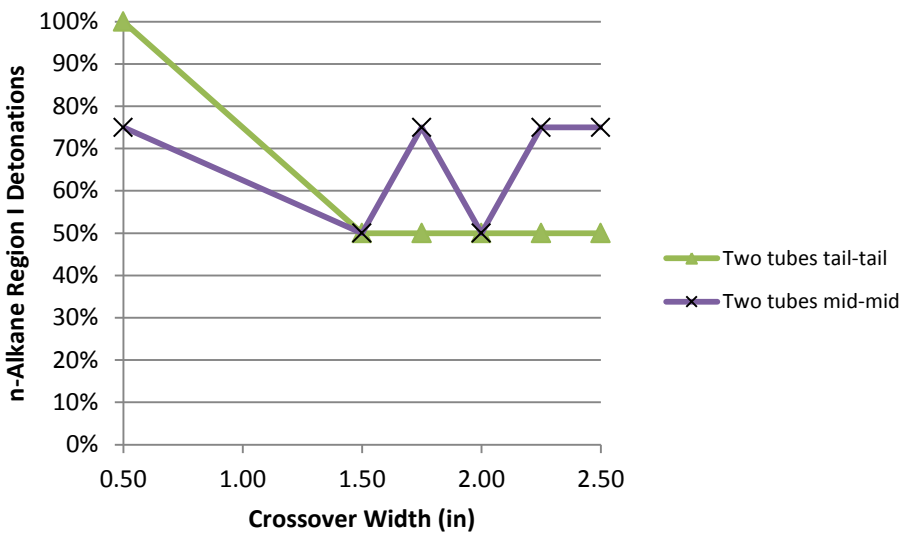

Figure 46. n-Alkane Region I detonations for tail-tail and mid-mid configurations

9. Crossover width

Figure 47 depicts the crossover width and detonation tube height.

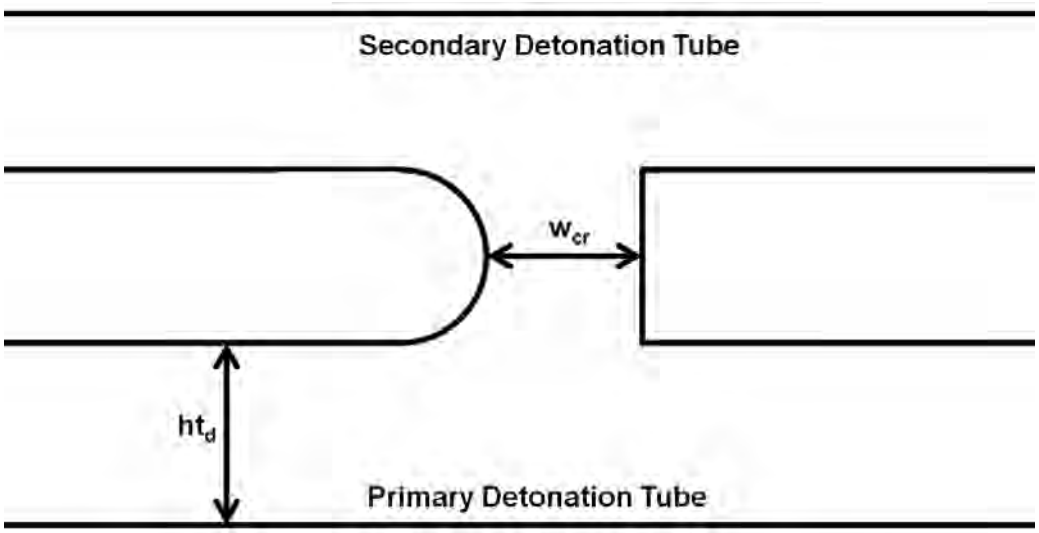

Figure 47. Depiction of crossover width, w_{cr}, and detonation tube height, ht_d

The crossover ratio, r_{cr}, is defined in Eq. (23).

$$r_{cr} = w_{cr}/ht_d \tag{23}$$

For hydrogen and ethylene in the mid-mid configuration with a crossover ratio of 1.0, the Region III detonation reinitiates, recouples across the height of the secondary detonation tube and becomes planar in the case of hydrogen and nearly-planar in the case of ethylene before the detonations leave the Schlieren field of view. The crossover ratio of 1 appears to reduce the distance in which the shock and combustion front recouple across the entire tube and become planar, possibly indicating a more efficient branched detonation and an optimal crossover ratio. Reinitiated planar detonations can be seen in Figs. 48 and 50 as compared to Figs. 49 and 51. Each pair of figures depicts a 13 μs interval. A crossover width of 1.5 in is shown in Figs. 49 and 51 as an example of the crossover ratio not equal to unity. Crossover ratios less than unity were less consistent in producing successful detonation reinitiations.

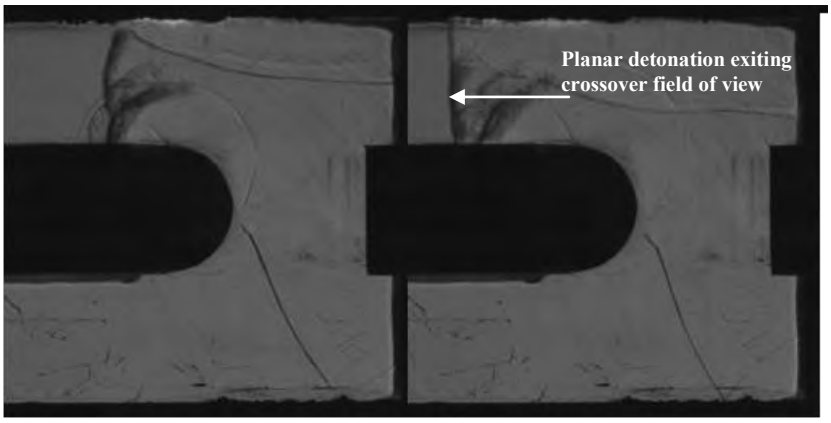

Figure 48. Mid-mid configuration hydrogen-air detonation with 2.0 in crossover width reinitiates, recouples across the entire secondary detonation tube and becomes planar in secondary tube prior to leaving the visible section of the crossover

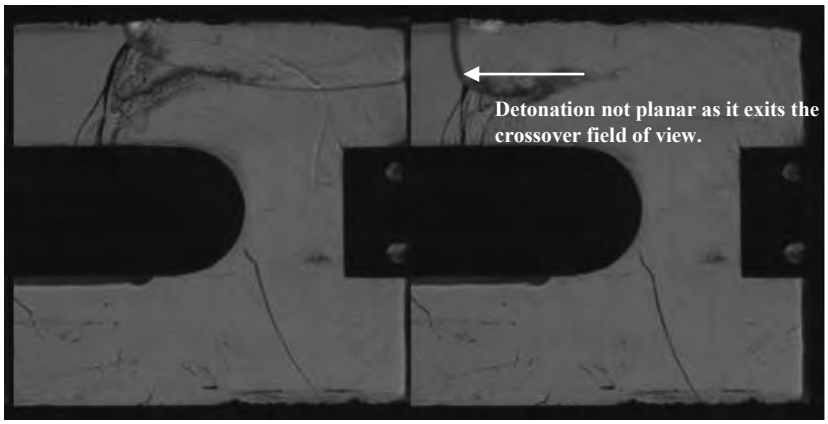

Figure 49. Mid-mid configuration hydrogen-air detonation with 1.5 in crossover width reinitiates but is neither coupled across the entire secondary tube nor planar prior to leaving the visible section of the crossover

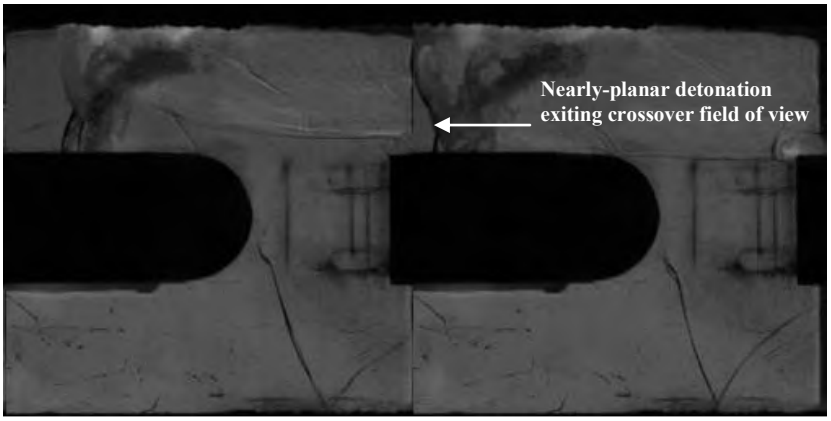

Figure 50. Mid-mid configuration ethylene-air detonation with 2.0 in crossover width reinitiates, recouples across the entire secondary tube and becomes nearly-planar prior to leaving the visible section of the crossover

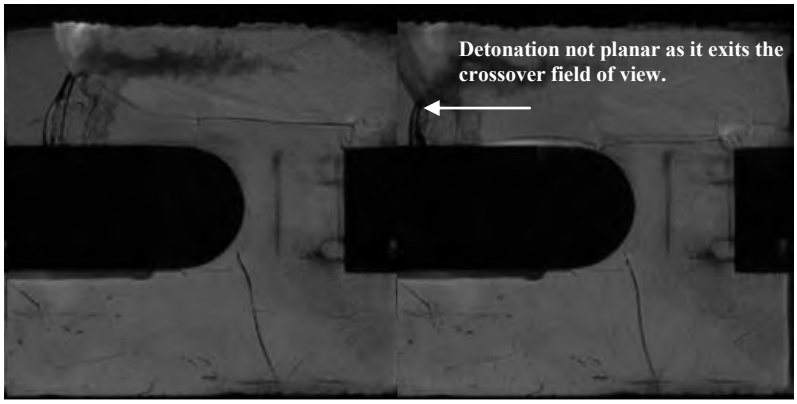

Figure 51. Mid-mid configuration ethylene-air detonation with 1.5 in crossover width reinitiates but is neither coupled across the entire secondary tube nor planar prior to leaving the visible section of the crossover

Figure 52 shows that the effects of crossover width on the distance required for a reinitiated planar n-alkane detonation are inconclusive due to the quality of the Schlieren photographs.

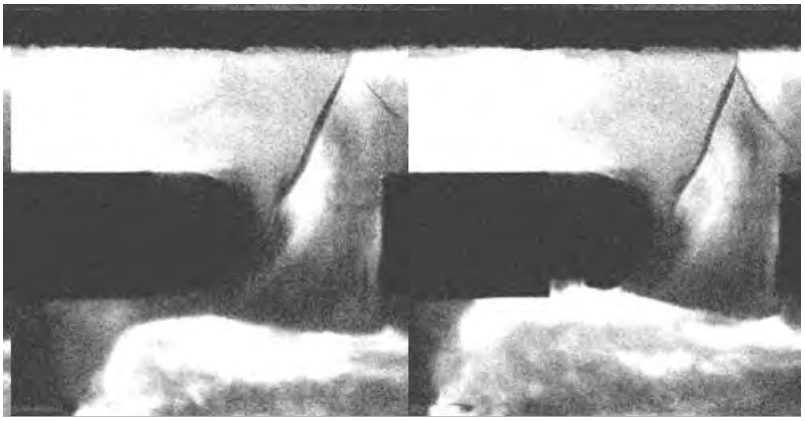

Figure 52. Mid-mid configuration n-alkane-air detonation with 2.0 in crossover width. It is not clear whether the detonation is planar or not due to the quality of the photograph.

V. Conclusions

This research reports on how crossover location and width affect tube-to-tube initiation in a PDE. Branched detonations were observed in Regions II and III for a crossover width of 2.0 in regardless of crossover location. For the mid-mid crossover location, branched detonations were observed 100% of the time for crossover widths of 1.75-2.5 in.

1. Effects of crossover location

The mid-mid crossover location is more conducive to hydrocarbon branched detonation propagation than the tail-tail configuration. The mid-mid location produces 100% detonations in Regions II and III with a crossover width between 1.75-2.5 in. The mid-mid crossover is less affected than the tail-tail crossover location by the leaned-out equivalence ratio in the crossover section due to entrainment of the ambient air. It will be important to note in the employment of multiple mid-mid crossover locations across multiple detonation tubes, that the crossovers should be alternating and offset from each other far enough that the branched detonation is able to reinitiate and begin traveling in the direction of the detonation tube before diffracting into another crossover duct. Ensuring that the detonation has enough distance to reinitiate and begin traveling down the tube will avoid undesired detonation diffraction across multiple mid-mid crossover locations simultaneously.

2. Effects of crossover width

Branched detonations propagate more successfully through crossover widths approximately equal to the detonation tube height. Ethylene detonations occur in Regions II and III 100% of the time for crossover widths of 1.5-2.5 in for the mid-mid configuration. A crossover width of 2.25-2.5 in produces ethylene detonations in all three regions in the mid-mid configuration every time there was a spark. The n-Alkane detonations occur in Regions II and III 100% of the time

for crossover widths of 2.0-2.5 in for either the tail-tail or the mid-mid configuration. A crossover width of 2.5 in produces n-alkane detonations in all three regions in the mid-mid configuration for every spark.

3. Future Work

a. Crossover width

By repeating the tests in this research with multiple detonation tube sizes, the results could be used to validate the optimal crossover ratio. Based on data from tests with multiple detonation tube sizes, the optimal crossover ratio that provides the most consistent branched detonation could be utilized in an application regardless of the size of the detonation tube.

b. Thrust

Thrust measurements were not taken during this research. It would be worth examining whether the tail-tail or mid-mid configuration has any effect on the amount of thrust produced. Additionally, the amount of thrust produced from the secondary detonation tube may be affected by the distance required for the reinitiated detonation to become planar, because a planar detonation may produce thrust more efficiently than a reinitiated detonation that is not yet planar. If the detonation becomes planar in a shorter distance, the amount of thrust produced from the secondary detonation tube may be greater. Utilizing the ratio of crossover width to detonation tube height that results in the shortest distance required to produce a planar detonation may help maximize the thrust in the secondary detonation tube regardless of the detonation tube height.

c. Region I detonations

This research focused on how crossover location and width affected branched detonations in Regions II and III. As seen in the results, Region I detonations were not consistent. Future testing could vary spiral length and tube size in order to isolate which combination of variables

produce consistent Region I detonations. A spiral length and tube size that consistently produce Region I detonations combined with the crossover width and crossover location that consistently produce Region II and III detonations may be utilized in an overall best configuration to most consistently produce branched detonations.

d. Ion probes

Due to the limited number of ion probe channels, this research did not use ion probes on the tail end of the secondary detonation tube. Future tests may include these ion probes to ensure that the branched detonation is propagating out the tail end of the secondary detonation tube. Detonations that fail to successfully propagate out the tail end of the secondary detonation tube in either the tail-tail or mid-mid configuration would likely decrease the amount of thrust produced.

Appendix A. Summary of tests

Each run in Tables A-1 through A-3 consisted of 4 sparks at 10 Hz. A dash mark in the wave speed column indicates a failed detonation attempt with no recorded wave speeds. For the hydrogen and n-alkane tests, detonations in Region II were assumed in accordance with Fig. 23, although Region II detonation wave speeds were not recorded due to having only one good ion probe voltage drop.

Table A-1. Hydrogen test summary

Run #	Crossover width (in)	Configuration	Wave Speed (m/s)	
			Region I	Region III
1	2.50	Tail-Tail	1924	2351
			1895	2247
			1895	2228
			1895	2396
2	2.25	Tail-Tail	1909	2351
			1924	2228
			1909	2351
			1895	2419
3	2.00	Tail-Tail	1895	2309
			1924	2208
			1909	2373
			1881	2099
4	1.75	Tail-Tail	1895	2288
			1909	2309
			1909	2170
			1895	2288
5	1.50	Tail-Tail	1895	2288
			1881	2330
			1881	2189
			1881	2330
6	0.50	Tail-Tail	1909	2048
			1909	2540
			1909	1971
			1881	2396
7	2.50	Mid-Mid	1909	2247
			1924	2065
			-	-
			-	-
8	2.50	Mid-Mid	-	-
			1909	2267
			1924	2048
			1895	2419
9	2.25	Mid-Mid	1881	2247
			1909	2048
			1895	2330
			1881	2228
10	2.00	Mid-Mid	1924	2015
			1895	2267
			1909	2396
			1909	2330
11	1.75	Mid-Mid	1895	2208
			1909	2351
			1895	2466
			1867	2309
12	1.50	Mid-Mid	1909	2288
			1924	2351
			1909	2208
			1881	2228
13	0.50	Mid-Mid	1909	2288
			1895	3527
			1909	2267
			1881	2267

Table A-2. Ethylene test summary

Run #	Crossover width (in)	Configuration	Wave Speed (m/s)		
			Region I	Region II	Region III
1	2.50	Tail-Tail	-	-	-
			2081	488	2099
			-	-	-
			-	-	-
2	2.50	Tail-Tail	2000	266	1673
			-	-	-
			-	-	-
			1881	476	2134
3	2.50	Tail-Tail	2000	276	2116
			-	-	-
			-	-	-
			1827	2437	2134
4	2.50	Tail-Tail	-	-	-
			2032	635	2116
			-	-	-
			-	-	-
5	2.50	Tail-Tail	2152	352	2330
			-	-	-
			1968	2437	2351
			2116	2457	2228
6	2.25	Tail-Tail	2000	448	2189
			1840	3175	2170
			2330	1313	2099
			1854	2540	2152
7	2.00	Tail-Tail	2048	1537	2189
			1854	2540	2208
			2228	2116	2170
			1801	2020	2116
8	1.50	Tail-Tail	1763	2116	1806
			1968	2241	2116
			-	-	-
			1909	2005	2134
9	0.50	Tail-Tail	-	-	-
			1867	2721	907
			1881	1313	984
			2442	1465	686
10	2.50	Mid-Mid	2099	2381	2170
			1827	2721	2170
			1968	2116	2170
			1984	2540	2189
11	2.25	Mid-Mid	1953	2381	2081
			1909	1465	2247
			2000	2540	2189
			1840	2540	2170
12	2.00	Mid-Mid	-	-	-
			-	-	-
			1468	2005	2189
			1895	2241	2228
13	1.75	Mid-Mid	-	-	-
			-	-	-
			2152	2241	2081
			1682	2005	2208
14	1.50	Mid-Mid	-	-	-
			1502	2005	1895
			-	-	-
			-	-	-
15	1.50	Mid-Mid	-	-	-
			-	-	-
			2267	2021	2170
			1628	1524	2134
16	0.50	Mid-Mid	-	-	-
			2170	1860	705
			1739	1792	1226
			-	-	-

Table A-3. n-Alkane test summary

Run #	Crossover width (in)	Configuration	Wave Speed (m/s)	
			Region I	Region III
1	2.50	Tail-Tail	-	-
			793	858
			2091	2241
			1503	2381
2	2.25	Tail-Tail	339	1175
			1524	1336
			1275	2000
			1203	374
3	2.00	Tail-Tail	1785	2300
			900	711
			804	421
			1220	1854
4	1.50	Tail-Tail	2731	476
			1387	1840
			-	-
			-	-
5	0.50	Tail-Tail	1445	328
			1544	328
			1731	273
			1544	236
6	2.25	Mid-Mid	1814	1814
			1258	1428
			1020	782
			1727	1393
7	2.00	Mid-Mid	952	1716
			1208	1854
			1048	323
			1329	1827
8	1.75	Mid-Mid	1866	2152
			-	-
			1905	3298
			1284	1309
9	1.50	Mid-Mid	944	799
			1484	589
			1011	457
			1843	1544
10	2.50	Mid-Mid	1205	1671
			1344	1693
			1731	1854
			1344	1351
11	0.50	Mid-Mid	1242	384
			1222	374
			-	-
			1329	402

Appendix B. Hydrogen detonation photographs

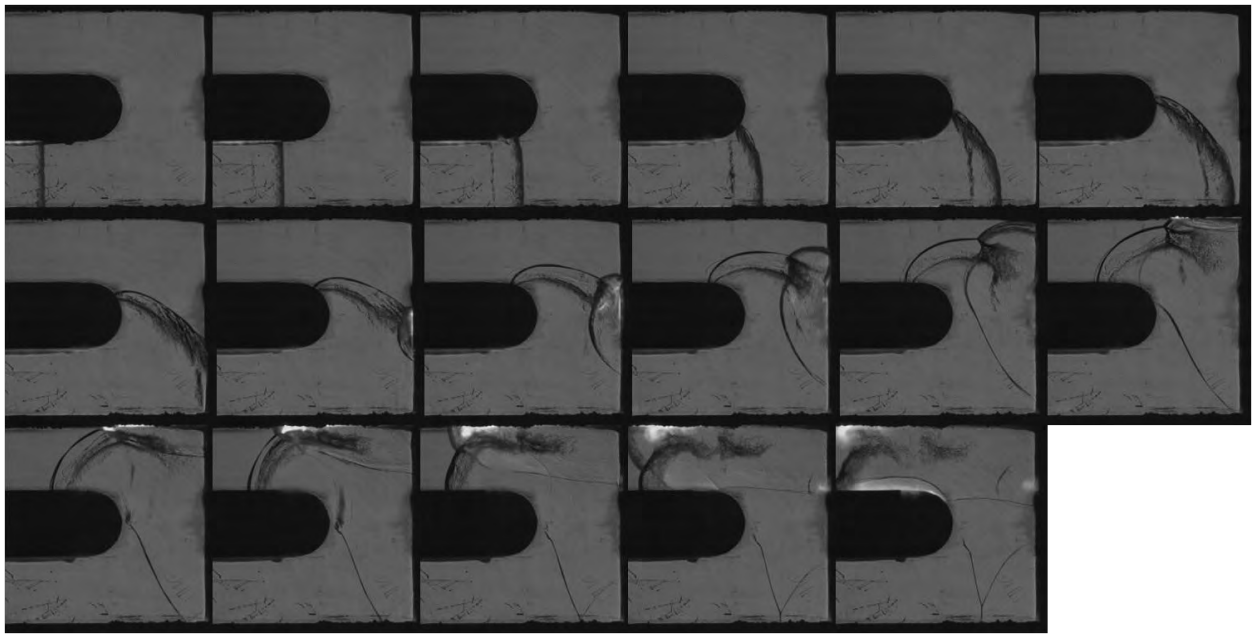

Figure B-1. Hydrogen-air detonation in tail-tail configuration with 2.5 in crossover width resulting in a successful Region III reinitiation

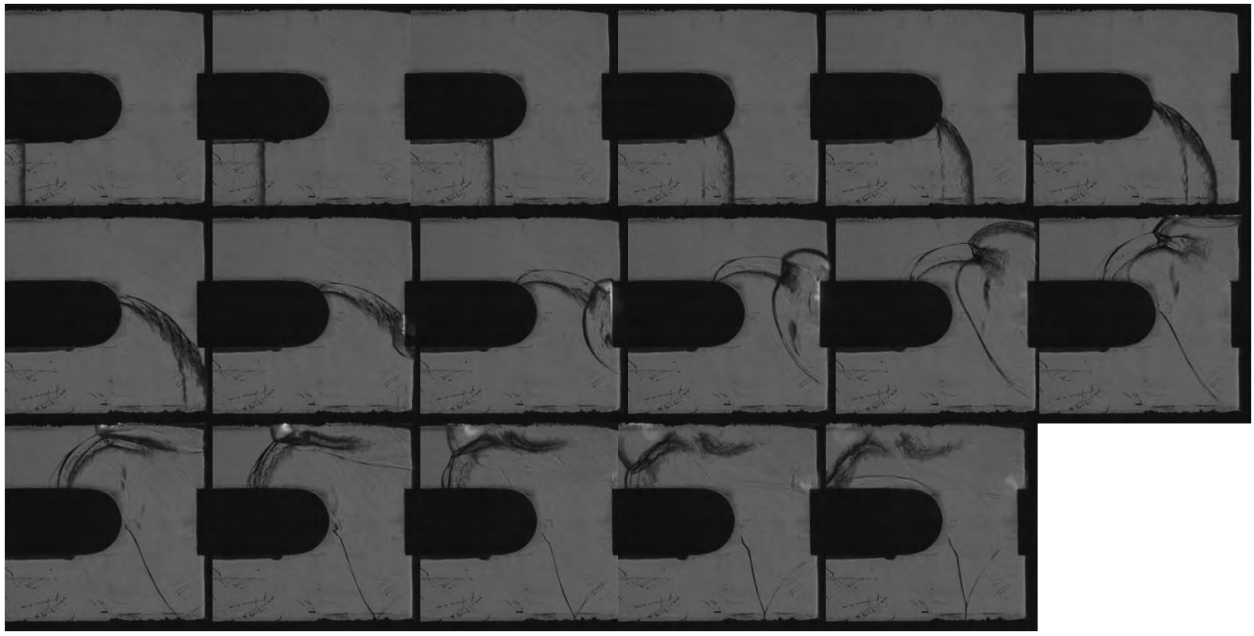

Figure B-2. Hydrogen-air detonation in tail-tail configuration with 2.25 in crossover width resulting in a successful Region III reinitiation

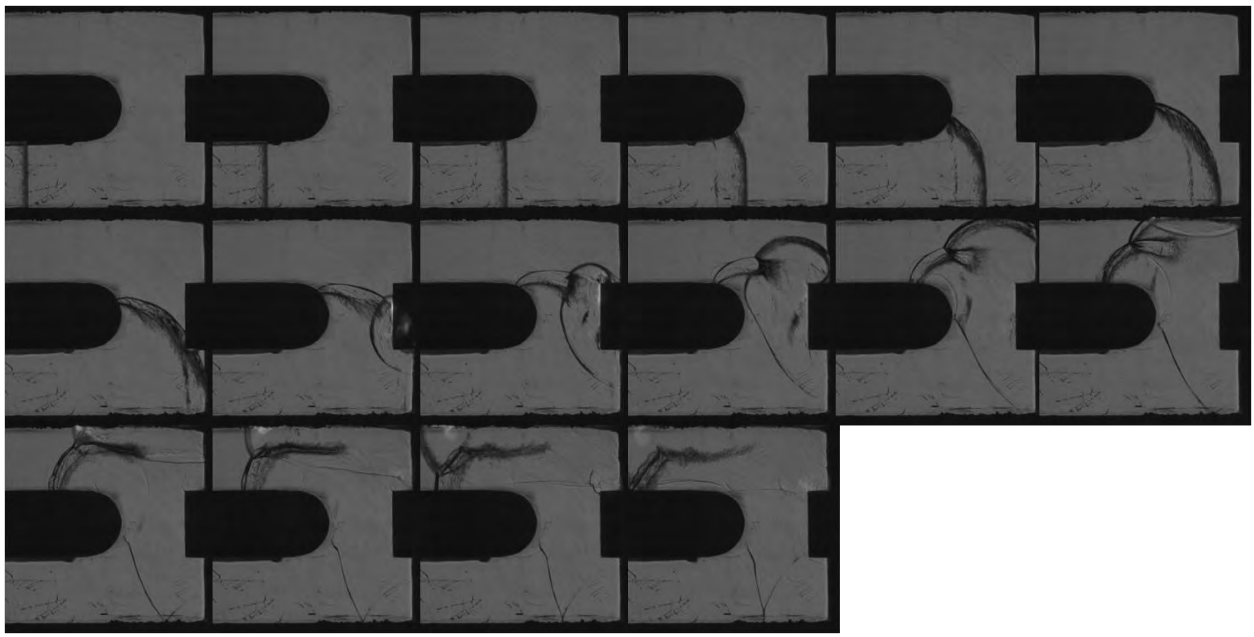

Figure B-3. Hydrogen-air detonation in tail-tail configuration with 2.0 in crossover width resulting in a successful Region III reinitiation

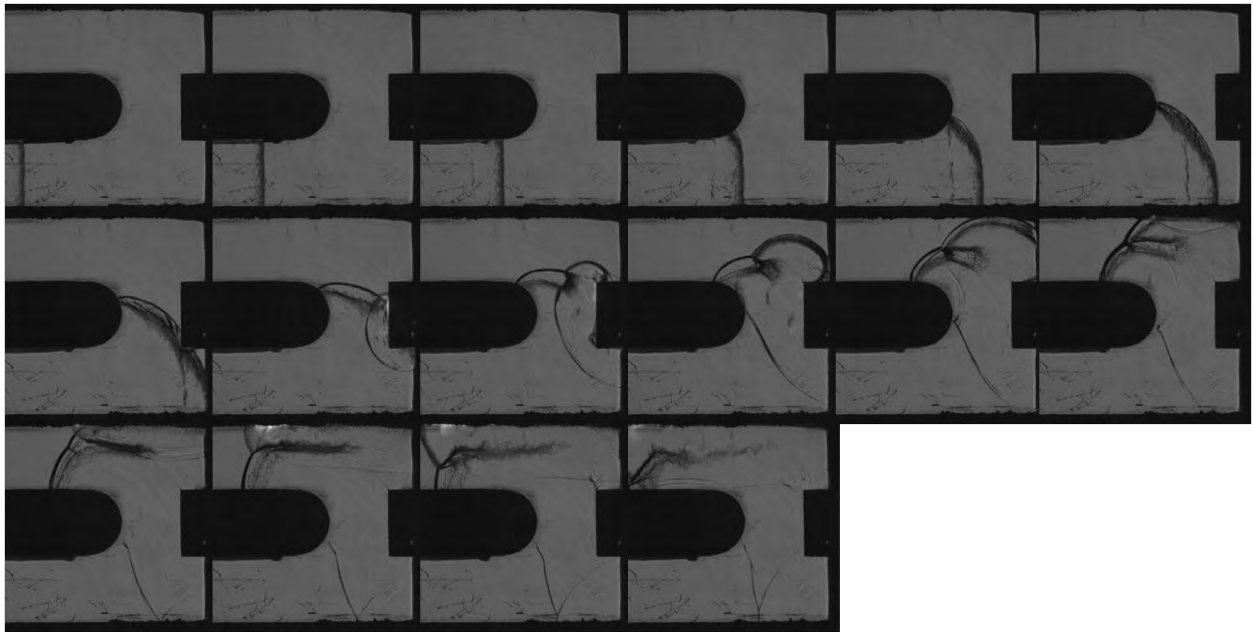

Figure B-4. Hydrogen-air detonation in tail-tail configuration with 1.75 in crossover width resulting in a successful Region III reinitiation

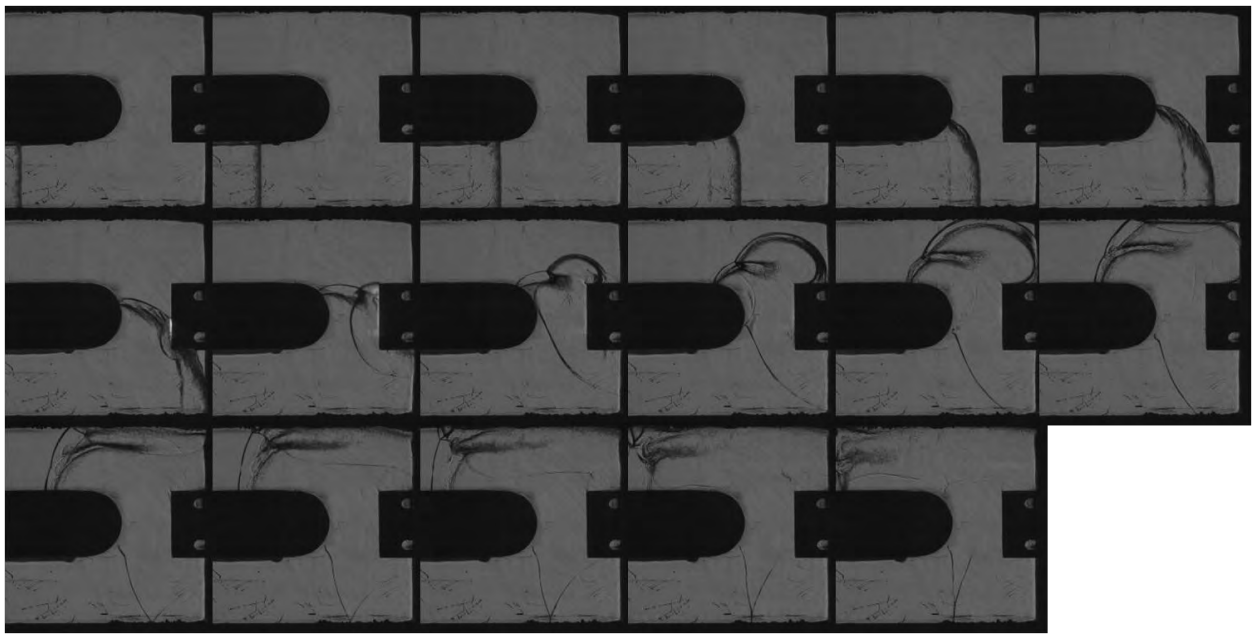

Figure B-5. Hydrogen-air detonation in tail-tail configuration with 1.5 in crossover width resulting in a successful Region III reinitiation

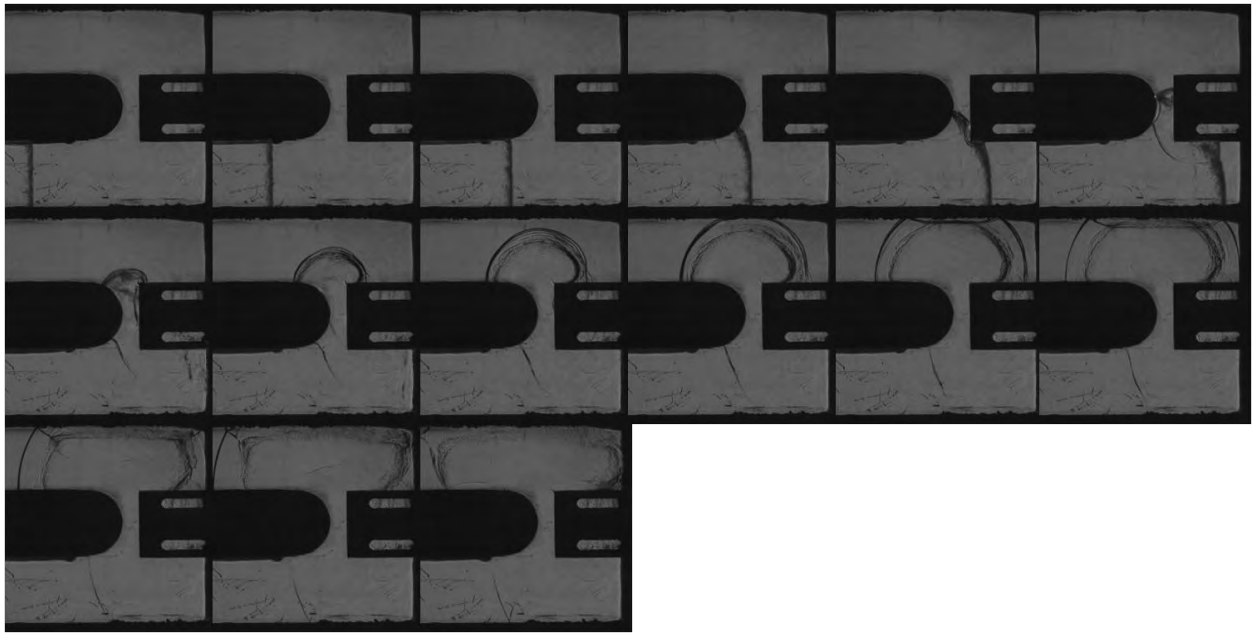

Figure B-6. Hydrogen-air detonation in tail-tail configuration with 0.5 in crossover width resulting in a successful Region III reinitiation

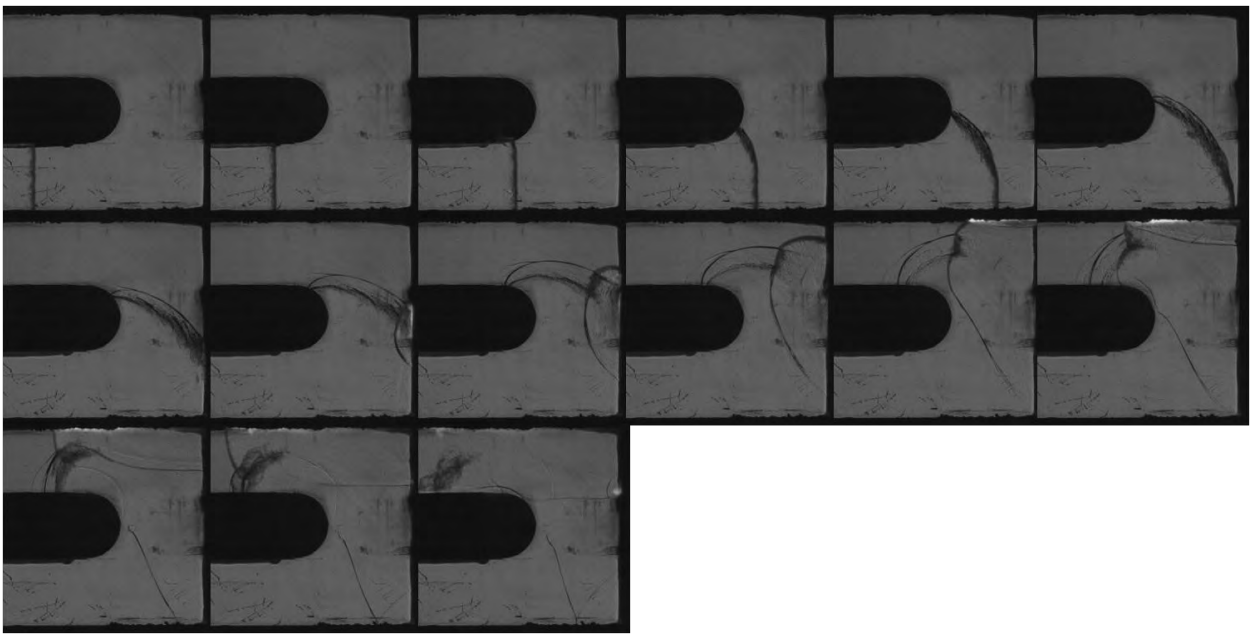

Figure B-7. Hydrogen-air detonation in mid-mid configuration with 2.5 in crossover width resulting in a successful Region III reinitiation

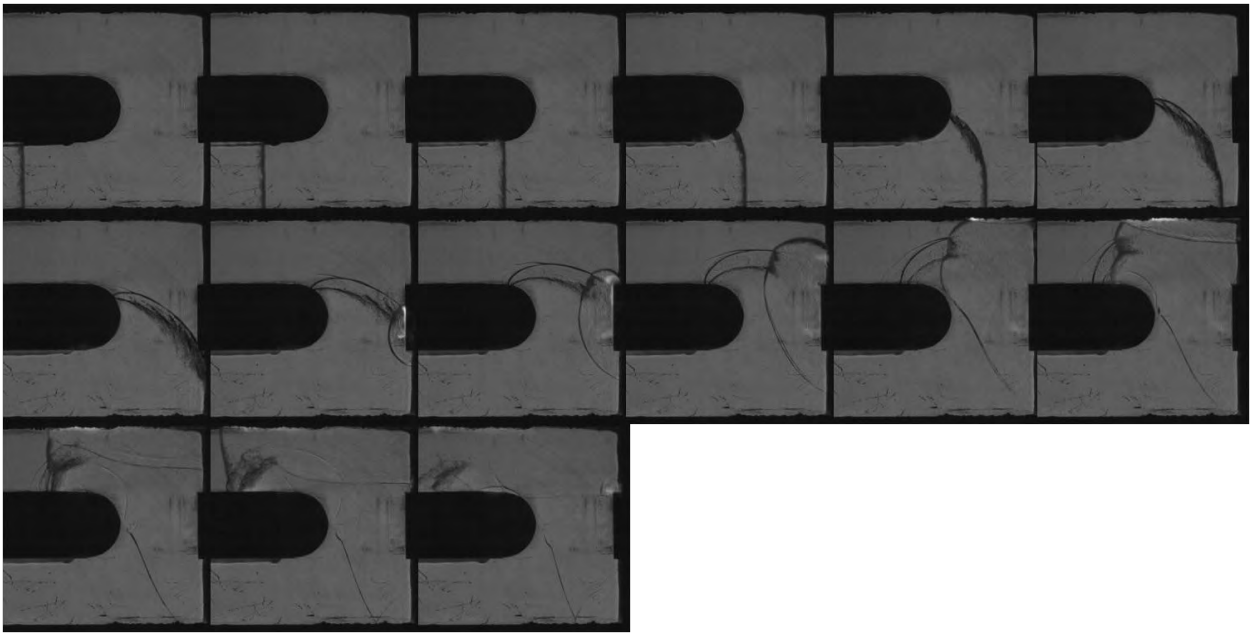

Figure B-8. Hydrogen-air detonation in mid-mid configuration with 2.25 in crossover width resulting in a successful Region III reinitiation

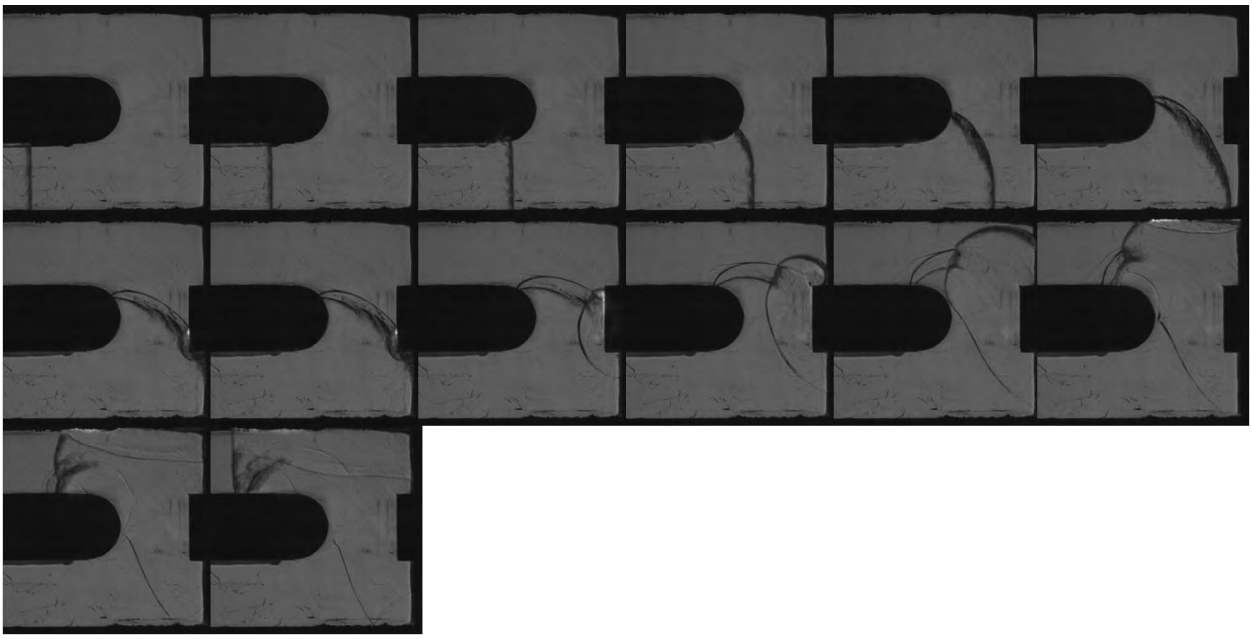

Figure B-9. Hydrogen-air detonation in mid-mid configuration with 2.0 in crossover width resulting in a successful Region III reinitiation

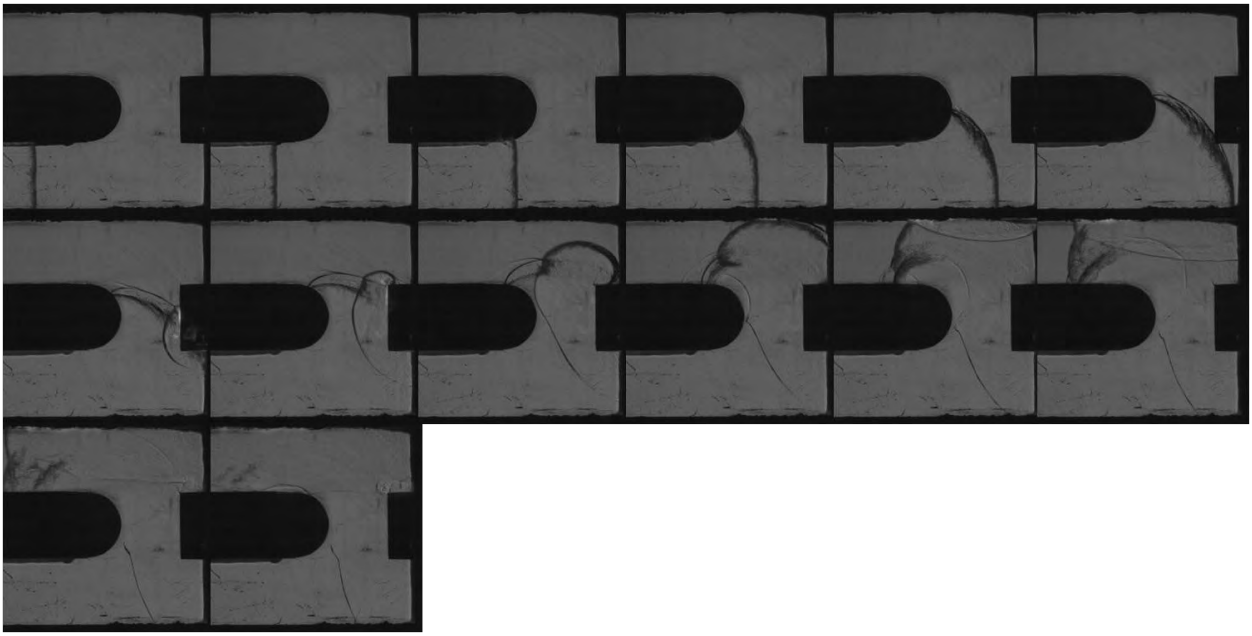

Figure B-10. Hydrogen-air detonation in mid-mid configuration with 1.75 in crossover width resulting in a successful Region III reinitiation

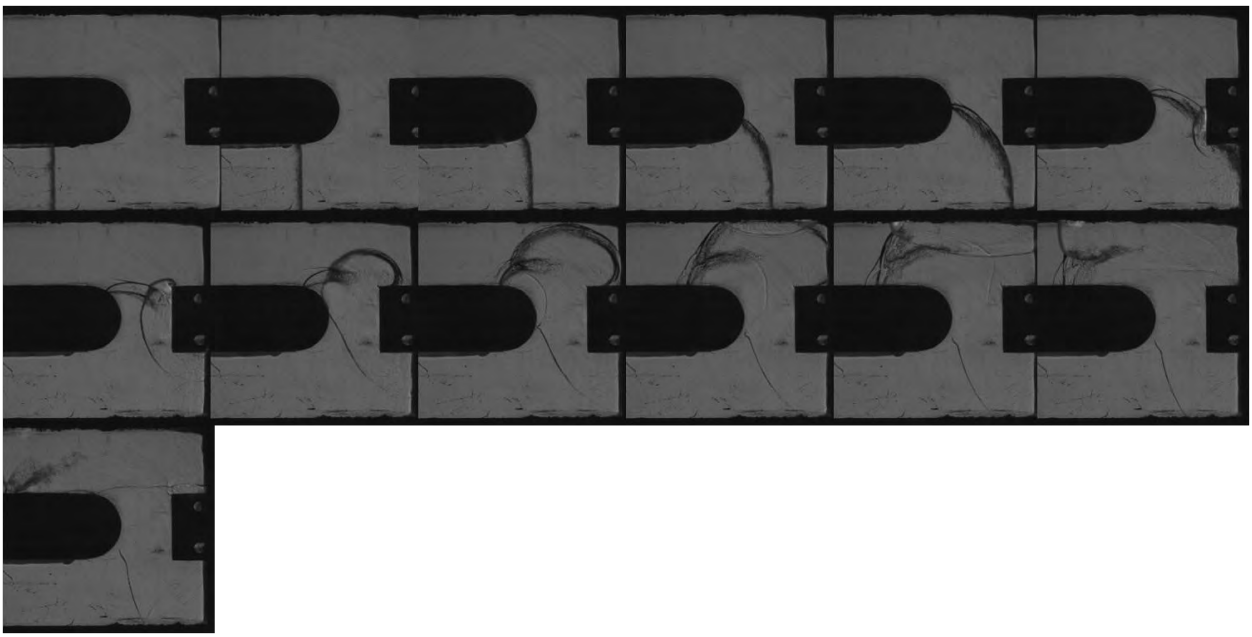

Figure B-11. Hydrogen-air detonation in mid-mid configuration with 1.5 in crossover width resulting in a successful Region III reinitiation

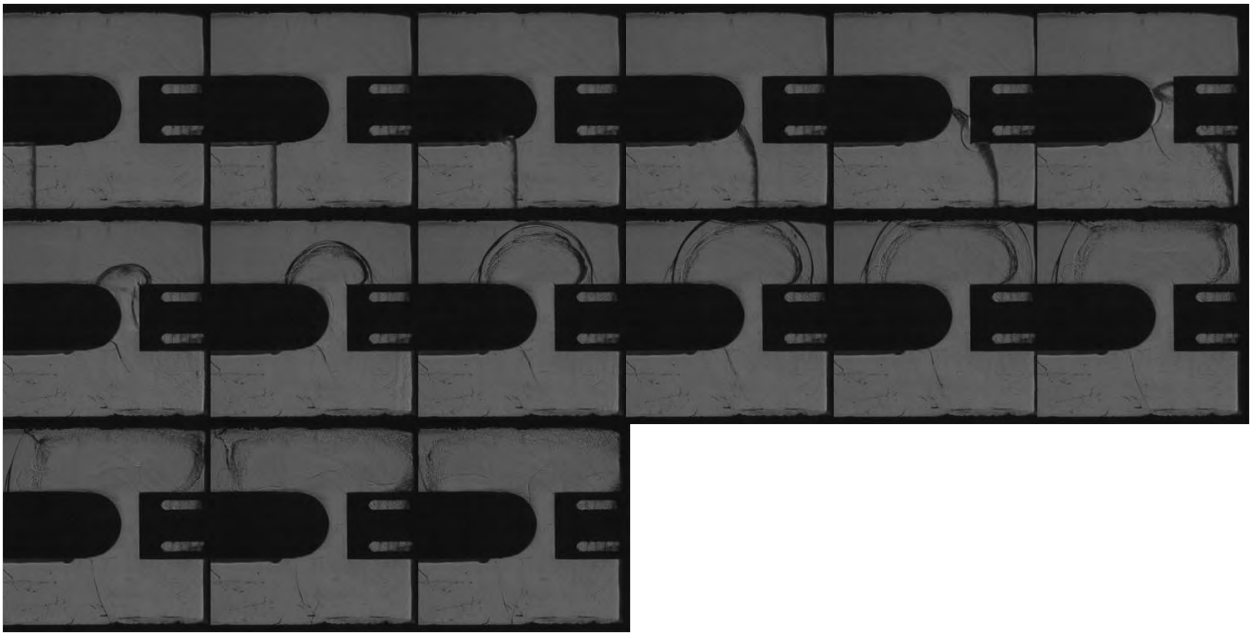

Figure B-12. Hydrogen-air detonation in mid-mid configuration with 0.5 in crossover width resulting in a successful Region III reinitiation

Appendix C. Ethylene detonation photographs

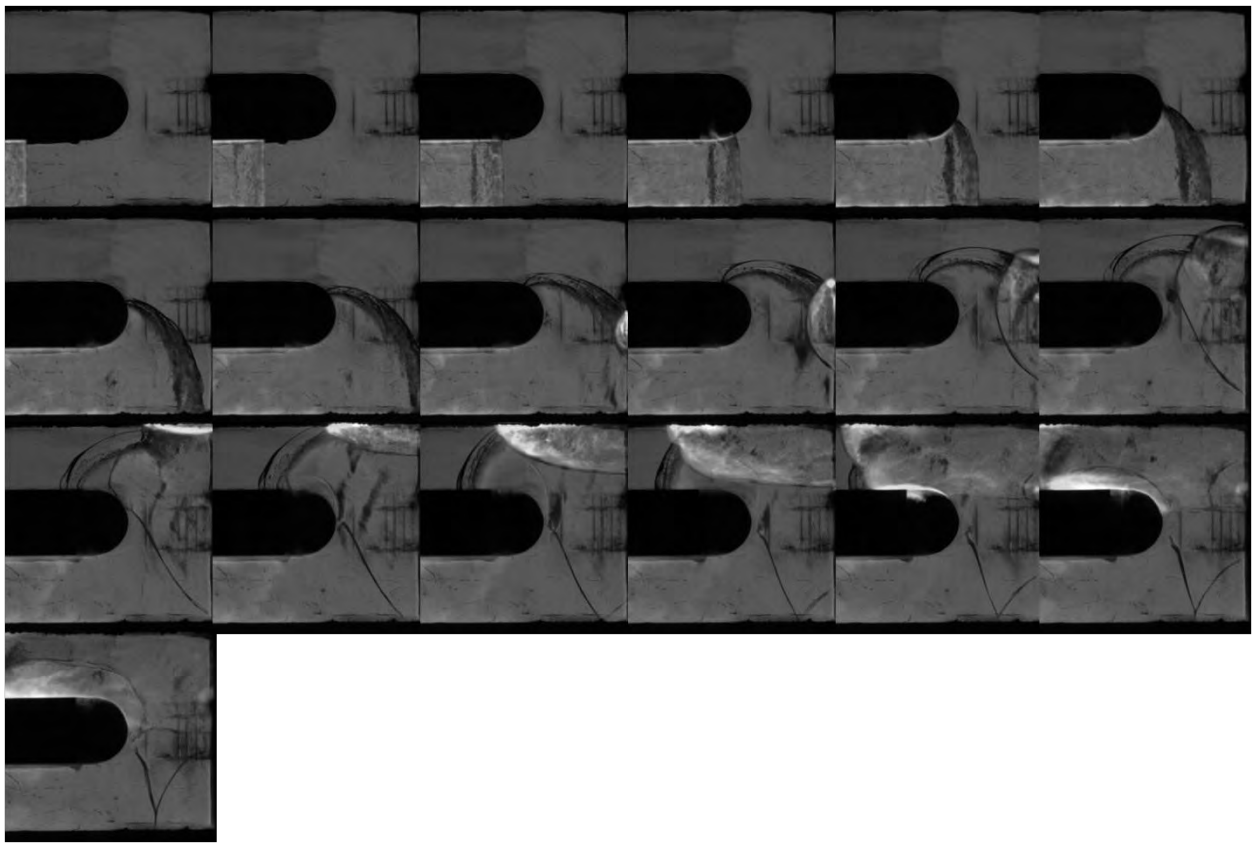

Figure C-1. Ethylene-air detonation in tail-tail configuration with 2.5 in crossover width resulting in a successful Region III reinitiation

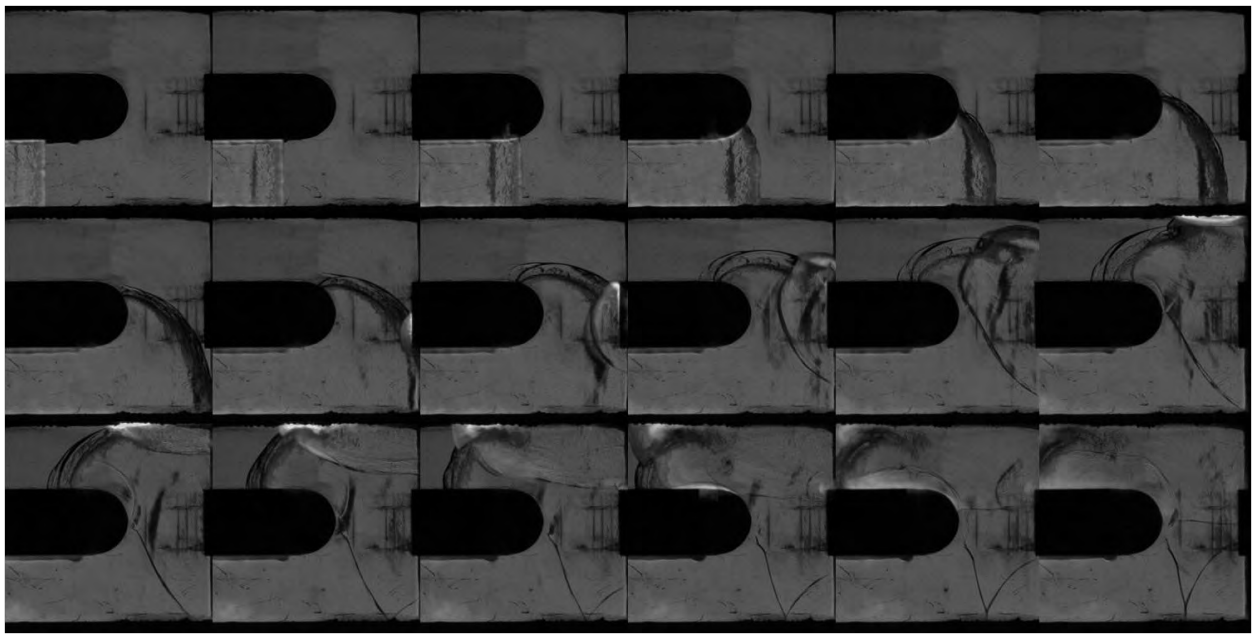

Figure C-2. Ethylene-air detonation in tail-tail configuration with 2.25 in crossover width resulting in a successful Region III reinitiation

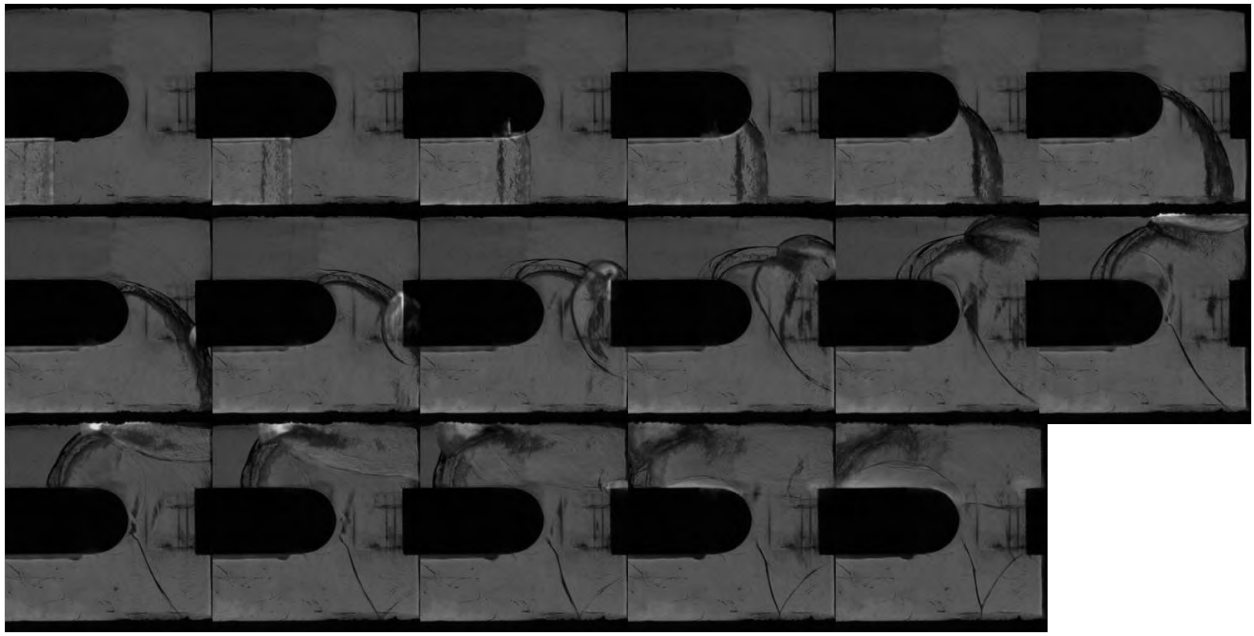

Figure C-3. Ethylene-air detonation in tail-tail configuration with 2.0 in crossover width resulting in a successful Region III reinitiation

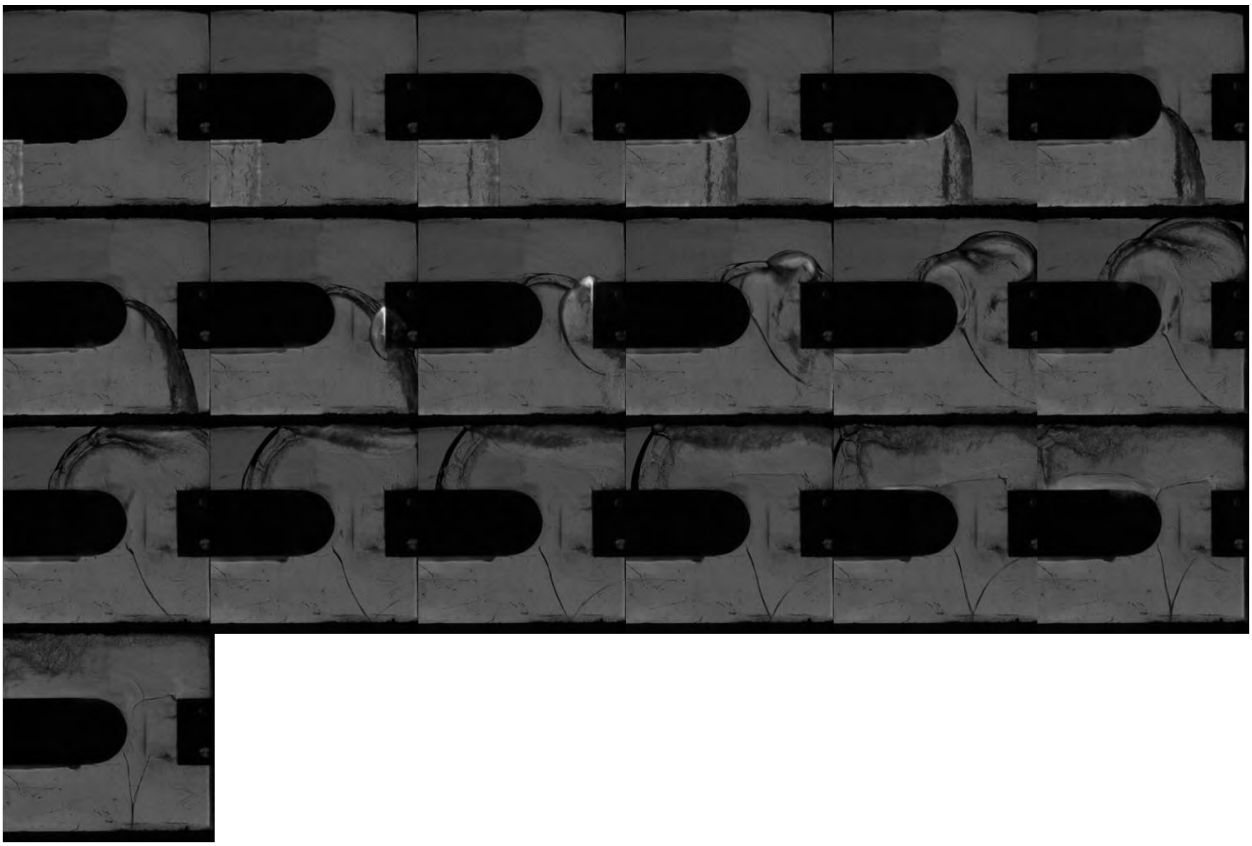

Figure C-4. Ethylene-air detonation in tail-tail configuration with 1.5 in crossover width resulting in a successful Region III reinitiation

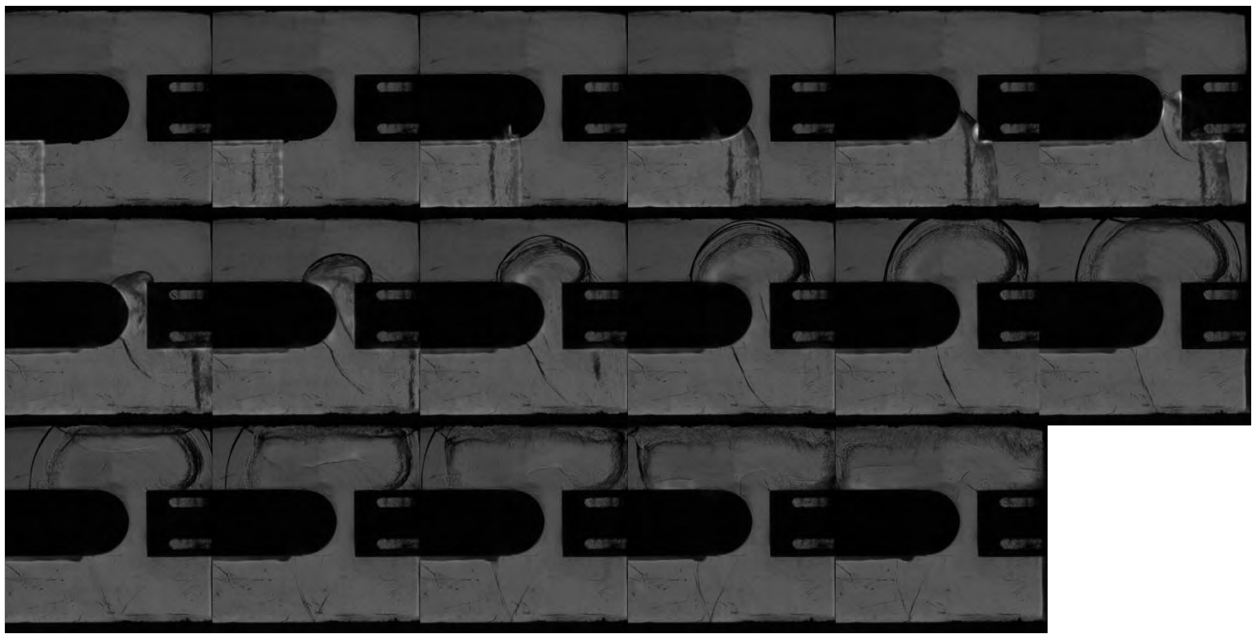

Figure C-5. Ethylene-air detonation in tail-tail configuration with 0.5 in crossover width resulting in a failed Region III reinitiation

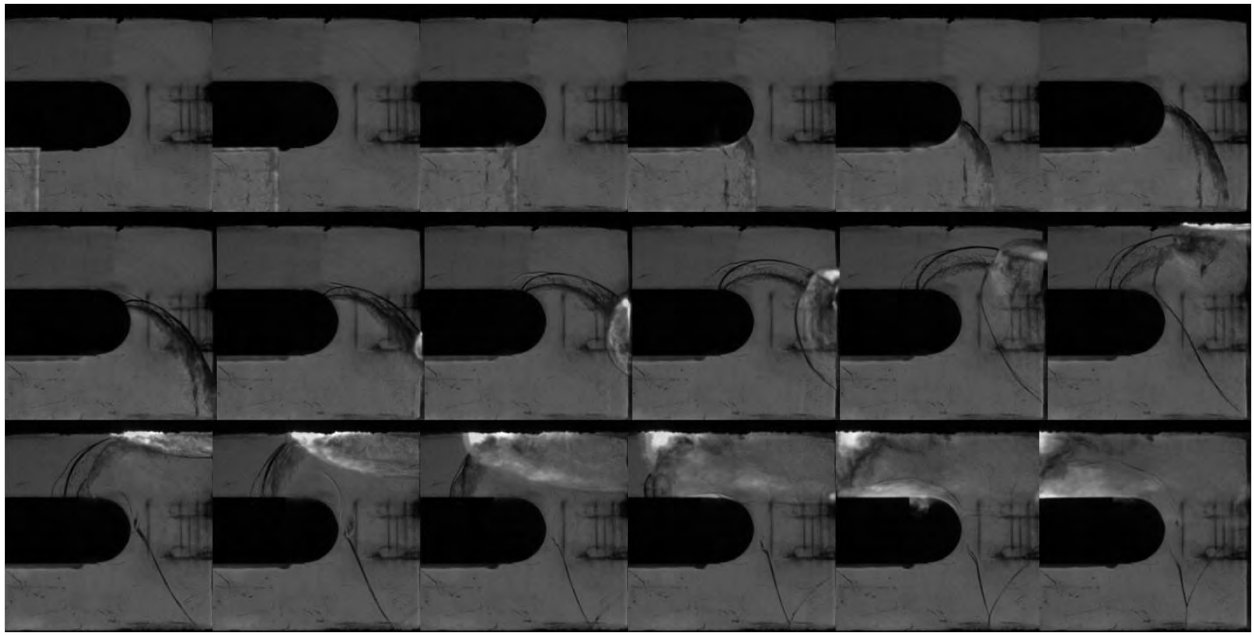

Figure C-6. Ethylene-air detonation in mid-mid configuration with 2.5 in crossover width resulting in a successful Region III reinitiation

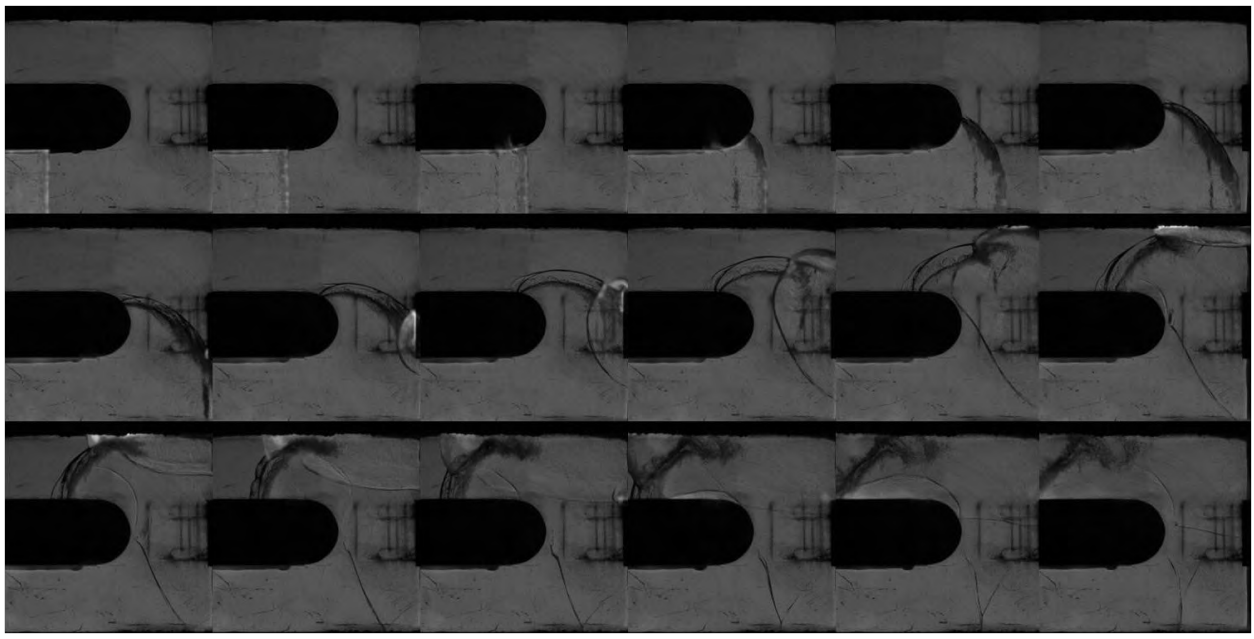

Figure C-7. Ethylene-air detonation in mid-mid configuration with 2.25 in crossover width resulting in a successful Region III reinitiation

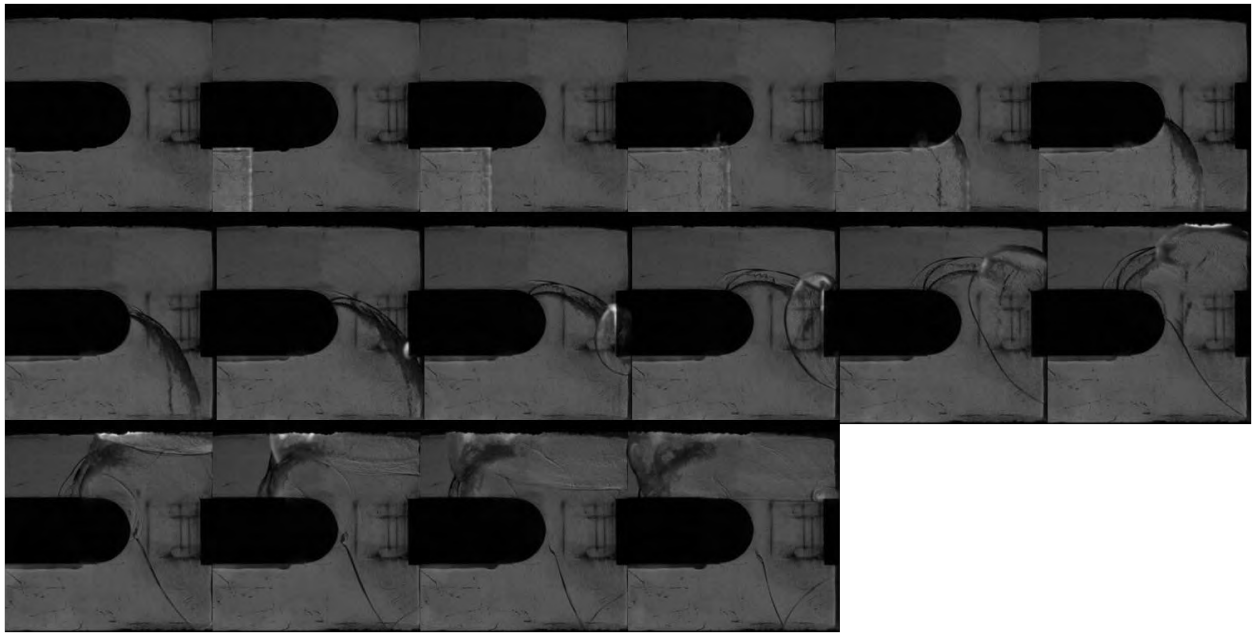

Figure C-8. Ethylene-air detonation in mid-mid configuration with 2.0 in crossover width resulting in a successful Region III reinitiation

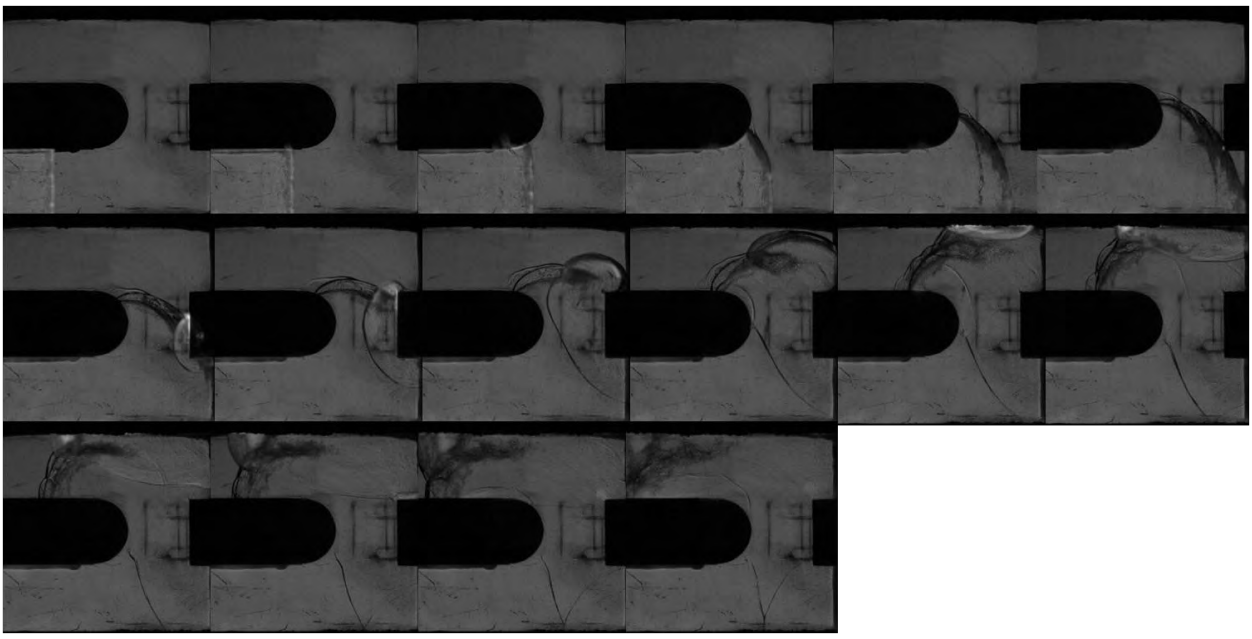

Figure C-9. Ethylene-air detonation in mid-mid configuration with 1.75 in crossover width resulting in a successful Region III reinitiation

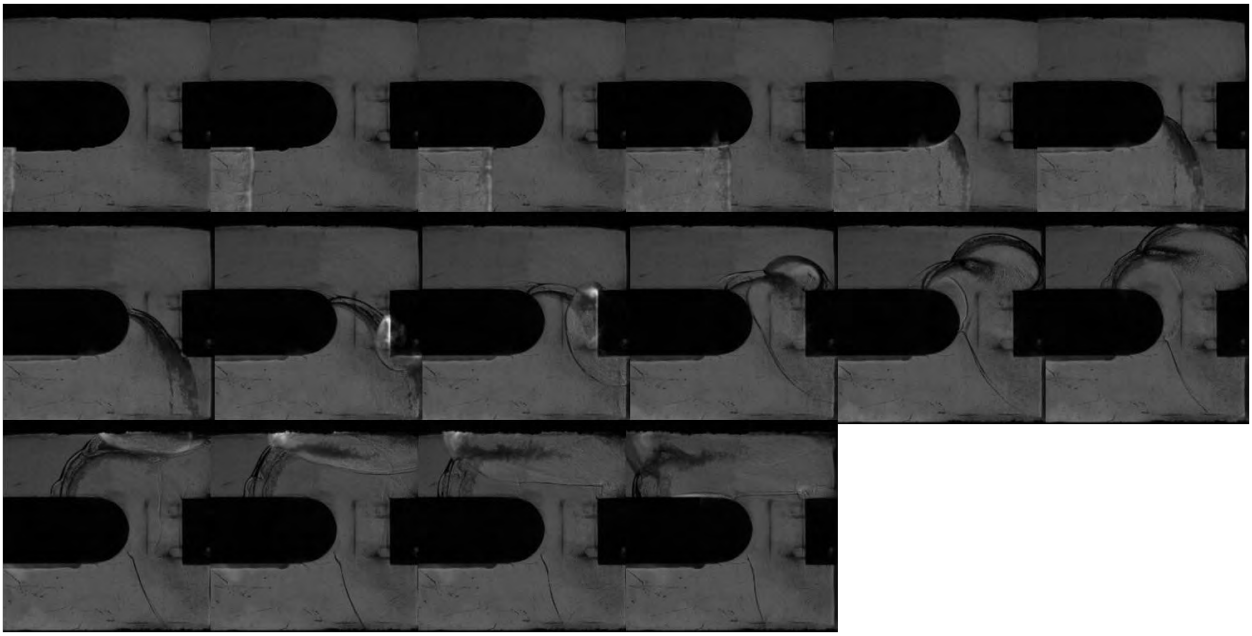

Figure C-10. Ethylene-air detonation in mid-mid configuration with 1.5 in crossover width resulting in a successful Region III reinitiation

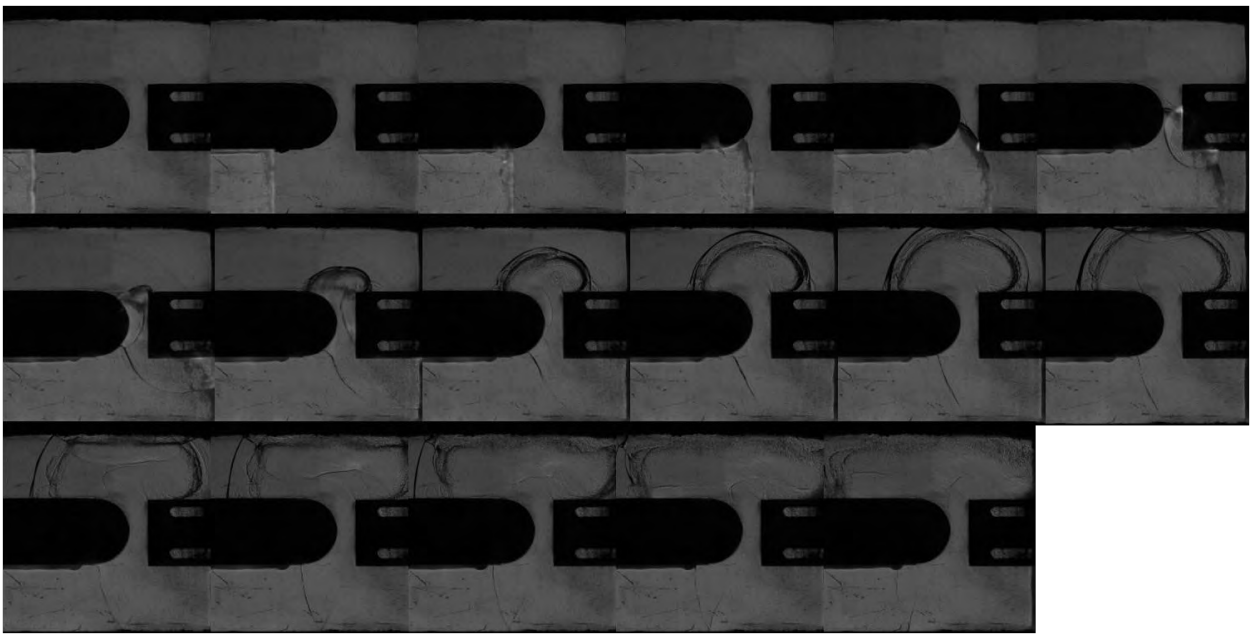

Figure C-11. Ethylene-air detonation in mid-mid configuration with 0.5 in crossover width resulting in a failed Region III reinitiation

Appendix D. n-Alkane detonation photographs

The DDT spiral and spark were switched into tube 2 in order to remedy initiation failures in tube 4 due to a valve that would not close properly. As a result, the n-alkane detonation photographs depict the primary detonation tube on the top and the secondary detonation tube on the bottom. The detonations proceed from top to bottom as opposed to proceeding from bottom to top as with hydrogen and ethylene. Additionally, oil was sprayed through the leaking valve in tube 4 and covered the polycarbonate window. As a result, the field of view in the Schlieren photographs is darker for the n-alkane detonations.

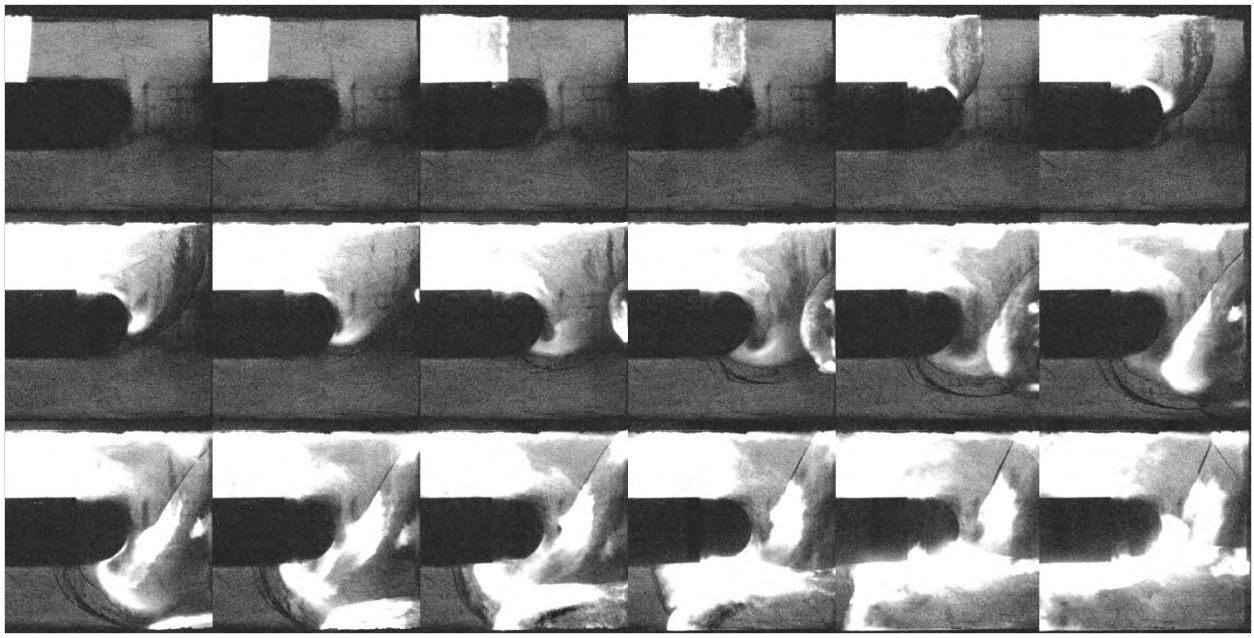

Figure D-1. n-Alkane-air detonation in tail-tail configuration with 2.5 in crossover width resulting in a successful Region III reinitiation

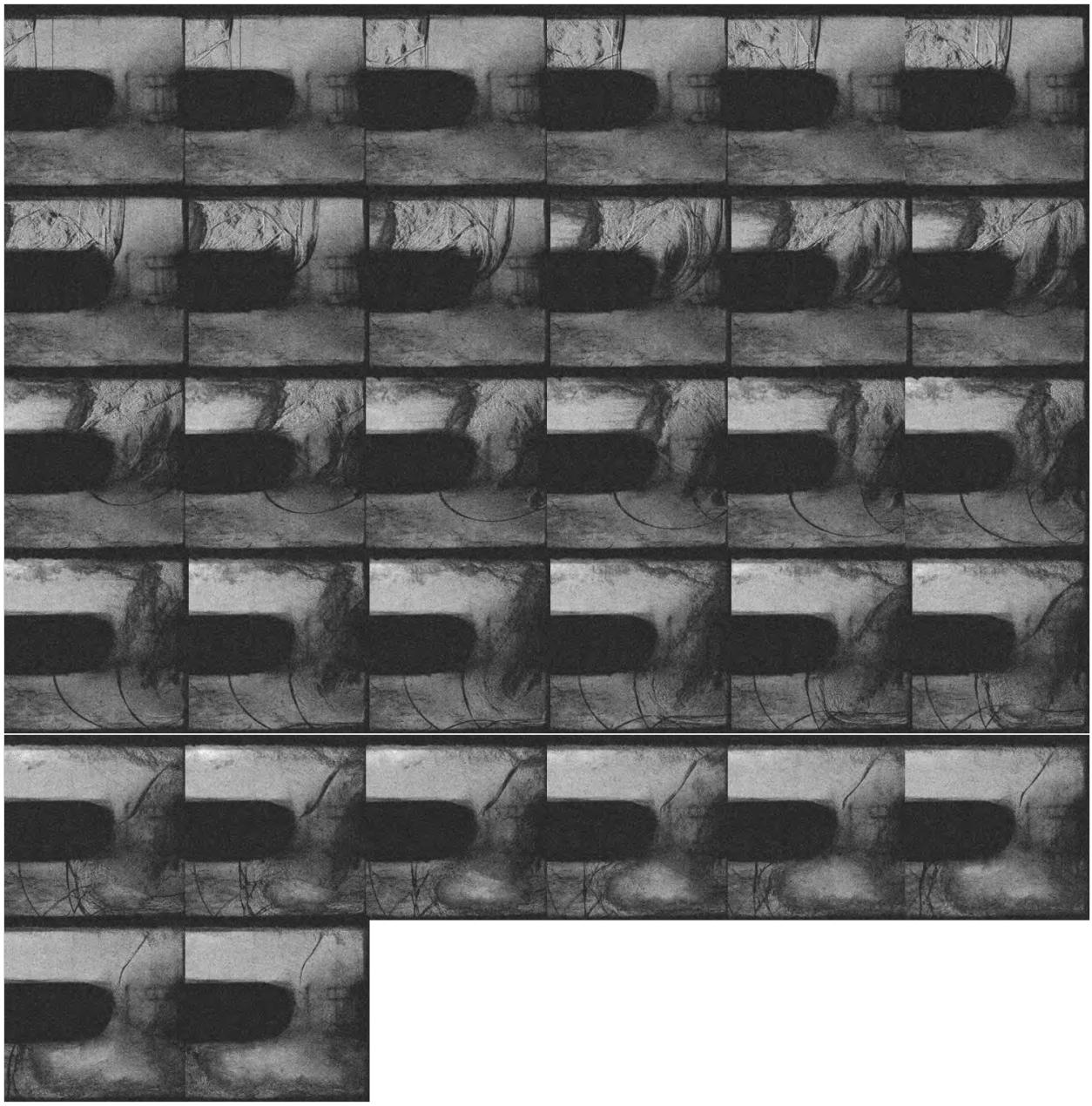

Figure D-2. n-Alkane-air failed detonation in tail-tail configuration with 2.25 in crossover width

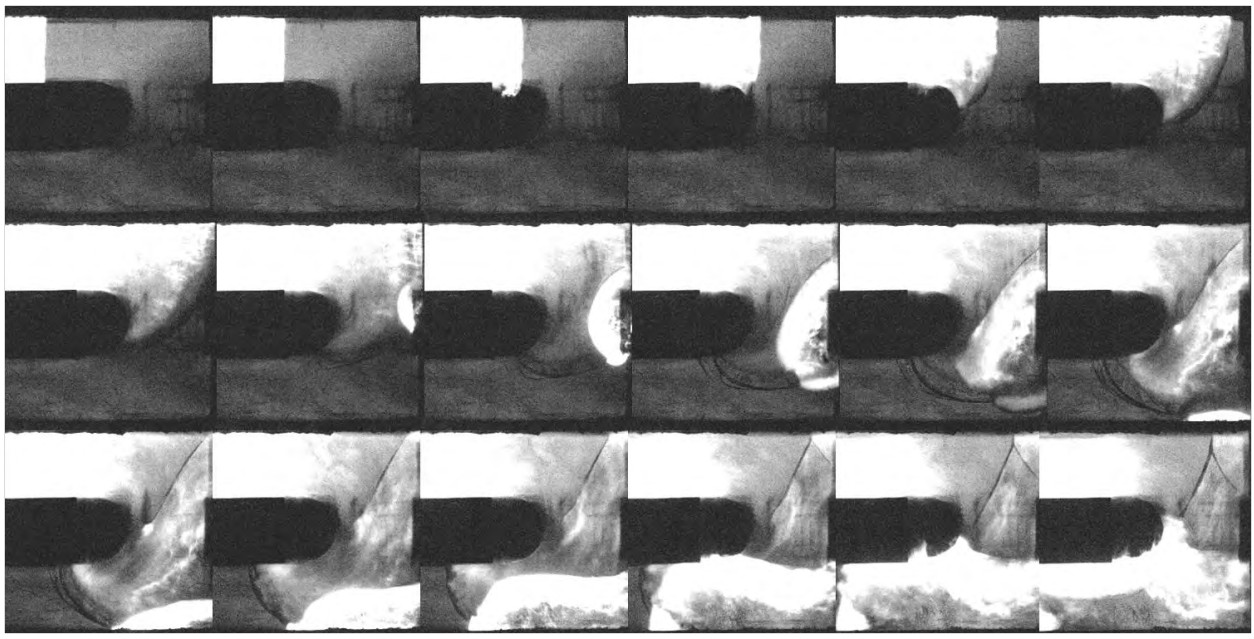

Figure D-3. n-Alkane-air detonation in tail-tail configuration with 2.25 in crossover width resulting in a successful Region III reinitiation

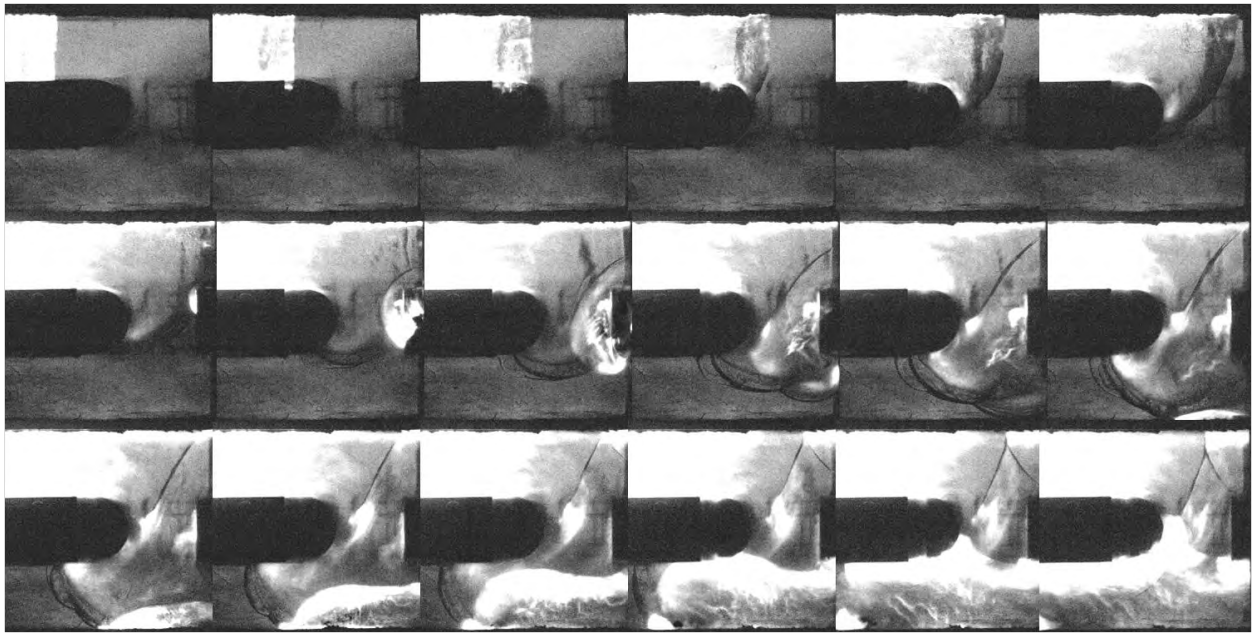

Figure D-4. n-Alkane-air detonation in tail-tail configuration with 2.0 in crossover width resulting in a successful Region III reinitiation

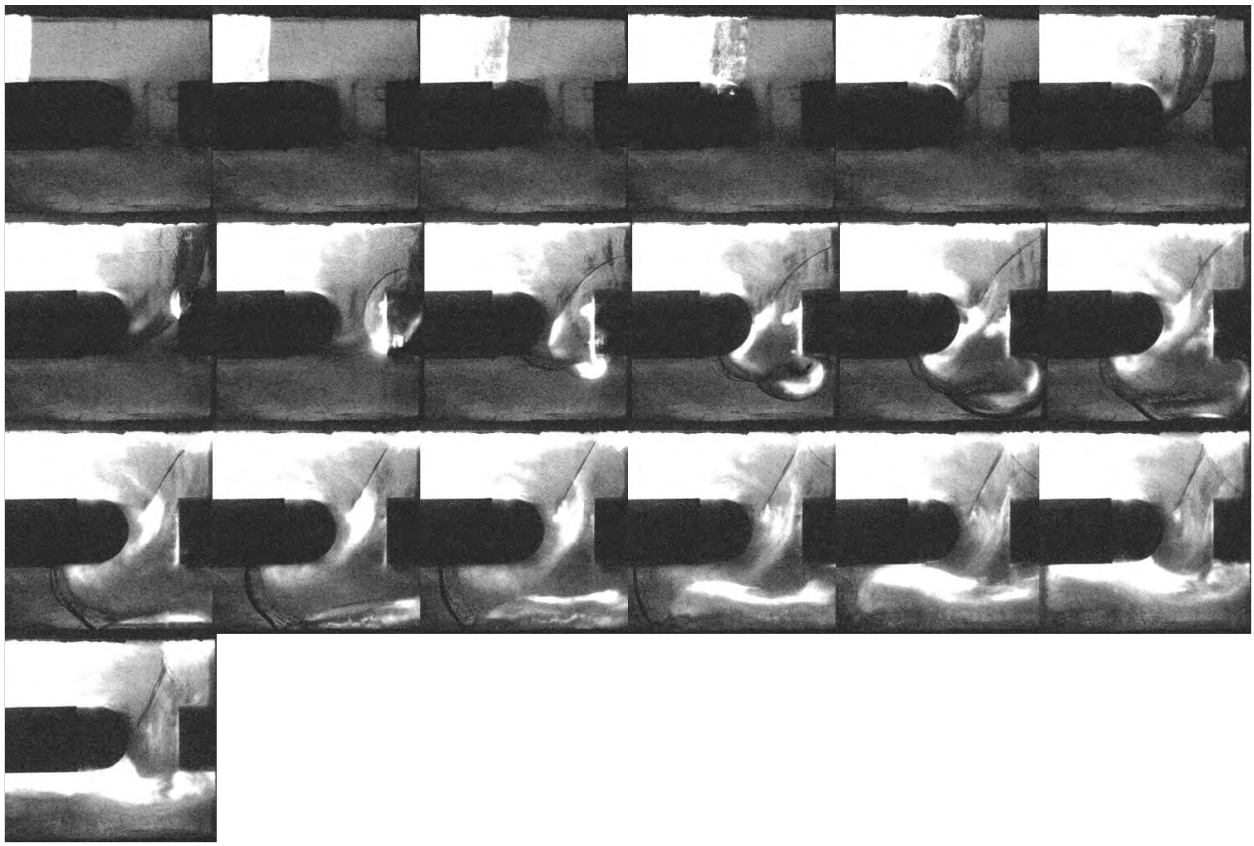

Figure D-5. n-Alkane-air detonation in tail-tail configuration with 1.5 in crossover width resulting in a failed Region III reinitiation

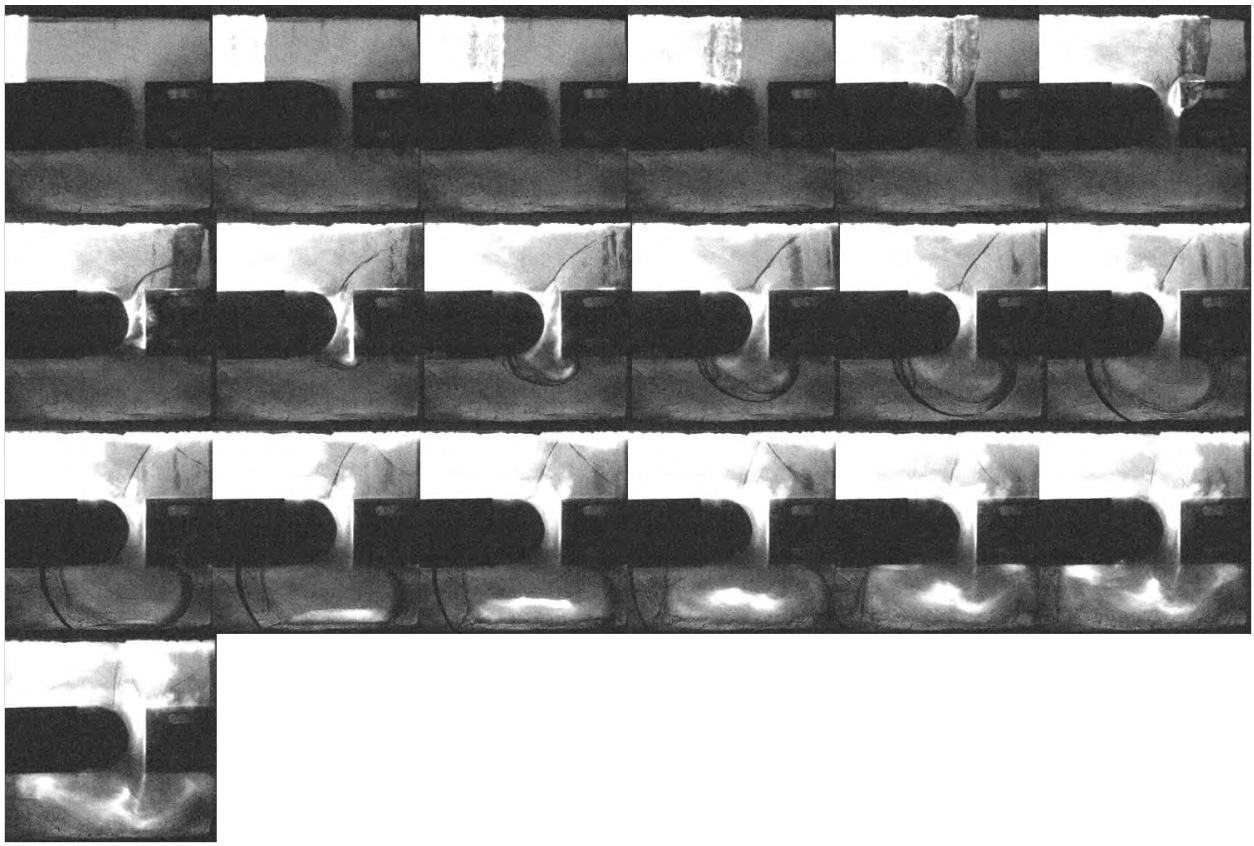

Figure D-6. n-Alkane-air detonation in tail-tail configuration with 0.5 in crossover width resulting in a failed Region III reinitiation

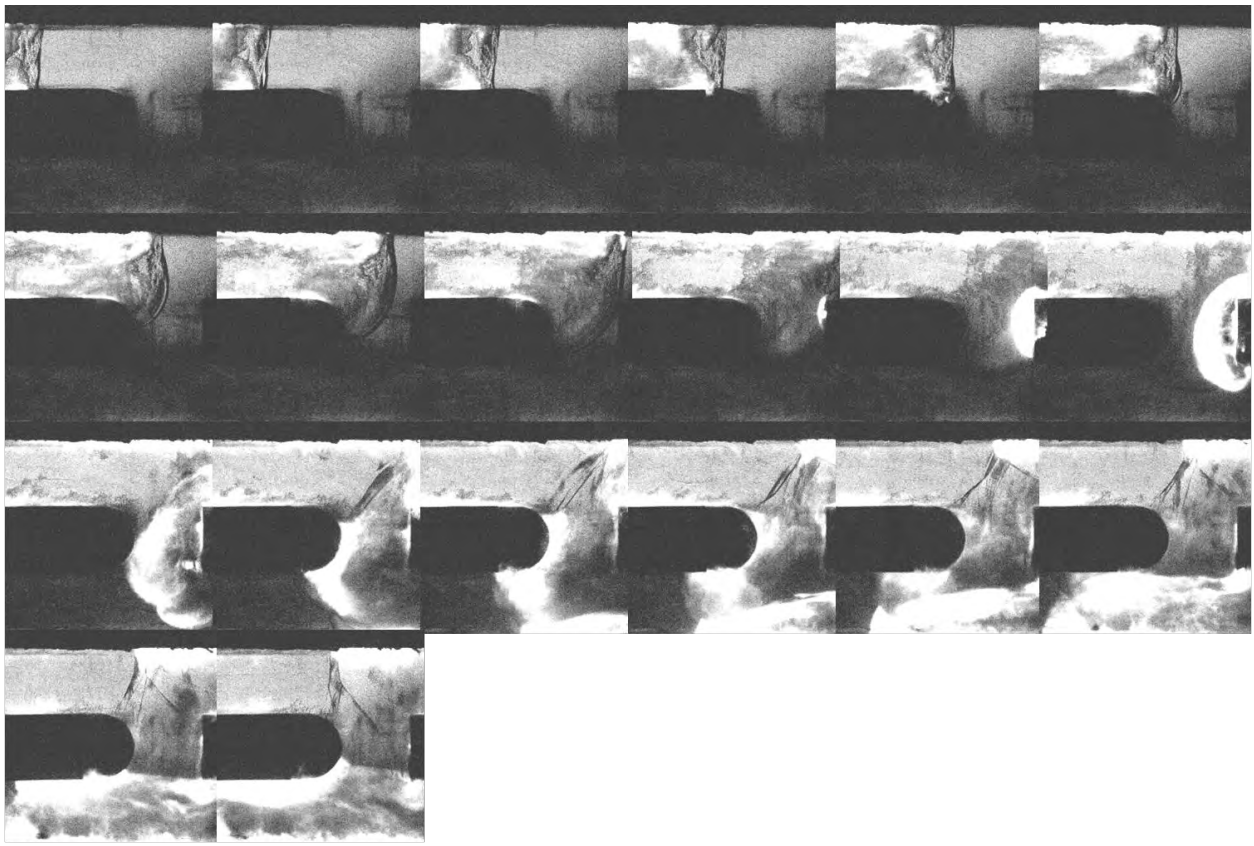

Figure D-7. n-Alkane-air detonation in mid-mid configuration with 2.0 in crossover width resulting in a failed Region I detonation, but a successful Region III reinitiation

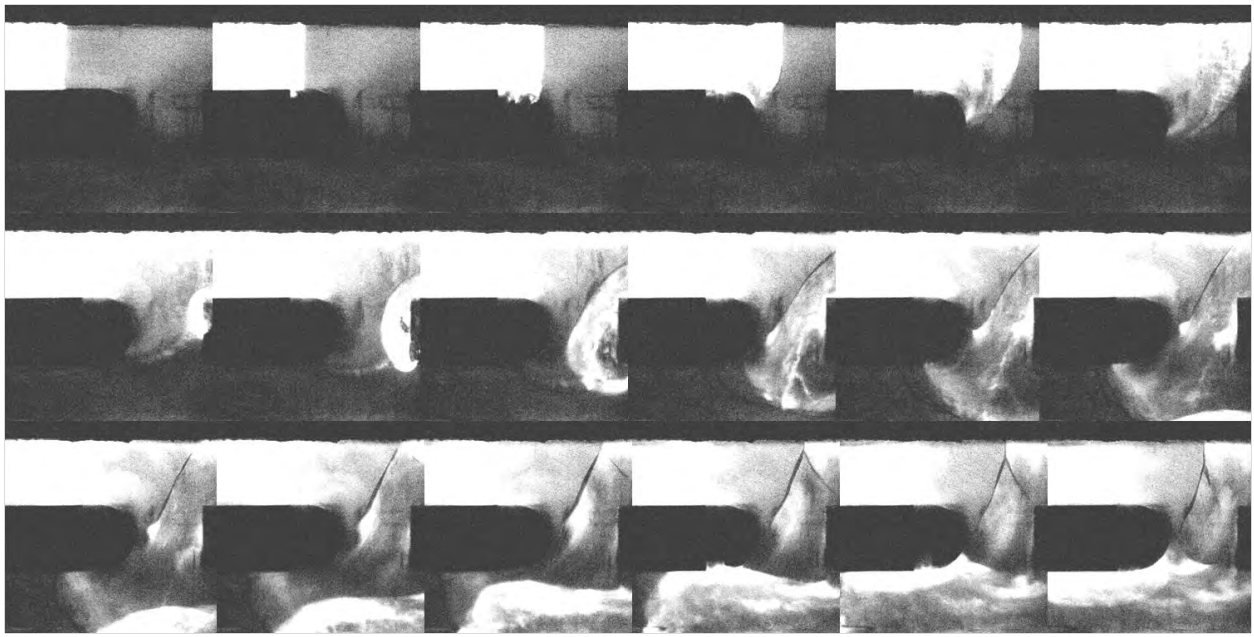

Figure D-8. n-Alkane-air detonation in mid-mid configuration with 2.0 in crossover width resulting in a successful Region III reinitiation

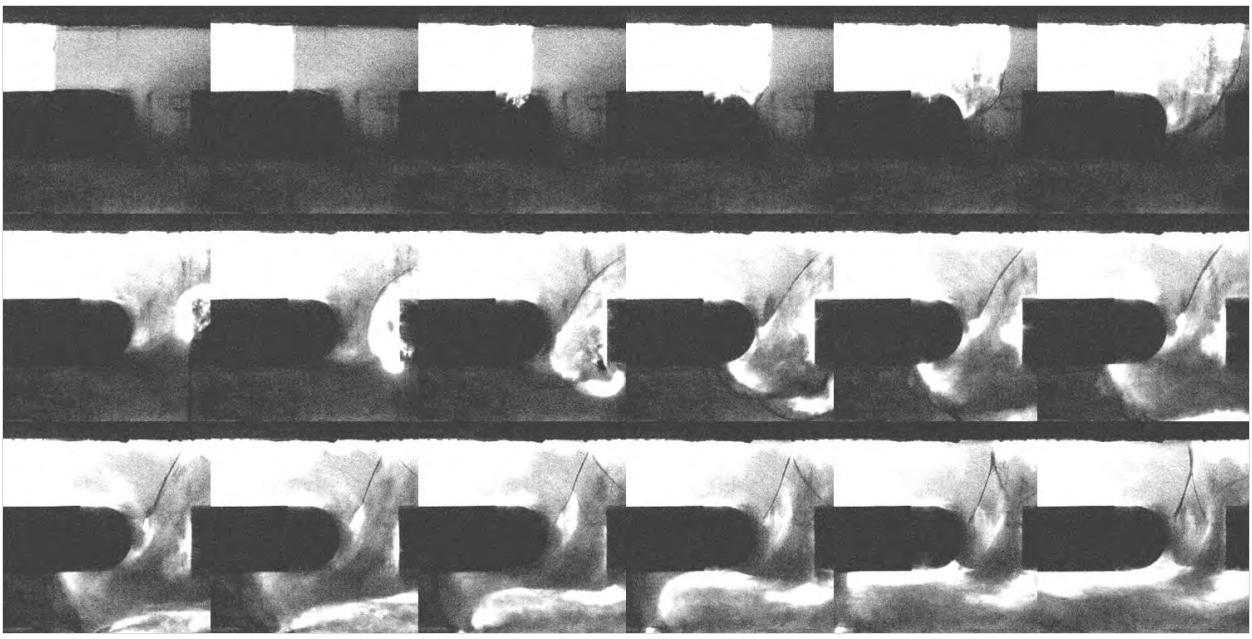

Figure D-9. n-Alkane-air detonation in mid-mid configuration with 1.75 in crossover width resulting in a successful Region III reinitiation

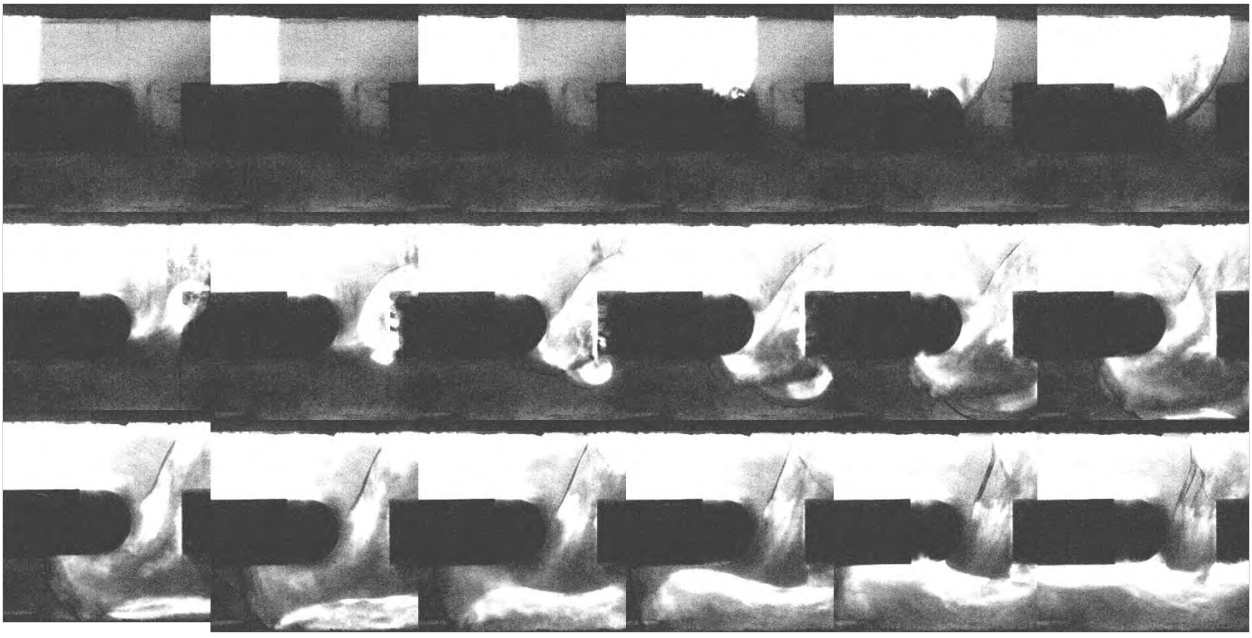

Figure D-10. n-Alkane-air detonation in mid-mid configuration with 1.5 in crossover width resulting in a failed Region III reinitiation

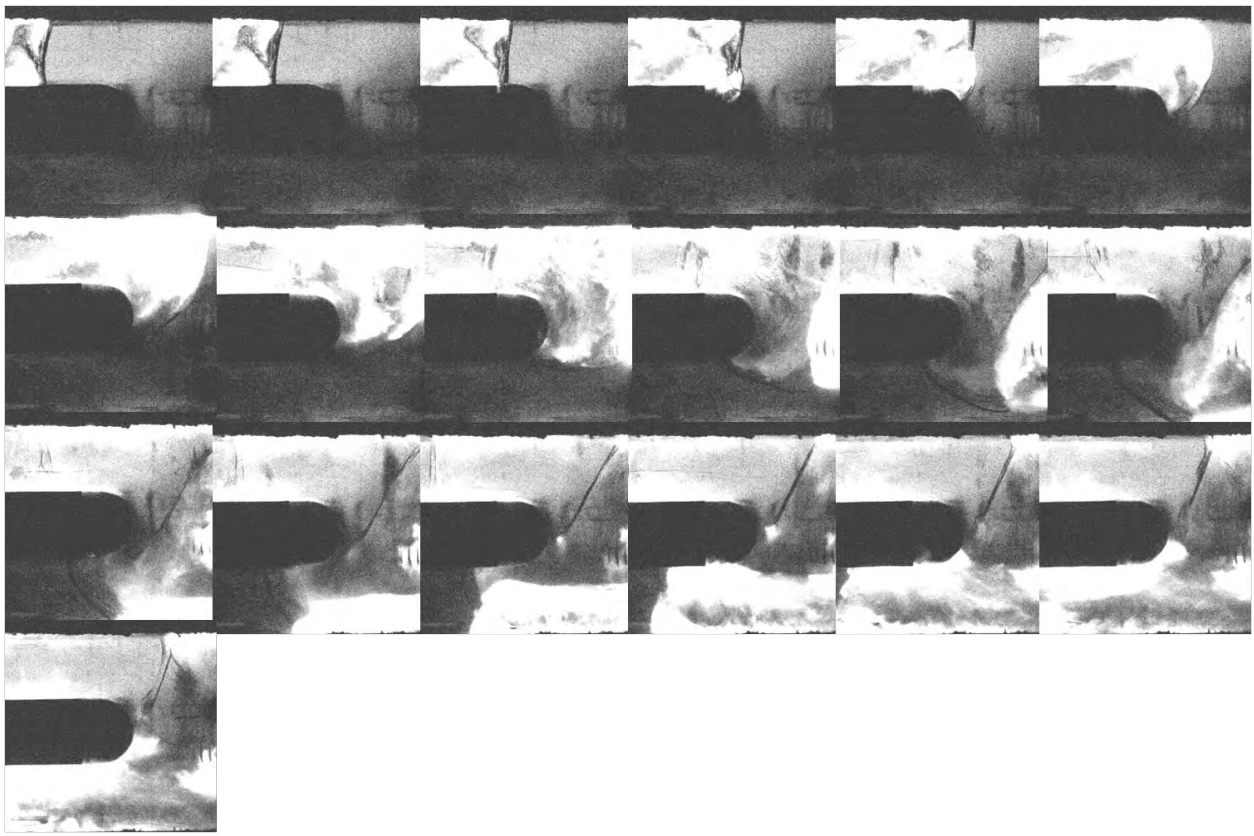

Figure D-11. n-Alkane-air detonation in mid-mid configuration with 2.5 in crossover width resulting in a successful Region III reinitiation

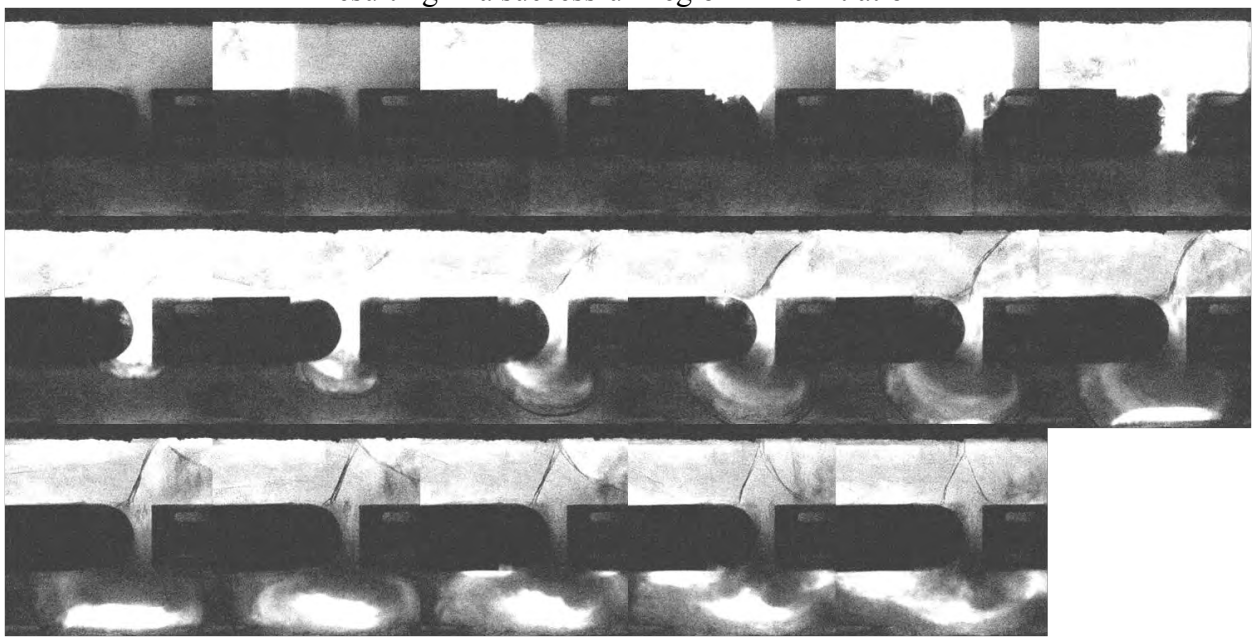

Figure D-12. n-Alkane-air detonation in mid-mid configuration with 0.5 in crossover width resulting in a failed Region III reinitiation

Bibliography

[1] Wu, Y., Ma, F., and Yang, V. "System Performance and Thermodynamic Cycle Analysis of Airbreathing Pulse Detonation Engines," *Journal of Propulsion and Power*, 19: 556-567 (2003).

[2] Bussing, T. and Pappas, G. "An Introduction to Pulse Detonation Engines," AIAA Paper No. 94-0263, 32nd Aerospace Sciences Meeting and Exhibit, Reno NV, 10-13 January 1994.

[3] Mindling, George. *U.S. Air Force Tactical Missiles*. Morrisville NC: Lulu.com Publishing, 2008.

[4] Oates, Gordon C. *Aerothermodynamics of Gas Turbine and Rocket Propulsion*. Reston VA: American Institute of Aeronautics and Astronautics, 1997.

[5] Roy, G.D., Frolov, S.M., Borisov, A.A., and Netzer, D.W. "Pulse Detonation Propulsion: Challenges, Current Status, and Future Perspective," *Progress in Energy and Combustion Science*, 30: 545-672 (2004).

[6] Bussing, T. and Pappas, G. "Pulse Detonation Engine Theory and Concepts," *Progress in Astronautics and Aeronautics*. 421-472. Reston VA: AIAA, 1996.

[7] Nielsen, Jeffrey M. *Detonation Propagation Through Ducts in a Pulsed Detonation Engine*. MS Thesis, AFIT/GAE/ENY/11-M21. Graduate School of Engineering and Management, Air Force Institute of Technology (AU), Wright-Patterson AFB OH, March 2011 (ADA540028).

[8] Panzenhagen, K.L. *Detonation Branching in a PDE with Liquid Hydrocarbon Fuel*. MS Thesis, AFIT/GAE/ENY/04-M13. Graduate School of Engineering and Management, Air Force Institute of Technology (AU), Wright-Patterson AFB OH, March 2004 (ADA424361).

[9] Hopper, D. *Direct Initiation of Multiple Tubes by Detonation Branching in a Pulsed Detonation Engine*. Air Force Institute of Technology (AU), Wright-Patterson AFB OH, August 2008 (ADB343653).

[10] Nielsen, J., King, P., Schauer, F., Stevens, C., Hoke, J. "Detonation Propagation Through Ducts in a Pulsed Detonation Engine," AIAA Paper No. 2011-585, 49th AIAA Aerospace Sciences Meeting including the New Horizons Forum and Aerospace Exposition, Orlando FL, 4-7 January 2011.

[11] Bartlma, F. "The Propagation of Detonation Waves in Channels of Varying Cross-Section," *Journal of Fluid Mechanics*, 218: 225-238 (1990).

[12] Gilbert, Jonathan M. *Direct Initiation of Multiple Tubes by Detonation Branching in a Pulsed Detonation Engine Using Hydrocarbon Fuels*. MS Thesis, AFIT/GAE/ENY/09-M09. Graduate School of Engineering and Management, Air Force Institute of Technology (AU), Wright-Patterson AFB OH, March 2009 (ADB347686).

[13] Lee, John H.S. *The Detonation Phenomenon*. New York: Cambridge University Press, 2008.

[14] Turns, Stephen R. *An Introduction to Combustion: Concepts and Applications*. Boston: The McGraw-Hill Companies, Inc., 2000.

[15] Zucker, Robert D. *Fundamentals of Gas Dynamics*. Chesterland OH: Matrix Publishers, Inc., 1977.

[16] Helfrich, Timothy M. *Cycle Performance of a Pulse Detonation Engine with Supercritical Fuel Injection*. MS Thesis, AFIT/GAE/ENY/06-M14. Graduate School of Engineering and Management, Air Force Institute of Technology (AU), Wright-Patterson AFB OH, March 2006 (ADA450884).

[17] Coleman, M.L. *Overview of Pulse Detonation Propulsion Technology*. CPTR 70. Chemical Propulsion Information Agency, 2001.

[18] Kuo, Kenneth K. *Principles of Combustion*. Hoboken NJ: John Wiley & Sons, Inc., 2005.

[19] Fievisohn, Robert T. *Numerical Investigation of Predetonator Geometries for PDE Applications*. MS Thesis, AFIT/GAE/ENY/10-M10. Graduate School of Engineering and Management, Air Force Institute of Technology (AU), Wright-Patterson AFB OH, March 2010 (ADA517597).

[20] Bartlma, F. and Schroeder, K. "The Diffraction of a Plane Detonation Wave at a Convex Corner," *Combustion and Flame*, 66: 237-248 (1986).

[21] Schultz, Eric. *Detonation Diffraction through an Abrupt Area Expansion*. PhD dissertation. California Institute of Technology, Pasadena CA, April 2000.

[22] Schauer, F., Stutrud, J., and Bradley, R. "Detonation Initiation Studies and Performance Results for Pulsed Detonation Engine Applications," AIAA Paper No. 2001-129, 39th AIAA Aerospace Sciences Meeting & Exhibit, Reno NV, 8-11 January 2001.

[23] Schultz, E. and Shepherd, J. *Validation of Detailed Reaction Mechanisms for Detonation Simulation*. Explosion Dynamics Laboratory Report FM99-5. Pasadena CA: Graduate Aeronautical Laboratories, February 2000.

[24] Tavoularis, Stavros. *Measurement in Fluid Mechanics*. Cambridge: Cambridge University Press, 2005.

REPORT DOCUMENTATION PAGE		*Form Approved* *OMB No. 0704–0188*

1. REPORT DATE (DD–MM–YYYY)	2. REPORT TYPE	3. DATES COVERED *(From — To)*
22-03-2012	Master's Thesis	SEP 2010 – MAR 2012

4. TITLE AND SUBTITLE	5a. CONTRACT NUMBER
Determination of Effective Crossover Location and Dimensions for Branched Detonation in a Pulsed Detonation Engine	5b. GRANT NUMBER
	5c. PROGRAM ELEMENT NUMBER
6. AUTHOR(S) Louis A. Camardo II, Maj, USMC	5d. PROJECT NUMBER
	5e. TASK NUMBER
	5f. WORK UNIT NUMBER

7. PERFORMING ORGANIZATION NAME(S) AND ADDRESS(ES)	8. PERFORMING ORGANIZATION REPORT NUMBER
Air Force Institute of Technology Graduate School of Engineering and Management (AFIT/ENY) 2950 Hobson Way WPAFB OH 45433-7765	AFIT/GAE/ENY/12-M05
9. SPONSORING / MONITORING AGENCY NAME(S) AND ADDRESS(ES) Attn: Dr. Frederick Schauer Air Force Research Laboratory Propulsion Directorate, Turbine Engine Division, Combustion Branch, Advanced Concepts Group Bldg 71A, D-Bay, 7th St. Wright Patterson AFB, OH 45433-7251 DSN 785-6462, frederick.schauer@wpafb.af.mil	10. SPONSOR/MONITOR'S ACRONYM(S) AFRL/RZTC
	11. SPONSOR/MONITOR'S REPORT NUMBER(S)

12. DISTRIBUTION / AVAILABILITY STATEMENT
APPROVED FOR PUBLIC RELEASE; DISTRIBUTION UNLIMITED

13. SUPPLEMENTARY NOTES This material is declared a work of the U.S. Government and is not subject to copyright protection in the United States.

14. ABSTRACT
A study is presented of the optimal crossover duct location and width to obtain consistent branched detonation transition from one detonation tube to another. On a Pulsed Detonation Engine (PDE) with detonation branching, the duct location at which the detonation crosses from one (primary) tube to a branched (secondary) tube impacts the number of successful detonations. In this paper, a comparison is made of the effects of the location and width of the crossover duct for hydrogen, ethylene and an n-alkane. The crossover location is varied from the aft end of the detonation tube to the middle of the detonation tube while the crossover width is varied from 2.5 in to 0.5 in. Detonation wave speeds are measured and compared to Chapman-Jouguet velocities in order to determine successful detonations. Regardless of crossover location, all three fuels are demonstrated 100% of the time to transition between 2 in detonation tubes with a crossover width of 2 in. With a mid-location crossover duct, all three fuels are demonstrated 100% of the time to transition detonations between 2 in detonation tubes with a crossover width between 1.75 in and 2.5 in.

15. SUBJECT TERMS
Detonation, Pulsed, Engine, Shock wave, Propagation, Cross-over, Wave speed, Combusion, Chapman-Jouguet, Schlieren, Reflection, Re-initiation

16. SECURITY CLASSIFICATION OF: Unclassified			17. LIMITATION OF ABSTRACT	18. NUMBER OF PAGES	19a. NAME OF RESPONSIBLE PERSON Dr. Paul I. King
a. REPORT	b. ABSTRACT	c. THIS PAGE	UU	111	19b. TELEPHONE NUMBER (Include Area Code) (937)255-3636, ext 4628 paul.king@afit.edu
U	U	U			

Standard Form 298 (Rev. 8–98)
Prescribed by ANSI Std. Z39.18